Available online at www.elsevier.com/locate/nds

Nuclear Data Sheets 139 (2017) 77-137

FISPACT-II: An Advanced Simulation System for Activation, Transmutation and Material Modelling

J.-Ch. Sublet,[1,*] J. W. Eastwood,[2] J. G. Morgan,[2] M. R. Gilbert,[1] M. Fleming,[1] and W. Arter[1]

[1] *United Kingdom Atomic Energy Authority, Culham Science Centre, Abingdon OX14 3DB, UK*
[2] *Culham Electromagnetics Ltd, Culham Science Centre, Abingdon OX14 3DB, UK*

(Dated: January 19, 2017; Received 25 August 2016; accepted XX 2016)

FISPACT-II is a code system and library database for modelling activation-transmutation processes, depletion-burn-up, time dependent inventory and radiation damage source terms caused by nuclear reactions and decays.

The FISPACT-II code, written in object-style Fortran, follows the evolution of material irradiated by neutrons, alphas, gammas, protons, or deuterons, and provides a wide range of derived radiological output quantities to satisfy most needs for nuclear applications. It can be used with any ENDF-compliant group library data for nuclear reactions, particle-induced and spontaneous fission yields, and radioactive decay (including but not limited to TENDL-2015, ENDF/B-VII.1, JEFF-3.2, JENDL-4.0u, CENDL-3.1 processed into fine-group-structure files, GEFY-5.2 and UKDD-16), as well as resolved and unresolved resonance range probability tables for self-shielding corrections and updated radiological hazard indices. The code has many novel features including: extension of the energy range up to 1 GeV; additional neutron physics including self-shielding effects, temperature dependence, thin and thick target yields; pathway analysis; and sensitivity and uncertainty quantification and propagation using full covariance data.

The latest ENDF libraries such as TENDL encompass thousands of target isotopes. Nuclear data libraries for FISPACT-II are prepared from these using processing codes PREPRO, NJOY and CALENDF. These data include resonance parameters, cross sections with covariances, probability tables in the resonance ranges, PKA spectra, kerma, dpa, gas and radionuclide production and energy-dependent fission yields, supplemented with all 27 decay types. All such data for the five most important incident particles are provided in evaluated data tables.

The FISPACT-II simulation software is described in detail in this paper, together with the nuclear data libraries. The FISPACT-II system also includes several utility programs for code-use optimisation, visualisation and production of secondary radiological quantities. Included in the paper are summaries of results from the suite of verification and validation reports available with the code.

CONTENTS

* Corresponding author: jean-christophe.sublet@ukaea.uk

http://dx.doi.org/10.1016/j.nds.2017.01.002

I. INTRODUCTION

FISPACT-II [1] is a code system and library database for the simulation of depletion, activation, transmutation processes and time dependent radiation damage source terms caused by nuclear reactions and decays. It has three main components:

1. software for simulation of depletion, activation, transmutation processes and radiation damage terms. This comprises a library of modules and a number of driver programs, the principal one of which is also called FISPACT-II.

2. nuclear data libraries. These are enhanced ENDF-6 [2] formatted group cross sections, decay and fission yield libraries with additional sub-group data for self-shielding, recoil matrices, full variance-covariance information and data for radiological quantities derived from activity. FISPACT-II links to nuclear data libraries for incident particles including neutron, deuteron, proton, alpha and gamma irradiation.

3. an extensive suite of validation and verification tests that cover all major applications from fusion to fission reactors, astrophysics, accelerator and high energy systems, medical applications, etcetera.

The core of the simulation system is the FISPACT-II code. This is described in the following section. The data libraries and their preparation in a suitable form for use by FISPACT-II are described in Section III and a summary of the FISPACT-II verification and validation tests are presented in Section IV. A summary of reaction/decay pathway and uncertainty methods is provided in Section V C 1.

II. FISPACT-II

FISPACT-II replaces the now obsolete FISPACT code, which was developed and maintained for more than 20 years [3–5] at UKAEA, and was itself based on the much earlier fission-orientated code FISPIN [6]. That system became too cumbersome and inflexible to adapt to the latest advances in nuclear physics and nuclear data, prompting the development of FISPACT-II. This was accomplished over a number of years using modern, object-style Fortran, focussing initially on recreating the functionality of FISPACT (see Eastwood and Morgan [7]), but then subsequently extending its capabilities significantly beyond what was available before. The new code has numerous improvements including upgraded numerical algorithms. The core of FISPACT-II is the LSODE [8] ordinary differential equation solver, which integrates the rate equations forward in time. It also uses dynamical memory allocation, and so may be readily adapted to any energy group structure. It contains four major

subsystems for handling (1) nuclear data reduction, (2) assembling and solving the rate equations for the inventory, (3) computing pathways and uncertainties and (4) computing and outputting derived radiological data. The present version works with any ENDF-6 compliant library for group cross-section data as well as the EAF-style nuclear data libraries [9] used by its predecessors, although without the full functionality of the enhanced ENDF-6 data.

A. Capabilities

The main FISPACT-II program is now a powerful and practical activation-transmutation engineering prediction tool that undertakes the following tasks:

1. extraction, reduction and storage of nuclear and radiological data from the nuclear data library files;
2. construction and solution of the rate equations to determine the time evolution of the inventory in response to different irradiation scenarios. These scenarios include
   (a) a cooling-only calculation;
   (b) a single irradiation pulse followed by cooling;
   (c) multiple irradiation pulses where only flux amplitudes change, followed by cooling;
   (d) multi-step irradiation where flux amplitude, flux spectra and cross sections may change, followed by cooling.
   (e) multi-projectile simulation
3. computation and output of derived radiological quantities;
4. subsidiary calculations to identify the key reactions and decays, and to quantify the uncertainties in the predictions. The four main subsidiary items are
   (a) pathway analysis;
   (b) uncertainty calculation and propagation from pathways;
   (c) reduced model calculations;
   (d) monte-carlo sensitivity and uncertainty calculations.

These items are described further in the following subsections.

The discussion in the following subsections will be in terms of neutrons as the irradiating projectile. FISPACT-II works equally well for other projectiles, when provided with the necessary data. Differences for projectiles deuteron, proton, alpha and gamma are treated in Section II O.

1. *Library Data Reduction*

The library reduction task comprises reading and *collapsing* the cross-section data with an incident-particle spectrum, reading, *condensing* and storing the decay data and fission data, and storing the regulatory radiological data (potential biological hazards, clearance data and legal transport data).

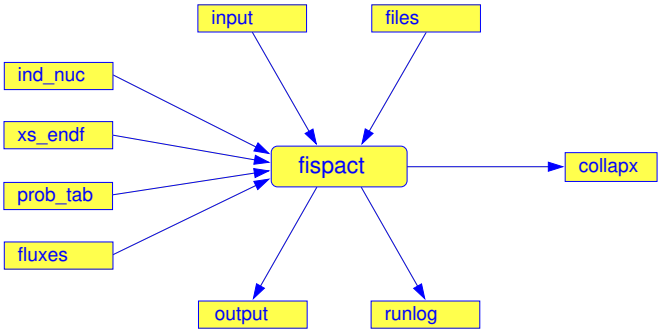

FIG. 1. (Color online) Input and output streams for cross section and uncertainty collapse.

Figure 1 summarises the *collapse* process where an incident particle spectrum is convolved with the reaction cross sections, including uncertainties and any self-shielding corrections. The `input` file contains keywords to specify a collapse run, and the `files` file contains mappings of the nuclear data files to the input streams. The code's ENDF processor reads data from the `xs_endf` folder and extracts cross-section (`MF`=3 and 10) and covariance data (`MF`= 33 and 40) for all nuclides in the master index file `ind_nuc`. Section II B contains a summary of the reactions for neutron irradiation. It then collapses these with the flux spectrum in the `fluxes` file and stores the collapsed cross sections in the `collapx` file. Error logging goes to the `runlog` file and other simulated quantities are written to the `output` file. The formulae used for data collapse are described in Section II C.

Keywords may be added to the `input` to cause self-shielding factors to be calculated and applied. If the subgroup method is specified, then the CALENDF [10, 11] probability table data are read from the `prob_tab` stream and are incorporated in the calculation of the collapsed cross section using the formulae presented in Section II D. If the universal sigmoid curve method (see Section II E) is specified, then `MF`=2 resonance data are read on stream `xs_endf` and the formulae given in Section II E are used.

Figure 2 illustrates the *condense* process where decay and fission yield data are processed for use in the rate equation solutions. If the keywords in the `input` file specify a condense, then `MF`=8, `MT`=457 data are read from the `dk_endf` stream. Decay constants, decay energies and spectra are extracted and data are stored in the file `arrayx` (see Section II F). The γ and X-ray spectral lines are used to construct 24-group spectra for use in computing gamma doses from the inventories (Section II G). In

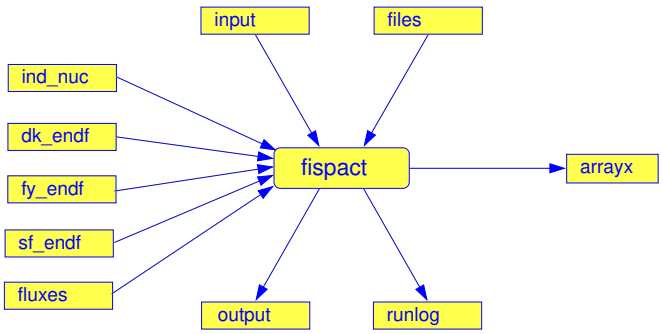

FIG. 2. (Color online) Input and output streams for decay and fission yield condense.

cases where the γ spectrum data are not available, then approximate spectra may be constructed for the purpose of estimating gamma doses (see Section II G 3).

If the use of fission yields is indicated, then `MF`=8, `MT`=454 or 459 (independent or cumulative yields, respectively) data are read on stream `fy_endf` and tables of fission daughters and yields are added to the data written to `arrayx`. More details of fission processing are given in Section II H. If, in addition, a keyword is used to specify the use of spontaneous fission yields, then similar data are read on stream `sf_endf` to give spontaneous fission yields and daughters.

Keywords may be added to the FISPACT-II `input` to cause summary tables of information on the cross-section, fission yield and decay data extracted from the nuclear data libraries.

2. *Inventory Calculation*

Figure 3 shows an inventory calculation. Library data reduction provides the cross sections (`collapx`) and decay constants with yields (`arrayx`) needed to construct the coefficients for the rate equations (Section II I). The rate equations describe the transmutation of the initial inventory by nuclear reactions induced by the projectiles and by spontaneous radioactive decay. The inventory calculation then proceeds by

1. setting the physical initial conditions of the target;
2. setting the output selections;
3. specifying the subsidiary calculations;
4. computing the irradiation steps;
5. performing the subsidiary calculations;
6. computing the cooling steps;
7. computing summary data.

The rate equations provide the inventory at each step. Radiological quantities derived from them are written to `output` as they become available at each step. Depending on the output selected, data files `absorp`, `a2data`, `clear` and `hazards` are read to provide respectively the factors needed to construct and output gamma dose, transport data, clearance data and biological hazard data. If selected, graphical output is sent to file `graph`. More information on these outputs are given in Section II L.

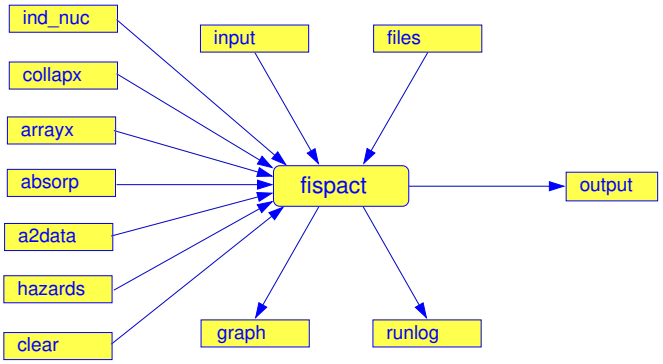

FIG. 3. (Color online) Input and output streams for the inventory calculation.

The sequence of timesteps performed in the calculation follows the sequence of steps specified in the user's `input` file controlling the run. The duration of a step is specified by the user, and typically ranges from fractions of a second to many years. During each step, the irradiating flux amplitude, cross sections and decay rates are kept constant. Also, it is assumed that the imposed projectile flux is not modified by the reactions and decays in the target material. As a consequence, the rate equations are linear and have constant coefficients for each timestep. The material is homogeneous, infinite and infinitely dilute (but in some circumstances, self-shielding can be accommodated in the model) and the description of the evolution of the nuclide numbers is reduced to a set of ordinary differential equations (see Section II I below). Unlike FISPACT 2007 [5], FISPACT-II does not use the equilibrium approximation for short-lived nuclides and includes the evolution of actinide sources in the rate equations. The core engine of the FISPACT-II stiff-ode solver is the LSODE package [8, 12, 13].

If the inventory calculation includes irradiation, then the first step must have a non-zero irradiating flux amplitude. The rate equation coefficients in subsequent steps may be changed in one or more of the following ways

- changing the flux amplitude;
- changing the library cross-section data (e.g., to take account of temperature effects);
- changing the flux spectrum;

The end of the irradiation (heating) phase triggers the subsidiary pathways and sensitivity calculations as well as resetting the elapsed time to zero.

The cooling phase is a sequence of timesteps, the same as the irradiation phase, although the projectile flux amplitude is usually (but not necessarily) set to zero and must be zero for the first cooling step. This functionality of including cooling steps with irradiation is to provide flexible applicability for pathway analysis and graphical output.

The principal output of an inventory calculation step is the inventory of nuclides at the end of the step. Secondary outputs are derived from the inventory, the choice of which is controlled by keywords in the FISPACT-II input file. See Section II L for a summary of the available output quantities.

The flux amplitude is generally specified for steps of the inventory calculation, but as an alternative, volumetric power based on kerma (total, fission or any partial specified by the user) may be used to set the normalisation of the particle flux during any timesteps. A list of all the available kerma values within the ENDF data is provided in Table II. This is a convenient alternative method for specifying the particle flux in units of burnup (*e.g.* GWd/tHM or any comparable units).

3. *Subsidiary Calculations*

The standard inventory calculation employing the ENDF library data uses all nuclides and all reactions that are catalogued in these libraries. The dominant nuclides at the end of a sequence of irradiation pulses can be readily identified from lists of nuclides ordered by various radiological quantities derived from the inventory. These lists do not show which dominant nuclide arose from which initial target nuclide, and by what series of reactions and/or decays.

The subsidiary calculations in FISPACT-II provide tools for the user to probe the reactions and decays in detail. Unlike its predecessor, pathways and sensitivity analyses can be undertaken for a series of irradiation pulses rather than for just a single irradiation pulse. Pathways calculations can be followed for an arbitrary number of irradiation and cooling periods (limited only by computational resources), and automatically identify loops that make significant differences to the contribution of the paths on which they lie.

The pathways calculation identifies how much of the inventory of each of the dominant nuclides came from which initial nuclide, and by what chains (and loops) of reactions and/or decays. Specific routes and paths can be probed independently from the dominant nuclide lists, and specific cross sections and decay rates can be changed to assess their effects. A description of the pathways algorithm used in FISPACT-II is given in Section V.

Uncertainty estimates are made by combining the pathways information with uncertainty data for cross sections and decay rates using the random walk approximation method described in Section II J.

FISPACT-II also has the capability to undertake repeated calculations and use Monte-Carlo methods to estimate uncertainty and sensitivity (see Section II K.) Correlation coefficients from these sensitivity calculations provide a complementary method of identifying important reactions. This approach is computationally intensive, but requires fewer assumptions than the random walk method based on pathways.

A reduced list of nuclides can be generated from the pathways information and full inventory calculations can be undertaken on the reduced set of nuclides and reactions to check whether all important reactions and decays are included. Reduced models can significantly reduce the computational time needed for Monte-Carlo sensitivity studies.

B. Neutron Activation

The main application of the code is for neutron activation calculations. In these the transmutation of a nuclide j to another nuclide i (and in some cases additional secondaries) may result from one of the neutron-induced reactions listed in Table I or one of the decay processes listed in Table VI. Activation by other projectiles (γ, d, p and α) is treated below in Section II O and decay processes are described in Section II F.

Data where the parent and daughter nuclides are the same are not used in constructing the rate equation matrix (except though self-shielding). 'Other reactions' (`MT`=5 in Table I) is a set of lumped channels with the same residuals and is a special case designated (z, O) for projectile z. Fission (`MT`=18 in Table I) is also a special case and is treated below in Section II H. The remaining `MT` in Table I describe reactions with one principal product plus a number of light nuclide secondaries.

Group cross sections for different `MT` values are tabulated as a function of energy in the ENDF cross-section libraries (cf. Section III D). These cross sections are reduced to energy-independent (one-group average) values using the collapse process described below in Section II C. The total cross section relating a given parent nuclide to a given daughter nuclide is formed by summing contributions from all different reaction `MT` values relating the parent to the daughter (see Section II I. The proportion each `MT` contributes to a parent-daughter pair is shown in the pathway analysis output (Section V).

1. *Other Reactions: Gas, Heat and Damage*

The TENDL-2011-15 libraries contain additional diagnostic tables for `MT` values listed in Table II. These reaction diagnostics are included in the `MF`=3 and `MF`=10 file sections together with the reaction cross-section data, and are collapsed in the same way. The primary responses are used to produce secondary responses including rates of gas production, DPA (Displacements Per Atom) and KERMA (Kinetic Energy Release in Materials). These

TABLE I. Neutron induced reactions.

Projectile	Products	MT	ΔZ	ΔA	NSEC	Secondaries
n	total	1	0	0	0	
n	E	2	0	0	0	
n	nonel	3	0	0	0	
n	n	4	0	0	0	
n	O	5			0	
n	2nd	11	−1	−3	1	^{2}H
n	2n	16	0	−1	0	
n	3n	17	0	−2	0	
n	F	18			0	
n	nα	22	−2	−4	1	^{4}He
n	n3α	23	−6	−12	3	^{4}He ^{4}He ^{4}He
n	2nα	24	−2	−5	1	^{4}He
n	3nα	25	−2	−6	1	^{4}He
n	np	28	−1	−1	1	^{1}H
n	n2α	29	−4	−8	2	^{4}He ^{4}He
n	2n2α	30	−4	−9	2	^{4}He ^{4}He
n	nd	32	−1	−2	1	^{2}H
n	nt	33	−1	−3	1	^{3}H
n	nh	34	−2	−3	1	^{3}He
n	nd2α	35	−5	−10	3	^{2}H ^{4}He ^{4}He
n	nt2α	36	−5	−11	3	^{3}H ^{4}He ^{4}He
n	4n	37	0	−3	0	
n	2np	41	−1	−2	1	^{1}H
n	3np	42	−1	−3	1	^{1}H
n	n2p	44	−2	−2	2	^{1}H ^{1}H
n	npα	45	−3	−5	2	^{1}H ^{4}He
n	γ	102	0	1	0	
n	p	103	−1	0	1	^{1}H
n	d	104	−1	−1	1	^{2}H
n	t	105	−1	−2	1	^{3}H
n	h	106	−2	−2	1	^{3}He
n	α	107	−2	−3	1	^{4}He
n	2α	108	−4	−7	2	^{4}He ^{4}He
n	3α	109	−6	−11	3	^{4}He ^{4}He ^{4}He
n	2p	111	−2	−1	2	^{1}H ^{1}H
n	pα	112	−3	−4	2	^{1}H ^{4}He
n	t2α	113	−5	−10	3	^{3}H ^{4}He ^{4}He
n	d2α	114	−5	−9	3	^{2}H ^{4}He ^{4}He
n	pd	115	−2	−2	2	^{1}H ^{2}H
n	pt	116	−2	−3	2	^{1}H ^{3}H
n	dα	117	−3	−5	2	^{2}H ^{4}He
n	5n	152	0	−4	0	
n	6n	153	0	−5	0	
n	2nt	154	−1	−4	1	^{3}H
n	tα	155	−3	−6	2	^{3}H ^{4}He
n	4np	156	−1	−4	1	^{1}H
n	3nd	157	−1	−4	1	^{2}H
n	ndα	158	−3	−6	2	^{2}H ^{4}He
n	2npα	159	−3	−6	2	^{1}H ^{4}He
n	7n	160	0	−6	0	
n	8n	161	0	−7	0	
n	5np	162	−1	−5	1	^{1}H
n	6np	163	−1	−6	1	^{1}H
n	7np	164	−1	−7	1	^{1}H
n	4nα	165	−2	−7	1	^{4}He
n	5nα	166	−2	−8	1	^{4}He
n	6nα	167	−2	−9	1	^{4}He
n	7nα	168	−2	−10	1	^{4}He
n	4nd	169	−1	−5	1	^{2}H
n	5nd	170	−1	−6	1	^{2}H
n	6nd	171	−1	−7	1	^{2}H
n	3nt	172	−1	−5	1	^{3}H
n	4nt	173	−1	−6	1	^{3}H
n	5nt	174	−1	−7	1	^{3}H
n	6nt	175	−1	−8	1	^{3}H
n	2nh	176	−2	−4	1	^{3}He
n	3nh	177	−2	−5	1	^{3}He
n	4nh	178	−2	−6	1	^{3}He
n	3n2p	179	−2	−4	2	^{1}H ^{1}H
n	3n2α	180	−4	−10	2	^{4}He ^{4}He
n	3npα	181	−3	−7	2	^{1}H ^{4}He
n	dt	182	−2	−4	2	^{2}H ^{3}H
n	npd	183	−2	−3	2	^{1}H ^{2}H
n	npt	184	−2	−4	2	^{1}H ^{3}H
n	ndt	185	−2	−5	2	^{2}H ^{3}H
n	nph	186	−3	−4	2	^{1}H ^{3}He
n	ndh	187	−3	−5	2	^{2}H ^{3}He
n	nth	188	−3	−6	2	^{3}H ^{3}He
n	ntα	189	−3	−7	2	^{3}H ^{4}He
n	2n2p	190	−2	−3	2	^{1}H ^{1}H
n	ph	191	−3	−3	2	^{1}H ^{3}He
n	dh	192	−3	−4	2	^{2}H ^{3}He
n	hα	193	−4	−6	2	^{3}He ^{4}He
n	4n2p	194	−2	−5	2	^{1}H ^{1}H
n	4n2α	195	−4	−11	2	^{4}He ^{4}He
n	4npα	196	−3	−8	2	^{1}H ^{4}He
n	3p	197	−3	−2	3	^{1}H ^{1}H ^{1}H
n	n3p	198	−3	−3	3	^{1}H ^{1}H ^{1}H
n	3n2pα	199	−4	−8	3	^{1}H ^{1}H ^{4}He
n	5n2p	200	−2	−6	2	^{1}H ^{1}H

are of value in the design and assessment of nuclear devices. For MT ={201–207}, the z denotes any projectile (γ, n, d, p, α) and X is a positive integer.

The method of evaluation of the gas production, DPA and KERMA coefficients is described in Section III D.

2. *Miscellaneous Reactions*

The new ENDF-style libraries of total or partial cross-section data may contain MT values not included in Tables I and II. Data for the MT numbers shown in Table III are silently ignored. Data for any other MT encountered cause warning messages to be issued.

TABLE II. `MT` numbers for gas production, DPA and KERMA.

`MT`	Description
201	(z,Xn) Total neutron production
202	(z,Xγ) Total gamma production
203	(z,Xp) Total proton production
204	(z,Xd) Total deuteron production
205	(z,Xt) Total triton production
206	(z,Xh) Total helion (^{3}He) production
207	(z,Xα) Total alpha particle production
301	Kerma total (eV-barns)
302	Kerma elastic
303	Kerma non-elastic (all but `MT`=2)
304	Kerma inelastic (`MT`={51-91})
318	Kerma fission (`MT`=18 or `MT`= {19, 20, 21, 38})
401	Kerma disappearance (`MT`={102-120})
402	Kerma for radiative capture
403	Kerma for proton emission
407	Kerma for alpha emission
442	Total photon (eV-barns)
443	Total kinematic kerma (high limit)
444	Dpa total (eV-barns)
445	Dpa elastic (`MT`=2)
446	Dpa inelastic (`MT`={51-91})
447	Dpa disappearance (`MT`={102-120})

TABLE III. Additional `MT` numbers for reactions that are silently ignored.

`MT`	Description
19	(n,f) First chance fission reaction
20	(n,nf) Second chance fission reaction
21	(n,2nf) Third chance fission reaction
38	(n,3nf) Fourth chance fission reaction
46–101	(z,n$_i$) Neutron production with residuals in excited states
110	Unassigned
118–150	Various multiple-emission reactions
219–253	Various
600–849	Various partial reactions
851–859	Lumped reaction covariances
875–891	Various double neutron productions

C. Reaction Data Collapse

The reaction data input to FISPACT-II are the projectile flux spectrum, multi-group reaction cross sections, reaction diagnostics, induced fission yields and covariances. These are tabulated in energy groups, where in general the cross-section data are tabulated in a much finer group structure than the fission yield or covariance data. These data are 'collapsed' using flux spectrum weighting into energy independent values for use in the inventory calculations.

Consider the collapsed cross section $\bar{X}$ and its uncertainty Δ that are used in FISPACT-II. The input data for $\bar{X}$ are cross sections X_i from the `xs_endf` data stream and the projectile flux ϕ_i from file `fluxes` in energy groups $i \in [1, N]$. ϕ_i is the flux (cm^{-2}s^{-1}) in energy range E_i to E_{i+1}, and we use it to define the weight for group i as

$$W_i = \phi_i / \sum_{i=1}^{N} \phi_i \,. \tag{1}$$

The collapsed cross section $\bar{X}$ is given by

$$\bar{X} = \sum_{i=1}^{N} W_i X_i \,. \tag{2}$$

Covariances for cross sections X_i and Y_j grouped in energy bins $i \in [1, N_X]$, $j \in [1, N_Y]$ are $Cov(X_i, Y_j)$. The collapsed covariance arising from these is given by

$$Cov(\bar{X}, \bar{Y}) = \sum_{i=1}^{N_X} \sum_{j=1}^{N_Y} W_i W_j Cov(X_i, Y_j) \,. \tag{3}$$

$Cov(\bar{X}, \bar{Y})$ where X and Y are distinct channels is a functionality which cannot be currently exploited due to the lack of available data in the nuclear data files, but is planned to be used in future Monte-Carlo sensitivity calculations. The case of interest at present is that where reactions X and Y are the same, and then the collapsed variance is given by

$$var = Cov(\bar{X}, \bar{X}) = \sum_{i,j=1}^{N} W_i W_j Cov(X_i, X_j) \,. \tag{4}$$

For EAF data, the uncertainty is defined at the three standard deviation point:

$$\Delta = 3\sqrt{var}/\bar{X} \,. \tag{5}$$

and for ENDF data, it is defined as

$$\Delta = \sqrt{var}/\bar{X} \,. \tag{6}$$

The covariance data are typically less complete than the cross-section data. Each covariance data energy group contains several cross-section energy groups, and in some cases the data in different energy groups are assumed to be uncorrelated. The covariance data in the EAF and TENDL-2011-15 libraries that FISPACT-II recognises are the ENDF [2] NI-type data with LB=1, 5, 6 or 8. The projection operator S_i^k maps cross-section energy bins to covariance energy bins as illustrated in Fig. 4, where the projection operator S_i^k is

$$S_i^k = \begin{cases} 1 & \text{bin i in bin k} \\ 0 & \text{otherwise} \end{cases} \,. \tag{7}$$

Using S_i^k, the formula used to construct estimates of the covariance matrix from the library data are respec-

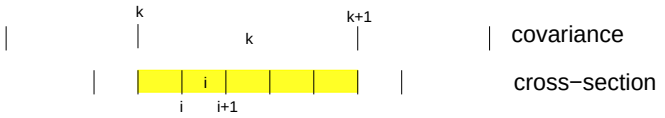

FIG. 4. (Color online) Projection operator S_i^k maps cross-section energy bins to covariance energy bins. The shaded energy bins have $S_i^k = 1$, and all others have $S_i^k = 0$.

tively for LB = 1, 5, 6, and 8 are

$$Cov(X_i, X_j) = \sum_{k=1}^{M} S_i^k S_j^k F_k X_i X_j \quad (8)$$

$$Cov(X_i, Y_j) = \sum_{k=1}^{M} \sum_{k'=1}^{M} S_i^k S_j^{k'} F_{kk'} X_i Y_j \quad (9)$$

$$Cov(X_i, Y_j) = \sum_{k=1}^{M} \sum_{k'=1}^{M'} S_i^k S_j^{k'} F_{kk'} X_i Y_j \quad (10)$$

$$Cov(X_i, X_j) = \sum_{k=1}^{M} S_i^k S_j^k 1000 F_k \quad (Koning) \quad (11)$$

$$(or = \sum_{k=1}^{M} S_i^k \delta_{ij} 1000 F_k)\,. \quad (12)$$

The LB=1 case (Eq. (8)) is the one that applies to the computation of uncertainty for the EAF data. Covariances are described by a fraction for each k bin and the different k bins are assumed to be uncorrelated.

The LB = 5, 6, and 8 cases appear in the TENDL-2011-15 libraries. The LB = 5 data for X and Y referring to the same reaction are used to compute the uncertainty, and are assumed to have LS=0. The LB = 6 data give cross-correlations between collapsed cross sections. These are read but not used in the present version of the code. The LB = 8 data are produced from the same source as the LB = 5 data for $X = Y$, with some of the cross-correlations ignored, and use definitions different from those in the ENDF manual [2]. FISPACT-II reads and discards these data.

D. Self-Shielding using Probability Tables

Keywords in the FISPACT-II `input` file may be used to cause probability table sub-group data generated by CALENDF [10, 14] to be used to model dilution effects in the computation of the collapsed effective cross sections. CALENDF provides data in five sets of macro-partial cross sections; the CALENDF set macro-`MT` numbers (cal-mt) are defined in Table IV. The sum of these macro-partial cross sections gives the total cross section in each energy group over the resonance regions covered.

The data provided by CALENDF are effective cross-section σ and probability values P depending on four parameters,

$$\sigma(x, n) \equiv \sigma(p, g, x, n) \quad (13)$$

$$P(x, n) \equiv P(p, g, x, n)\,, \quad (14)$$

where
p = parent nuclide number,
g = energy group number,
x = macro-partial (or total) index, and
n = Gaussian quadrature index.

In the expressions below, we suppress the explicit display of dependence of cross section on the parent nuclide p and energy group g except in the formulae for dilution. The infinite dilution ($d = \infty$) cross section for a given parent, energy group and component is

$$\sigma(x, d = \infty) = \frac{1}{E_{max} - E_{min}} \int_{E_{min}}^{E_{max}} \sigma(E)\, dE = \sum_{n=1}^{N} P(x, n)\sigma(x, n)\,. \quad (15)$$

When a nuclide is a part of a homogenous mixture of nuclides, then the effective cross sections in the resonance regions are reduced, and are parameterised using the dilution cross section d [10, 15–17],

$$\sigma(x, d) = \frac{\sum_{n=1}^{N} P(x, n)\sigma(x, n)/(\sigma_t(n) + d)}{\sum_{n=1}^{N} P(x, n)/(\sigma_t(n) + d)}\,, \quad (16)$$

where the total cross section is given by the sum of the macro-partials,

$$\sigma_t(n) = \sum_{x=1}^{X} \sigma(x, n)\,. \quad (17)$$

The total cross section for nuclide p in energy group g at dilution d is given by

$$\sigma^{tot}(d) = \sum_{x=1}^{X} \sigma(x, d_p)\,. \quad (18)$$

The probability table data from CALENDF are used in conjunction with the 709 and 1102 group data in the TENDL library, as well as the 616 energy group data of the legacy EAF library. In the following discussion,

TABLE IV. CALENDF macro-`MT` number.

cal-mt	Description	`MT` in set
2	elastic scattering	2
101	absorption (no outgoing neutron)	102 103 107
18	fission total	18
4	inelastic scattering (emitting one neutron)	4 11
15	multiple neutron production (excluding fission)	5 16 17 37

we use the term 'library' or 'LIB' to refer to either the TENDL or alternative ENDF-6 forms as appropriate. The dilution computed using the CALENDF data is applied either as scaling factors to the library cross-section data or as replacements over the energy ranges for which the probability table data are available. (This is selected by user input). If the CALENDF and library data were fully self-consistent, then the same self-shielding would be obtained for scaling and for replacement, but the absence of elastic scattering cross section in the EAF data leads to some differences. For both the scaling or replacement approach, partial or total scaling may be selected by user input.

a. Scaling applied to LIB data: Scaling is applied to the library data in one of two ways depending on user input. If the partial self-shielding scaling factor option is chosen, then the cross section for nuclide p in energy group g and for `MT` value y belonging to the macro-partial group x is scaled according to

$$\sigma^{new}(y,d) = \sigma^{LIB}(y)\left(\frac{\sigma(x,d)}{\sigma(x,d=\infty)}\right) \tag{19}$$

and for the total scaling factor

$$\sigma^{new}(y,d) = \sigma^{LIB}(y)\left(\frac{\sigma^{tot}(d)}{\sigma^{tot}(d=\infty)}\right). \tag{20}$$

The dilution $d(p,g)$ for a given nuclide p and energy group g is computed using a weighted sum over all the nuclides, $q \in [1,Q]$ in the mixture. The fraction of nuclide q in the mixture is f_q. Nuclides in the mixture may or may not be included in the list of nuclides to which the self-shielding correction is to be applied. Nuclides to which self-shielding corrections are applied must be in the mixture list. The first approximation is given using the total cross sections from the cross-section library as

$$d^{(0)}(p,g) = \sum_{\substack{q=1\\p\neq q}}^{Q} \frac{f_q \sigma^{LIB-tot}(q,g)}{f_p}, \tag{21}$$

where

$$\sigma^{LIB-tot}(p,g) = \sum_{y} \sigma^{LIB}(p,g,y). \tag{22}$$

Over the energy range for which the probability table data are available for those nuclides in the mixture for which self-shielding corrections are being applied, the approximation given by Eq. (21) is iteratively refined using

$$\begin{aligned} S^{(i)}(g) &= \sum_{q=1}^{Q} f_q \sigma^{LIB-tot}(q,g) \times \\ &\left(\frac{\sigma^{tot}(q,g,d^{(i)}(q,g))}{\sigma^{tot}(q,g,\infty)}\right) \end{aligned} \tag{23}$$

$$\begin{aligned} d^{(i+1)}(p,g) &= \frac{S^{(i)}(g)}{f_p} - \sigma^{LIB-tot}(p,g) \times \\ &\left(\frac{\sigma^{tot}(p,g,d^{(i)}(p,g))}{\sigma^{tot}(p,g,\infty)}\right). \end{aligned} \tag{24}$$

b. Replacement of LIB data: If there is only one reaction `MT` in the CALENDF macro-partial group, then the replacement formulae would be given by replacing the σ^{LIB} values in the above equations by the infinite dilution cross sections obtained from the CALENDF data. When there is more than one reaction in the macro-partial set, then the dilution effect has to be apportioned according to the LIB reaction cross sections.

If the partial self-shielding scaling factor option is chosen, then the cross section for nuclide p in energy group g and for `MT` value y belonging to the macro-partial group x is given by

$$\sigma^{new}(y,d_p) = \sigma(x,d_p)\left(\frac{\sigma^{LIB}(y)}{\sum_{y'\in x}\sigma^{LIB}(y')}\right) \tag{25}$$

and for the total scaling factor

$$\begin{aligned} \sigma^{new}(y,d_p) &= \sigma(x,\infty)\left(\frac{\sigma^{LIB}(y)}{\sum_{y'\in x}\sigma^{LIB}(y')}\right) \times \\ &\left(\frac{\sigma^{tot}(d_p)}{\sigma^{tot}(\infty)}\right). \end{aligned} \tag{26}$$

The initial values of the dilutions are given by Eqs (21) and (22) and the iterative refinements where CALENDF probability table data are available are given by

$$S^{(i)}(g) = \sum_{q=1}^{Q} f_q \sigma^{tot}(q,g,d^{(i)}(q,g)) \tag{27}$$

$$d^{(i+1)}(p,g) = \frac{S^{(i)}(g)}{f_p} - \sigma^{tot}(p,g,d_p^{(i)}). \tag{28}$$

The set of nuclides for which the self-shielding correction is calculated and the set of nuclides included in the mixture for computing the dilution cross section is specified user input. User input also allows the values of dilution given by Eq. (24) or (28) to be overridden by user-supplied dilution values.

The default method of computing self-shielding using the probability table method is to use Eqs (21) and (22) for initial values, Eq. (25) for cross section and iterate dilution using Eqs (27) and (28). When the iteration is complete, the new collapsed cross sections are computed by applying the ssf to produce the effective cross

sections. The effective self-shielding factor ssf for the collapsed cross section is given by

$$ssf(p,y) = \frac{\sigma^{new}(p,y)}{\sigma^{LIB}(p,y)}\,. \tag{29}$$

The self-shielding factors may be applied wherever probability table data are provided and can be used to correct specific sets of reaction rates for desired nuclides, for example the energy-dependent self-shielding factors applied to the ^{238}U neutron capture in a typical PWR spectrum and fresh fuel composition, which is shown in Fig. 5. These can be updated during irradiation, accommodating changes in both nuclide inventory and spectra to alter the dilutions and reaction rates, respectively.

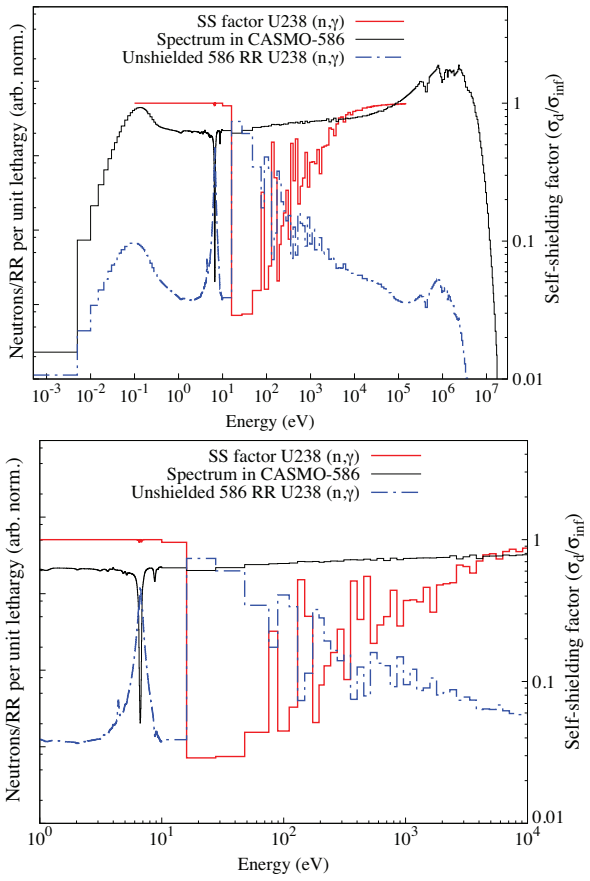

FIG. 5. (Color online) Neutron spectrum, the unshielded ^{238}U(n, γ) cross section and the energy-dependent probability table self-shielding factors calculated for the fresh fuel composition in FISPACT-IIusing ENDF/B-VII.1. Global and zoomed-in plots are provided. The integrated self-shielding factor for this cross section is 0.18.

E. Self-Shielding using the Universal Curve Model

FISPACT-II provides a second method of accounting for self shielding in thick targets with a variety of geometries. This can be used as an alternative to the probability table method described in the previous section which is appropriate for geometry relevant self-shielding effects. It is not possible to use both descriptions of self shielding simultaneously.

In a series of papers [18–20], the authors Martinho, Gonçalves and Salgado described a "universal sigmoid curve" model of self shielding to account for the reduction of the neutron flux by cross section resonances in the context of neutron activation analysis. They based their development on earlier experimental and theoretical work by Baumann [21].

The Martinho et al [18] model initially described the effect of a single resonance peak in a pure target consisting of a single nuclide. The self-shielding factor G_{res} is approximated as a simple function of a single dimensionless length parameter that depends on the physical size and shape of the target as well as the peak cross section at the resonance and the resonance widths for elastic scattering and radiative capture. The final form of the model [20] accommodates a group of isolated resonances of a pure target, and the target geometry could be a foil, wire, sphere or cylinder of finite height. This model has been generalised further and applied to the mixture of nuclides required for a FISPACT-II calculation.

FISPACT-II user input invokes this model of self shielding and defines the type and dimensions of the target, as detailed in Table V.

TABLE V. Target geometry recognised by FISPACT-II.

ID	Type	Dimension(s)	Effective length (y)
1	foil	thickness (t)	$y = 1.5t$
2	wire	radius (r)	$y = 2r$
3	sphere	radius (r)	$y = r$
4	cylinder	radius (r), height (h)	$y = 1.65rh/(r+h)$

The initial form of the model [18] that accounts for the effect of a single resonance in a pure target containing a single nuclide defines a dimensionless parameter,

$$z = \Sigma_{tot}(E_{res})y\sqrt{\frac{\Gamma_\gamma}{\Gamma}}, \tag{30}$$

that depends on the physical length y, the macroscopic cross section $\Sigma_{tot}(E_{res})$ at the energy E_{res} of the resonance peak, the resonance width Γ_γ for radiative capture and the total resonance width Γ. Then the self-shielding factor is

$$G_{res}(z) = \frac{A_1 - A_2}{1 + (z/z_0)^p} + A_2 \tag{31}$$

where the parameters defining this "universal sigmoid curve" are

$$A_1 = 1.000 \pm 0.005\,, \tag{32}$$
$$A_2 = 0.060 \pm 0.011\,, \tag{33}$$
$$z_0 = 2.70 \pm 0.09\,, \tag{34}$$
$$p = 0.82 \pm 0.02\,. \tag{35}$$

These parameters were determined empirically by Martinho et al [18] by fitting to a set of points generated by performing Monte-Carlo simulations with the MCNP code for a variety of targets of different shapes, sizes and compositions. Six nuclides that exhibit strong resonances were used individually, not as mixtures.

The model was then extended by Martinho et al [19], who defined an effective length y for cylinders of finite height, but a more significant extension was provided by Salgado et al [20], who defined an average $\langle G_{res}\rangle$ by assigning weights to each resonance and forming an average of the individual G_{res} factors calculated for each resonance individually. The weight of resonance i is

$$w_i = \left(\frac{\Gamma_\gamma}{E_{res}^2}\cdot\frac{g\Gamma_n}{\Gamma}\right)_i , \tag{36}$$

where

Γ_n is the neutron scattering width;

g is the statistical factor, $(2J+1)/(2(2I+1))$;

J is the spin of the resonance state;

I is the spin of the target nucleus.

Then the effective self-shielding factor is

$$\langle G_{res}\rangle = \frac{\sum_i w_i G_{res}(z_i)}{\sum_i w_i} . \tag{37}$$

where each z_i is calculated from Eq. (30) using the effective length of the target, y and the resonance parameters for resonance i.

This model has been generalised further in two ways to make it suitable for application in FISPACT-II.

First, the average self-shielding factor is computed from the resonance parameters given in the resolved resonance range defined in the ENDF `MF=2` data for a subset of the nuclides selected by user input. It is assumed that the resonances for the mixture of nuclides are separated in energy sufficiently for them not to overlap significantly.

Note that the TENDL data use a unique approach to create parameters for resolved statistical resonances for a large number of isotopes that did not have any. This method invokes global average parameters from the different systematics and from the TALYS reaction code [22]. These parameters are then used by either the CALENDF code or by the R-matrix code AVEFIT. Statistical resonance parameters are then obtained from zero up to the first excited level, reflecting the average resonance parameters coming from compound model calculations. Above the first inelastic level, grouped inelastic cross sections with local fluctuations are obtained. This method complements the measured resonance parameters, or provides a resolved resonance range when measurements do not exist. In between these two cases, statistical resonance parameters are adjusted to integral measurements when available. This method, which has been successfully applied to all isotopes living longer than one second, has been used to populate the resonance ranges of the TENDL libraries [23].

The cross section at a resonance peak is not supplied in the ENDF data. The simple expression provided by Fröhner [Eq. (186)][24] is used to supply this information.

Secondly, $\langle G_{res}\rangle$ is made energy dependent by taking averages separately for each energy bin used for the group-wise cross sections, including only those resonances with peaks in the relevant energy bin. Then this array of energy-dependent self-shielding factors is applied to each energy-dependent cross section before the cross section collapse.

The principle underlying this model of self shielding is that the resonances perturb the spectrum of the applied neutron flux. Consequently, the self shielding factors should modify the cross sections for all reactions. Note that the effect of self shielding varies from reaction to reaction because of the differing energy dependencies of the cross sections.

F. Decay Data

FISPACT-II reads the `MF=8`, `MT=457` decay data from the ENDF library decay files. Table VI lists the decay modes that the code recognises. The index `IRT` is the index used in the code. The index `RTYP` is the ENDF-6 reaction type code used for reaction product code `MT` = 457 [2, Sec. 8.3, 8.5]. The table also includes two unused `IRT` codes and another to indicate an unknown decay mode, so the maximum `IRT` is 27. The decay constant λ_{ij} appearing in Eq. (52) is the sum of the decay constants for the transmutation of nuclide j to i. In terms of the directed graph, the 'edge', or connection between two nuclides, shown in Fig. 9 corresponds to the combination of a subset of the possible decay edges from j to i (cf. Eqs (61)–(64)).

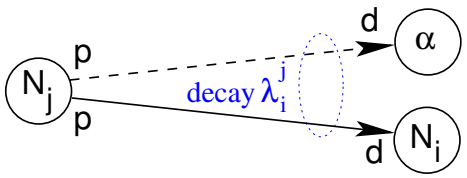

FIG. 6. (Color online) Decay processes (e.g., α-decay) may produce secondary gas nuclides that are included in the inventory calculation.

Some of the decay modes listed in Table VI have secondary gas nuclides that are included in the inventory calculation. The number of these is given by `NSEC` and their species are included in the right hand column of the table. This is illustrated in Fig. 6. The primary reaction leads to a secondary edge in the directed graph, and other products from these decays are regarded as debris that is ignored. When there are gas nuclide secondaries, then a secondary edge from nuclide j to the gas nuclide is associated with the decay from j to i. There may be 0, 1, 2 or 3 secondaries associated with a decay type; see

TABLE VI. Decay Types (MF=8, MT=457) recognised by the code. The column labelled 'Code' is the description used in output from FISPACT-II, NSEC is the number of secondaries and 'Secs' is an abbreviation for 'Secondaries'.

IRT	RTYP	Description	ΔZ	ΔA	Code	NSEC	Secs
1	1	β^- decay	1	0	b-	0	
2	2	β^+ decay or electron capture	−1	0	b+	0	
3	3	isomeric transition (IT)	0	0	IT	0	
4	4	α decay	−2	−4	a	1	^{4}He
5	5	neutron emission	0	−1	n	0	
6	6	spontaneous fission (SF)	−999	−999	SF	0	
7	7	proton emission	−1	−1	p	1	^{1}H
8	8	not used	0	0	0		
9	9	not used	0	0	0		
10	10	unknown	0	0	0		
11	1.5	β^- decay + neutron emission	1	−1	b-n	0	
12	1.4	β^- decay + α emission	−1	−4	b-a	1	^{4}He
13	2.4	β^+ decay + α emission	−3	−4	b+a	1	^{4}He
14	2.7	β^+ decay + proton emission	−2	−1	b+p	1	^{1}H
15	3.4	IT followed by α emission	−2	−4	IT+a	1	^{4}He
16	1.1	double β^- decay	2	0	b-b-	0	
17	1.6	β^- decay followed by SF	−999	−999	b-SF	0	
18	7.7	double proton emission	−2	−2	pp	2	^{1}H ^{1}H
19	2.2	double β^+ or electron capture	−2	0	b+b+	0	
20	1.55	β^- and double neutron emission	1	−2	b-2n	0	
21	1.555	β^- and triple neutron emission	1	−3	b-3n	0	
22	1.5555	β^- and quadruple neutron emission	1	−4	b-4n	0	
23	5.5	double neutron emission	0	−2	2n	0	
24	5.55	triple neutron emission	0	−3	3n	0	
25	2.77	β^+ decay + double proton emission	−3	−2	b+2p	2	^{1}H ^{1}H
26	2.777	β^+ decay + triple proton emission	−4	−3	b+3p	3	^{1}H ^{1}H ^{1}H
27	2.6	β^+ decay followed by SF	−999	−999	b+SF	0	

Table VI for details.

By default, FISPACT-II will not follow the yields of spontaneous fission processes. However, if spontaneous fission yield ENDF-6 data (MF=8, MT=454 or 459) for the yield fractions are available, then they can be read and used as shown in Eq. (64).

TABLE VII. Decay Radiation Types (MF=8, MT=457) recognised by FISPACT-II The column headed 'Code' is the description used in output from FISPACT-II.

STYP	Radiation Type		Code
0	γ	gamma rays	gamma
1	β^-	beta rays	beta
2	ec,(β^+)	electron capture and/or positron emission	ec, beta+
3		not known	not known
4	α	alpha particles	alpha
5	n	neutrons	n
6	SF	spontaneous fission fragments	SF
7	p	protons	p
8	e^-	discrete electrons	e-
9	x	X-rays and annihilation radiation	x

1. *Decay Radiation Spectra*

The decay radiation types recognised by FISPACT-II are listed in Table VII. FISPACT-II reads from the MF=8 MT=457 sections of the ENDF decay files the information on radiation resulting from the decay and extracts the following information for use in diagnostic output from activation calculations:

a. Decay heating The average decay energies for light particles, electromagnetic radiation and heavy particles are read and stored for use respectively in the calculation of beta, gamma and alpha decay heating powers in FISPACT-II inventory calculations (cf. Section II L).

b. Gamma spectrum Discrete gamma and X-ray spectral lines (STYP= 0 or 9) are read and optionally stored. These are used to create 22- or 24-group histogram spectra by nearest grid point binning of the intensities of discrete gamma and X-ray lines. Energy bins used are listed in Table VIII. Each spectral line is characterised by an energy er, in eV, a relative intensity ri and a normalisation fd. If bin i lies between energies $E(i)$ and $E(i+1)$, and $E(i) \leq er < E(i+1)$, then the contribution of the line to the spectrum in bin i is $(fd \times er \times ri)$ eV. The spectrum for the nuclide is the sum of all lines from all its decay modes.

Section II G describes how these spectra are used in

predicting gamma doses. In cases where spectral line data are not available, then approximate spectra may optionally be used (cf. Section II G 3).

TABLE VIII. Spectrum energy bins and their energy ranges.

24 groups		22 Groups	
Bin	Range (MeV)	Bin	Range (MeV)
1	0.00–0.01	1	0.00–0.01
2	0.01–0.02	2	0.01–0.10
3	0.02–0.05	3	0.10–0.20
4	0.05–0.10	4	0.20–0.40
5	0.10–0.20	5	0.40–1.00
6	0.20–0.30	6	1.00–1.50
7	0.30–0.40	7	1.50–2.00
8	0.40–0.60	8	2.00–2.50
9	0.60–0.80	9	2.50–3.00
10	0.80–1.00	10	3.00–3.50
11	1.00–1.22	11	3.50–4.00
12	1.22–1.44	12	4.00–4.50
13	1.44–1.66	13	4.50–5.00
14	1.66–2.00	14	5.00–5.50
15	2.00–2.50	15	5.50–6.00
16	2.50–3.00	16	6.00–6.50
17	3.00–4.00	17	6.50–7.00
18	4.00–5.00	18	7.00–7.50
19	5.00–6.50	19	7.50–8.00
20	6.50–8.00	20	8.00–10.00
21	8.00–10.00	21	10.00–12.00
22	10.00–12.00	22	12.00–14.00
23	12.00–14.00		
24	>14.00		

c. Spontaneous fission neutron yield The spontaneous fission neutron yields (`IRT`=6, 17 or 27, `STYP`=5) are accumulated using the decay yields contained in the fd field of the decay radiation lists.

G. Gamma Radiation

In addition to the activity of irradiated materials, another measure of acceptability is the dose rate from emitted γ rays. FISPACT-II provides two approximate estimates of the γ dose rate due to irradiation by neutrons: contact dose from the surface of a semi-infinite slab or dose at a given distance from a point source. For both measures, the contribution of high-energy β-particle bremsstrahlung to the total dose rate can be significant, and a keyword in the `input` file may be used to activate its output. The formulae used for these are given in the following sub-subsections.

1. Contact Gamma-Dose Rate

Equation (38) shows the formula used to calculate the γ dose rate at the surface of a semi-infinite slab of material. It is taken from Jaeger [25]:

$$D = C\frac{B}{2}\sum_{i=1}^{N_\gamma}\frac{\mu_a(E_i)}{\mu_m(E_i)}S_\gamma(E_i)\,, \tag{38}$$

where

D = surface γ dose rate (Sv h^{-1})

N_γ = number of spectrum energy bins

E_i = mean energy of the i-th bin (cf. Table VIII)

μ_a = mass energy absorption coefficient (μ_{en}/ρ) of air (m^2 kg^{-1})

μ_m = mass energy attenuation coefficient (μ/ρ) of the material (m^2 kg^{-1})

B = build up factor (= 2)

S_γ = rate of γ emission (MeV kg^{-1} s^{-1})

$C = 3.6\times10^9|e|$ converts (MeV kg^{-1} s^{-1}) to (Sv h^{-1})

The library file `absorp` (see Section III G) contains μ/ρ [cm^2 g^{-1}] for all elements in increasing Z order, μ [m^{-1}] and μ_{en}/ρ [cm^2 g^{-1}] for air and the mean energies of the 24-group structure.

The value of μ_m for the material is calculated from the elemental values μ_{mj} provided by the `absorp` data file using

$$\mu_m = \sum_j f_j\mu_{mj}\,, \tag{39}$$

where f_j = (mass of element j)/(total mass).

The value of the emission rate S_γ is calculated using

$$S_\gamma(E_i) = I_iA(t)\,, \tag{40}$$

where I_i is the intensity of energy group i (MeV) and $A(t)$ is the specific activity of material at time t (Bq kg^{-1}). If discrete spectral line data are available, then I_i is obtained by summing the contributions from spectral lines in energy group i read from the `decay` data files. If data are not available, then an approximate value may be computed as described below in Section II G 3.

2. Gamma Dose Rate from Point Source

Equation (41) shows the standard formula (taken from Ref. [25]) for calculation of the dose rate from a point source in air,

$$D = C\sum_{i=1}^{N_\gamma}\frac{\mu_a}{4\pi r^2}e^{-\mu(E_i)r}m_sS_\gamma(E_i)\,, \tag{41}$$

where C, N_γ, μ_a, S_γ are as defined above for Eq. (38), and

m_s = mass of source (kg)

r = distance from source (m)

$\mu(E_i)$ = energy attenuation coefficient of air (m^{-1})

Both Eqs (38) and (41) are approximations suitable for FISPACT-II calculations, but it should be noted that they may not be adequate for specific health physics problems.

3. *Approximate Gamma Spectrum*

Wherever possible ENDF decay data have been used to construct the decay data library (cf. Section III E) used with FISPACT-II. Intensity in a spectrum energy group is computed from the sum of intensities of discrete spectral lines lying in the energy group as described in Section II F 1 b. However, for some unstable nuclides the file contains only the average γ energy; no data for the γ spectrum are available. Without the γ spectrum FISPACT-II is unable to calculate the γ dose rate contribution for these nuclides. In order to check if any of these nuclides are likely to contribute significantly to the total dose rate, the following method is used to calculate an approximate spectrum if selected by user input.

The maximum γ energies (E_m) for decays assumed in the method are given in Table IX.

TABLE IX. Maximum γ energies for various decay modes.

Decay mode	E_m
β^-	$2\langle\beta\rangle$
β^+	5 MeV
α	0
Isomeric transition	$\langle\gamma\rangle$

The intensity in the i-th group (I_i) is given by

$$I_i = \frac{a\langle\gamma\rangle}{E_m}\left(\frac{e^{-a\eta_{i-1}} - e^{-a\eta_i}}{1-(1+a)e^{-a}}\right), \quad (42)$$

where

$a = 14$ (arbitrary constant)

$\eta_i = E_i/E_m$

Gamma doses for approximate spectra are found using the intensity from Eq. (42) to find the emission rate (Eq. (40)), and then using this rate in Eq. (38) or (41) as appropriate.

4. *Bremsstrahlung Corrections*

The contribution of high-energy β-particle bremsstrahlung to the total γ dose rate can be significant in cases where the γ emission is small. FISPACT-II uses a similar approach to Jarvis [26] who considers γ emission from a mono-energetic electron.

The energy distribution of γ rays emitted by a mono-energetic electron in a matrix of charge Z is given by

$$dN = \begin{cases} aZ\left(\frac{E_0-E}{E}\right)dE & 0 \le E < E_0 \\ 0 & E \ge E_0 \end{cases}, \quad (43)$$

where

dN = number of γ-rays with energy E (keV)

E_0 = energy of electron (keV)

$a = 2.76 \times 10^{-6}$ (keV^{-1})

Integrating Eq. (43) over the energy bins gives the number of γ-rays associated with that bin.

For $E_0 \ge E_{i+1}$

$$N(i) = aZ[E_0 \log(E_{i+1}/E_i) - (E_{i+1} - E_i)]\,. \quad (44)$$

For $E_{i+1} > E_0 > E_i$

$$N(i) = aZ[E_0 \log(E_0/E_i) - (E_0 - E_i)] \quad (45)$$

and for $E_0 \le E_i$

$$N(i) = 0\,, \quad (46)$$

where E_i and E_{i+1} are the lower and upper energy bounds of group i. The intensity for group i is given by

$$I_i = N(i)(E_i + E_{i+1})/2\,. \quad (47)$$

The bremsstrahlung corrections to gamma doses are found using the intensity from this equation to find the emission rate (Eq. (40)), and then using this rate in Eq. (38) or (41) as appropriate.

The above discussion is valid only for mono-energetic electrons, but it is assumed that the same expressions are valid for the emission of β particles which have a continuous energy distribution if the mean β energy is used for E_0.

The value of Z used in Eqs (43)-(45) is calculated from

$$Z = \sum_j Z_j f_j\,, \quad (48)$$

where Z_j = atomic number of the j-th element and f_j = atomic fraction of the j-th element (i.e., number of atoms of j / total number of atoms).

5. *Bremsstrahlung Candidates*

Only a subset of all the nuclides in the decay library needs to be considered for bremsstrahlung production. Nuclides may make a contribution to the γ dose rate because of bremsstrahlung emission from energetic β particles.

The following criteria are applied by the code to the decay library (Section III E) to give the nuclides displayed in the Bremsstrahlung candidates output table:

- the nuclide is radioactive with a half-life ≥ 0.1 years or in the case of a short-lived nuclide, the half-life of the parent ≥ 0.1 years;
- the nuclide is radioactive with a half-life $\le 5.0\times10^{16}$ years;
- the nuclide has an average β-energy >average γ-energy;
- the nuclide has an average β-energy > 0.145 MeV.

H. Fission

The new TENDL and other ENDF-6 libraries have fission yield data for many nuclides, and these data are tabulated in energy bins in the same manner as for cross sections and covariances. With data available for many nuclides, the fission association and surrogate daughter algorithms, utilised in previous versions, are no longer needed.

The induced fission yield data, like the covariance data, are on coarser energy grids than the flux and cross sections. To collapse the fission yield, the weights are calculated using

$$W_k = \sum_{i=1}^{N} S_i^k \phi_i / \sum_{i=1}^{N} \phi_i \,, \tag{49}$$

where there are $k \in [1, K]$ fission yield energy groups and S_i^k is the projection operator (cf. Fig. 4). The yields are collapsed using

$$Y = \sum_{k=1}^{K} W_k Y_k \,, \tag{50}$$

where the energy dependent yields Y_k are drawn from the files, as from Fig. 7. The variance of the collapsed fission yield is given by

$$var = \sum_{k=1}^{K} (W_k F_k)^2 \,, \tag{51}$$

where F_k are the tabulated 1σ errors in the ENDF file, as shown in Fig 8. The fractional uncertainty is $\Delta = \sqrt{var}/Y$.

The spontaneous fission yield data are read and processed in the similar manner as for induced yield.

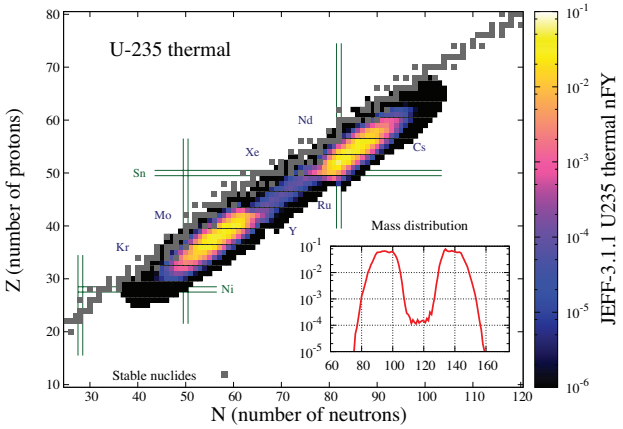

FIG. 7. (Color online) Fission yields from the JEFF-3.1.1 neutron-induced fission yield file, as read and utilised by FISPACT-II when fission is employed.

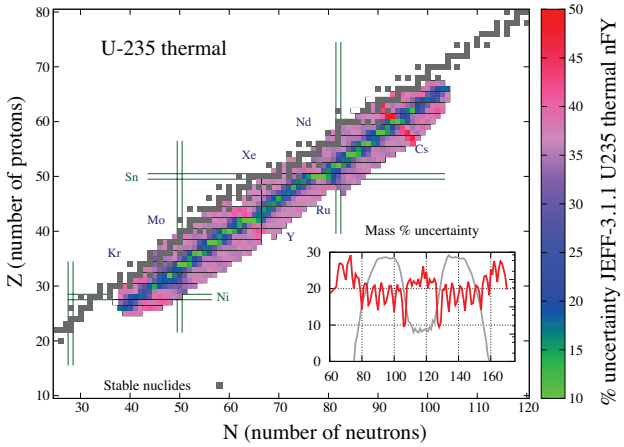

FIG. 8. (Color online) Fission yield uncertainties from the JEFF-3.1.1 neutron-induced fission yield file, as read and utilised by FISPACT-II when fission is employed. Note that since these include no (anti-)correlations, they do not provide a complete, consistent set for uncertainty propagation.

I. The Rate Equations

FISPACT-II follows the evolution of the inventory of nuclides in a target material that is irradiated by a time-dependent projectile flux, where the projectiles may be neutrons, protons, deuterons, α-particles or γ-rays. The material is homogeneous, infinite and infinitely dilute and the description of the evolution of the nuclide numbers is reduced to the stiff-ode set of rate equations [27],

$$\frac{dN_i}{dt} = \sum_j (\lambda_{ij} + \phi^{int}(t)\sigma_{ij}) N_j \,, \tag{52}$$

where

N_i = number of nuclide i at time t
ϕ^{int} = projectile flux (cm^{-2}s^{-1})
for $j \neq i$:
  λ_{ij} = decay constant of nuclide j producing i (s^{-1})
  σ_{ij} = cross section for reactions on j producing i (cm^2)
for $j = i$:
  $\lambda_j = -\lambda_{jj}$ = total decay constant of nuclide j (s^{-1})
  $\sigma_j = -\sigma_{jj}$ = total cross section for j (cm^2), excluding those where the parent and daughter nuclides are the same (cf., Eq. (54)).

The processes described by Eq. (52) may be interpreted in terms of a directed graph, with vertices corresponding to nuclides and edges giving the flow from parent to daughter nuclides via a decay process or an induced reaction. Figure 9 schematically presents a fragment of this graph. Graph theoretic methods are used to construct pathways (see Section V on page 51).

The total flow out from vertex j by decay is equal to

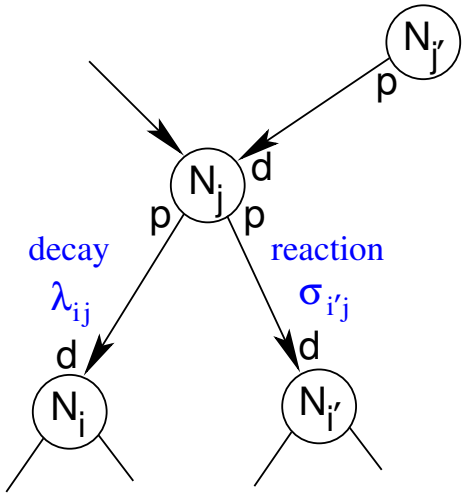

FIG. 9. (Color online) Directed graph representation of reactions and decays: The flow from the parent nuclide at vertex j to the daughter nuclide at vertex i along the directed edge ji is given by the sum of decay and reaction flows.

the total flow into other vertices i:

$$\lambda_j = -\lambda_{jj} = \sum_{i \neq j} \lambda_{ij} \,. \tag{53}$$

Similarly, the balances of the flows by projectile-induced reactions give

$$\sigma_j = -\sigma_{jj} = \sum_{i \neq j} \sigma_{ij} \,, \tag{54}$$

where the sums are over all nuclides.

Nuclides included in the rate equations are specified by a master index read by FISPACT-II. Only nuclides (including stable ones) for which there is a decay data file may be included. Users may change which nuclides are included in their calculations by removing or adding them to their master index. Daughter nuclides from a reaction or decay may or may not be included in the master index. To maintain correct accounting, daughter nuclides not included in the master index are assigned to a fictitious 'sink' nuclide (removing them from the inventory and responses) and secondary decay products are assigned to the appropriate gas nuclides. Similarly, fission products not in the master index are sent to the sink, and if the fragment yields for a fission are not known, then all the products of the fission reaction (or spontaneous fission) are sent to the sink.

Reaction cross sections depend on the projectile energy, and the source data for cross sections give values for a set of energy groups. In the code, an effective ('collapsed') cross section is computed as an average cross section weighted by projectile fluxes in each energy group:

$$\sigma_i^j = \sum_k \tilde{\sigma}_i^j(E_k)\phi_n(E_k) / \sum_k \phi_n(E_k) \,, \tag{55}$$

where $\tilde{\sigma}_i^j(E_k)$ is the cross section at projectile energy group k, $\phi_n(E_k)$ is the integrated projectile flux in energy group k, and the sums are over all energy groups k. See Sections II C and II H for further discussions of data collapse.

A consequence of the modelling assumptions underlying FISPACT-II is that the imposed projectile flux is not modified by the reactions and decays in the target material. It is the responsibility of the user or code which generates the incident-particle spectrum to update this as required. The decay rates and cross sections appearing in Eq. (52) are all independent of the nuclide numbers N_j and the equation can be rewritten compactly as

$$\frac{d\mathbf{N}}{dt} = \mathsf{A}\mathbf{N} = (\mathbf{\Lambda} + \phi\mathbf{\Sigma})\mathbf{N} \,, \tag{56}$$

where the matrix A is independent of the inventory $\mathbf{N}$.

The elements σ_{ij} of cross section matrix $\mathbf{\Sigma}$ are assembled by looping over all reaction `MT` values for parent j and adding contributions (δ) of that collapsed cross section σ_j^{MT}

$$\delta\sigma_{jj} = -\sigma_j^{MT} \tag{57}$$
$$\delta\sigma_{ij} = \sigma_j^{MT} \tag{58}$$
$$\delta\sigma_{kj} = s_k\sigma_j^{MT} \,, \tag{59}$$

where j labels the parent nuclide, i labels the daughter nuclide and k labels the secondary, where the number of secondaries produced is s_k. For fission (`MT`=18), the contribution for fragment i is given by

$$\delta\sigma_{ij} = F_{ij}\sigma_j^{MT} \,, \tag{60}$$

where F_{ij} is the branching fraction. Table I summarises the reaction `MT` values recognised by FISPACT-II for neutron irradiation.

The elements λ_{ij} of the decay constant matrix are similarly assembled by adding contributions from decay constants λ_j^{RTYP} of decay types `RTYP` and parent j,

$$\delta\lambda_{jj} = -\lambda_j^{RTYP} \tag{61}$$
$$\delta\lambda_{ij} = \lambda_j^{RTYP} \tag{62}$$
$$\delta\lambda_{kj} = s_k\lambda_j^{RTYP} \tag{63}$$

and for spontaneous fission (`RTYP`=6)

$$\delta\lambda_{ij} = S_{ij}\lambda_j^{RTYP} \,, \tag{64}$$

where S_{ij} is the spontaneous fission yield fraction from parent j to fission fragment i. Table VI summarises the decay `RTYP` values recognised by FISPACT-II.

In FISPACT-II the projectile flux is constant during each time interval, so that A is also piecewise-constant in time. Furthermore, the matrix A is sparse. Its sparsity pattern gives the adjacency matrix and its components give weighting factors for constructing the directed graphs (digraphs) used for pathway analysis. The full master index for TENDL contains 3875 distinct nuclides

so A has a size of 3876 × 3876, including the 'sink' nuclide. If actinides are not relevant to a calculation, the fission reactions can be omitted and about 150 000 elements of A remain non-zero. This number drops to less than 10 000 during cooling periods when only decays are required. Including the fission of all the actinides in the library increases the number of non-zero elements to almost 480 000 and substantially increases the necessary computer storage and time used in calculating the evolution of the inventory. This is noteworthy as in many codes only a small fraction of the fission products and fission yields for a fraction of the fissionable nuclides are used for simulations. By default, only fission of ^{235}U, ^{238}U and ^{239}Pu are included, in which case there are less than 160 000 non-zero elements. User controls are provided in the input to FISPACT-II to allow fission to be switched off completely or to be included for selected subsets of the actinides in the master index. These properties of the system matrix are relevant to the method of solution described below.

1. *ODE Method of Solution*

The rate equations (56) and subsets of the rate equations used for pathway calculations are all specific examples of first-order systems of differential equations with the general form

$$\frac{dy_i}{dt} = F_i(\{y_j\}, t)\,, \tag{65}$$

with initial conditions

$$y_i(t=0) = y_{i,0} \text{ given}\,, \tag{66}$$

for $1 \le i, j \le N$. These initial value problems can be solved to give $\{y_i(t)\}$ using numerical methods.

The rate equations are linear because of the level of approximation used in FISPACT-II. The matrix A in Eq. (56) is sparse; each reaction or decay typically produces a single principal daughter nuclide and a few secondary products, although fission reactions are an exception. Even with fissions included, less than 3% of the matrix elements of the system matrix A are non-zero, and without fissions this proportion drops to about 0.8%. The very large range of decay rates ensures that all practical FISPACT-II calculations with the full inventory for many applications are always stiff, i.e. the solutions have large fluctuations and many numerical methods are unstable. Thus the key characteristics of the rate equations are that they are linear, stiff and sparse. A well established solver suitable for such equations is the package LSODE [8, 12, 13] written at Lawrence Livermore Laboratory. FISPACT-II uses LSODE as a "black box", and no significant modifications to its internal details have been made. FISPACT-II uses a Fortran 95 module wrapper around LSODE to dynamically allocate its arrays and provide a simpler encapsulated interface for the program.

The stiffness of the system of equations limits the choice of numerical method. LSODE uses the backward differentiation formula method, also known as Gear's method. When the equations are not stiff, other methods are feasible and LSODE can use an implicit Adams method. For simplicity of implementation, FISPACT-II always calls on LSODE to apply Gear's method. The automatic error control (see below) ensures that the results of Gear's method remain accurate, although LSODE may well be more efficient, using fewer internal timesteps if the Adams method had been used instead.

LSODE calculates error estimates for each component of the solution vector, but it uses a single error criterion to control its internal iterations and choices of timestep. By default, this error criterion is based on a weighted root-mean-square average of the individual component error estimates. The weighting is a combination of absolute and relative terms, allowing the possibility of a very small or zero component in the solution. This is appropriate to FISPACT-II, since inventories of interest can involve a vast range of abundances from nuclide to nuclide, commonly with contrasts exceeding a ratio of 10^{20}.

The LSODE solver controls the accuracy of its calculations by refining its internal timesteps to satisfy a criterion placed on its estimate of the error. Estimates are produced separately for each component of the solution vector, but these are combined into a single measure of the error using a root-mean-square norm.

The acceptance criterion is based on the sum of relative and absolute tolerances, so that for the dominant nuclides in a FISPACT-II calculation the error is determined by the chosen `rtol` parameter, while for the minor nuclides the tolerance is relaxed by the addition of the `atol` parameter. This avoids the problems that would occur for a pure relative error estimate in the case of zero or very small inventories.

The solver returns the error estimates of the individual components of the solution vector to its calling program. This information is used in FISPACT-II to flag the nuclides with larger than usual error estimates. The criterion for flagging outlying nuclides is that the estimate should exceed the specified tolerance by a factor of more than the dimensionless error factor which is set in the code to 1.5. Specifically, LSODE computes a vector

$$w_i = rtol\, y_i + atol \tag{67}$$

from the solution vector, where the parameters `rtol` and `atol` may be reset by the user. The weights w_i are used with the local estimates of the component-wise errors, e_i to compute

$$D = \left[\frac{1}{N}\sum_{i=1}^{N}\frac{e_i}{w_i}\right]^{1/2}. \tag{68}$$

D is used as a single measure of acceptability; if $D > 1$ then LSODE refines its internal timesteps until a satisfactory D is obtained.

Users should be aware that LSODE works with local errors. Estimation of the global error is much harder and, in common with many numerical methods, LSODE does not attempt this error estimation. The convergence of FISPACT-II predictions may be tested by re-running with different `rtol` and `atol`.

J. Uncertainty

The pathways, the number of atoms created at target nuclide t due to the reaction and decay chain along path p to that nuclide together with uncertainties in the reaction cross sections and decay half lives associated with the edges of the pathways are used in FISPACT-II to provide estimates of the uncertainties [28]. Pathways arising from a fission are assumed to be correlated and their uncertainties are summed. All other pathway contributions are treated as uncorrelated and are combined in a random walk approximation. The uncertainty contributions from the reactions along the edges of each pathway are also combined using random walks. If only variances of cross sections are known, then the cross sections are assumed to be uncorrelated. If covariance data are known for cross sections, then the independent variables are obtained by diagonalising the covariance matrix. In deriving the formulae used in FISPACT-II it is also assumed that the number of nuclides formed along path p of length n to target nuclide t at time T

$$N_{tp} = N_{10}\left(\prod_{i=1}^{n-1}\beta_i\right)\sum_{i=1}^{n} e^{-\alpha_i T}/\prod_{\substack{j=1\\ j\neq i}}^{n}(\alpha_i-\alpha_j) \quad (69)$$

may be approximated by

$$N_{tp} = C_{tp}\prod_{i=1}^{n-1}\beta_i\,, \quad (70)$$

where C_{tp} is a constant along path p to target t, α_i gives the total rate of decay and induced destruction of a nuclide, and β_i is the rate of decay and transmutation of nuclide i specifically to nuclide $i+1$ (see Eq. (96) and Eq. (97) in Sec. V).

Given a set of target nuclides S_t, then the uncertainty in some radiological quantity $Q = \sum_{t\in S_t} q_t$ is given by ΔQ, where

$$(\Delta Q)^2 = \sum_{t\in S_t}\left(\frac{\Delta N_t}{N_t}\right)^2 q_t^2\,, \quad (71)$$

where q_t may, for example, be activity, gamma dose or some radiotoxicity measure. N_t is the number of atoms of target nuclide t formed from the initial inventory and ΔN_t is the error in N_t. N_t and q_t are known from the inventory calculation. ΔN_t is computed from the pathways inventories and the fractional squared error Δ^2_{tp} in the number of atoms of target nuclide t formed along pathway p to that target.

If we let the set of pathways to target t be S_p, then $S_p = (\cup_{a\in S_{sa}} S_a)\cup S_o$ where S_a is the subset of these pathways that start from the fission of an actinide source nuclide a and S_o is the set of other pathways. S_{sa} is the subset of the set of source nuclides that are actinides.

If all the pathways to a target nuclide t are uncorrelated, then the uncertainty in the inventories along pathways p to t can be combined using a random walk approximation to give an estimate of the uncertainty of the target nuclide inventory ΔN_t as

$$(\Delta N_t)^2 = \sum_p (\Delta N_{tp})^2\,. \quad (72)$$

However, pathways arising from a fission are correlated and so are combined linearly as

$$\Delta N_t = \sum_p \Delta N_{tp}\,. \quad (73)$$

Combining these gives the expression for the total ΔN_t

$$(\Delta N_t)^2 = \sum_{p\in S_o}\Delta N_{tp}^2 + \sum_{a\in S_{sa}}\left(\sum_{p\in S_a}|\Delta N_{tp}|\right)^2\,. \quad (74)$$

If we treat each cross section as independent, then on edge e of a pathway, $\beta_e = \sigma_e = \sum_r \sigma_r$, and so from Eq. (70), the contribution (δ) of reaction r on edge e is

$$\delta\left(\frac{\Delta N_{tp}}{N_{tp}}\right) = \frac{\Delta\sigma_r}{\sigma_e}\,. \quad (75)$$

If there are off-diagonal covariance matrix terms for the cross sections, the independent variables are found by diagonalising the covariance matrix. Let reaction r belong to the set of reactions $\{X_1 \ldots X_D\}$ for a parent where $cov(X_i, X_j)$ are nonzero for $i \neq j$, then we can find a similarity transformation matrix M such that $cov(Y,Y) = M^T cov(X,X) M$ is diagonal with diagonal elements $var(Y)$, and $Y = M^T X$. Components of Y are the independent variables, and from Eq. (70) the contribution to the uncertainty of inventory N_{tp} becomes

$$\delta\left(\frac{\Delta N_{tp}}{N_{tp}}\right) = \frac{M_{i(r)j}\Delta Y_j}{\sigma_e}\,, \quad (76)$$

where the dependence of index i on reaction r is indicated.

Using the random walk assumption and ignoring any off-diagonal covariance matrix terms gives

$$\begin{aligned}\Delta^2_{tp} &= \left(\frac{\Delta N_{tp}}{N_{tp}}\right)^2 \\ &= \sum_{e,r}\left(\frac{\Delta\sigma_r}{\sigma_e}\right)^2 + \sum_{e\in D_e}\left(\frac{\Delta\tau_j}{\tau_e}\right)^2\,,\end{aligned} \quad (77)$$

where the first sum is over all edges e on each pathway p, all reactions r on each edge and over all $\Delta Y_j = \sqrt{var(Y_j)}$ from the diagonalised covariance matrix for reaction r.

The second term gives the contribution of decay constant uncertainties and is summed over the set of edges. Equation (77) is generalised to handle multi-pulse irradiation scenarios by replacing the first term by

$$\sum_{e,r} \left(\frac{R_r(\Delta\sigma_r/\sigma_r)}{R_e} \right)^2 ,$$

where R_r and R_e are respectively the pulse averaged reaction rates of reaction r and the pulse averaged reaction rate on edge e.

In FISPACT-II, the pulse averaged fractional squared errors Δ^2_{tp} are precomputed from the nuclear data and are used in conjunction with values of N_{tp} from pathways calculations and with q_t and N_t from the main inventory calculation to provide error estimates for all cooling steps of the calculation.

K. Monte-Carlo Uncertainty and Sensitivity

FISPACT-II uses a Monte-Carlo approach to sensitivity analysis. A series S of inventory calculations is performed with the set of I independent variables $\{X_i^s;\ i = 1,\ldots,I;\ s = 1,\ldots,S\}$ chosen from distributions with means $\langle X_i\rangle$ and standard deviations $\langle \Delta X_i\rangle$. These runs produce a set of J dependent variables $\{Q_j^s;\ j = 1,\ldots,J;\ s = 1,\ldots,S\}$. With the TENDL and ENDF-6 libraries it is possible to take into account covariance data to get a complete assessment of the uncertainties of results.

The TENDL libraries contain covariance data between some reactions of given parents [22]. FISPACT-II reads these data and collapses the covariances as described in Section II C. Given a rank D symmetric positive definite covariance matrix, we can find a $D \times D$ similarity transformation matrix M such that $Y = M^T X$ and $cov(Y,Y) = M^T cov(X,X) M$ is diagonal with diagonal elements $var(Y)$. The transformed cross sections Y are treated as the independent variables, and random samples with means $\langle Y_i\rangle$ and standard deviations $\langle \Delta Y_i\rangle$ are chosen, and the input sample cross sections are computed using $X = MY$.

The dependent variables are the numbers of atoms of nuclides j or some related radiological quantity. The pathways summaries created by pathway analysis provide a good guide as to which cross sections and decays are likely to be important to include as independent variables in the sensitivity calculation.

Selecting a sensitivity calculation in FISPACT-II causes the series of S runs with different independent variables to be undertaken to compute, process and output the set $\{Q_j^s\}$. The default independent variable distribution is taken to be log-normal, but other options are provided (normal, log-uniform and uniform). Any sequence of irradiation pulses, changes in cross section, etc., that are possible with FISPACT-II can be used in the sensitivity calculations. The code performs the base calculation with full output, then repeats S times the sequence of steps with different sets $\{X_i^s\}$. The results of the base calculation are not included in the sensitivity calculation.

Sensitivity calculations provide both uncertainty and sensitivity output. Summary uncertainty output of means $\bar{X}_i$ and $\bar{Q}_j$ and standard deviations ΔX_i and ΔQ_j is produced. The code writes tables of means, standard deviations and Pearson correlation coefficients, and outputs the raw data $\{X_i^s,\ Q_j^s;\ i = 1,\ldots,I;\ j = 1,\ldots,J;\ s = 1,\ldots,S\}$ to file for possible post-processing.

L. Inventory Run Output

FISPACT-II produces various categories of output in human-readable form, as well as several types of tabular output for post-processing such as the preparation of graphs.

1. *Step Output*

At times specified in the `input` file, FISPACT-II outputs tables of inventory data for all nuclides with a number of atoms greater than the (adjustable) minimum threshold. Table X lists these, where

$A_{r,i}$ = atomic weight of nuclide i (amu);

N_A = Avogadro constant (mol^{-1});

$E_{\beta,i}$ = β decay energy for nuclide i (eV);

$E_{\alpha,i}$ = α decay energy for nuclide i (eV);

$E_{\gamma,i}$ = γ decay energy for nuclide i (eV);

C_1 = conversion from eV to kJ ($= 10^{-3}e$);

e_i^{ing}, e_i^{inh} = factors to convert activity of an ingested or inhaled nuclide into the dose received by an average person over 50 years (Sv);

L_i = specific activity below which a material is given clearance for disposal (Bq kg^{-1});

m_{tot} = total mass of material (kg);

$A_{2,i}$ = activity level for safe transport;

C_2 = conversion factor from TBq to Bq ($= 10^{12}$)

Section III G provides more information on the factors e_i^{ing}, e_i^{inh}, L_i and $A_{2,i}$.

Similar elemental output tables are printed, and formulae for these are given by summing the nuclide contributions over isotopes for each element. Summary data are also output. There are totals of activity, inhalation dose, ingestion dose and heating powers (alpha, beta, gamma and total) that are sums over all nuclides of quantities listed in Table X. Transport indexes *Total Bq/A2 ratio* and the effective transport index, $\langle A_2\rangle$, by

$$Total\ Bq/A2\ ratio = \sum_{i=1}^{N_n} \left(\frac{A_i}{A_{2,i} C_2} \right) , \qquad (78)$$

TABLE X. Inventory table output definitions.

Description	Value	Units
number of atoms	N_i	
mass	$N_i A_{r,i}/N_A$	g
activity	$A_i = N_i\lambda_i$	Bq
β-power	$A_i E_{\beta,i} C_1$	kW
α-power	$A_i E_{\alpha,i} C_1$	kW
γ-power	$A_i E_{\gamma,i} C_1$	kW
dose rate	Eq. (38) or Eq. (41)	$\mathrm{Sv\,h^{-1}}$
ingestion dose	$A_i e_i^{ing}$	Sv
inhalation dose	$A_i e_i^{inh}$	Sv
clearance index	$A_i/(m_{tot} L_i)$	
transport index	$A_i/(A_{2,i} C_2)$	
half-life	$\lambda_i^{-1} \log_e 2$ or 'Stable'	s

$$\langle A_2 \rangle = (\sum_{i=1}^{N_n} A_i)/(Total\ Bq/A2\ ratio) \tag{79}$$

and clearance indexes [29] are given

$$Clearance\ index = \sum_{i=1}^{N_n} \left(\frac{A_i}{M_{tot} L_i} \right) . \tag{80}$$

For cases where diagnostic cross-section data are available in the ENDF libraries, gas production, KERMA and DPA summaries are output. Gas production rates (in $\mathrm{s^{-1}}$) are given by

$$Gas\ rate = \phi \sum_{i=1}^{N_n} N_i \bar{\sigma}_i^{gas} , \tag{81}$$

where ϕ is the flux amplitude and $\bar{\sigma}_i^{gas}$ is the collapsed total gas production cross section in $\mathrm{cm^2}$. The collapse follows the same procedure as for reaction cross sections (cf. Section II C). A list of the total gas production cross sections recognised by the code is given in Table II.

The KERMA (kinetic energy released in materials) rates are given by

$$kerma\ rate = \phi \sum_{i=1}^{N_n} \bar{\kappa}_i , \tag{82}$$

where $\bar{\kappa}_i$ is the collapsed kerma cross section for one of the kerma cross sections listed in Table II. Specific values of this energy per kilogram and per $\mathrm{cm^3}$ are obtained by scaling the total kerma using the initial mass and density.

The displacements per atom (DPA) for a single element is given by [30, Eq.(90)]. For mixtures of elements with different lattice displacement energies, the total displacements rate, D_{tot} may be estimated using the ratio of the mean total available energy to the mean displacement energy,

$$D_{tot} = e_d \phi \sum_{i=1}^{N_n} N_i \bar{d}_i / 2\bar{E}_d , \tag{83}$$

TABLE XI. Atomic displacement energies used to compute DPA. E_d is 25 eV for all other elements.

Element	E_d in eV	Element	E_d in eV
Be	31	Co	40
C	31	Ni	40
Mg	25	Cu	40
Al	27	Zr	40
Si	25	Nb	40
Ca	40	Mo	60
Ti	40	Ag	60
V	40	Ta	90
Cr	40	W	55
Mn	40	Au	30
Fe	40	Pb	25

where ϕ is the flux amplitude in $\mathrm{cm^{-2}\,s^{-1}}$, N_i is the number of atoms of nuclide i and $\bar{d}_i$ is the collapsed DPA reaction cross section in eV-$\mathrm{cm^2}$. The constant e_d is the DPA efficiency factor and is set to 80% [30, p. 2757]. A list of the DPA cross sections recognised by FISPACT-II is given in Table II.

The mean atomic displacement energy $\bar{E}_d$ is given by

$$\bar{E}_d = \sum_{i=1}^{N_n} N_i E_d(Z_i) / \sum_{i=1}^{N_n} N_i , \tag{84}$$

where Z_i is the atomic number of nuclide i and E_d are atomic displacement energies (in eV) taken from Table II of Ref. [30], with the exception of the value 55 eV used for tungsten (see Table XI).

Alternatively, the displacement rate may be estimated using the mean of the displacement rates of the constituents,

$$D_{tot} = e_d \phi \sum_{i=1}^{N_n} N_i \bar{d}_i / 2E_d(Z_i) . \tag{85}$$

Both options have been evaluated and have been shown to give similar results. Equation (85) is used in the present version of FISPACT-II.

The displacements per atom rate is given by dividing D_{tot} by the total number of atoms

$$DPA\ rate = D_{tot} / \sum_{i=1}^{N_n} N_i . \tag{86}$$

The decay radiation data (cf. Section II F 1) are used to provide output of the total powers ($\mathrm{MeV\,s^{-1}}$) from α, β and γ radiations and the total number of spontaneous fission neutrons, the γ spectrum ($\mathrm{MeV\,s^{-1}}$ per group) and number of gammas per group ($\mathrm{cm^{-3}\,s^{-1}}$) in either a 24- or 22-group form, depending on user input.

The total dose rate is given in one of two forms depending on user selection; contact dose from a semi-infinite slab of the material (see Eq. (38)) and for the dose from a point source at a specified distance (Eq. (41) on page 13).

If most of the dose rate is produced by nuclides with approximate γ-spectra (Section II G 3) then a warning message is given. A bremsstrahlung correction to the gamma dose is calculated using either plane or point source formulae as appropriate and it is printed.

At each step the inventory is sorted into descending order of radiological quantities, and tables of nuclides at the tops of these lists are printed. Radiological quantities include activity, total heat production, dose rate, gamma heating and beta heating, ingestion dose, inhalation dose, and clearance index.

2. *Pathways and Uncertainty*

A typical FISPACT-II run comprises one or more irradiation steps followed by cooling steps. If pathways or uncertainty output are selected, then at the end of the final irradiation step, a pathways analysis is performed. A detailed description of the resulting output appears in Section V A 3.

If uncertainties are selected, then the set of pathway inventories and the cross section uncertainties derived from collapsed covariance data are combined to provide output of uncertainties in radiological quantities (cf. Section II J).

If sensitivities are selected, then a series of calculations is performed and mean values, uncertainties and Pearson correlation coefficients are computed and output is generated (cf. Section II K).

A new functionality for uncertainty quantification in nuclide depletion has been added after the 3-00 code version. While pathways-based uncertainty handles the *production* of radionuclides for the purposes of quantifying uncertainty in radiological quantities, the uncertainty in the depletion of any nuclide – whether through reactions or decays – adds an additional contribution to uncertainty propagation. In comparison with the myriad of possible pathways which produce a nuclide, the depletion occurs only through an easily classed subset of reactions which are precisely the negative diagonal terms of the rate equation matrix.

A nuclide generally may have some combination of creation and destruction,

$$\frac{dN}{dt} = -\mathsf{D}N + \mathsf{C}, \tag{87}$$

where D is a specific rate of destruction while C is a rate of creation, i.e. units of s^{-1} and atoms/s, respectively. While C typically depends on a many quantities including potentially many inventories, decays and reactions, it can be determined by direct reference to the rate equation solutions and the depletion term.

The creation terms in turn have their own associated uncertainties and are the subject of the pathways-based uncertainty analysis in FISPACT-II. To address the depletion uncertainty, FISPACT-II considers three variables with their uncertainties

λ = total decay rate for the target nuclide

Φ = flux amplitude

σ = total non-scattering cross-section

The depletion specific rate $\mathsf{D} = \lambda + \Phi\sigma$, so using the standard identities for variance of sums or products of random variables we obtain

$$var(\mathsf{D}) = var(\lambda) + \Phi^2 var(\sigma) + \sigma^2 var(\Phi) + var(\sigma)var(\Phi). \tag{88}$$

FISPACT-II calculates the fractional uncertainties for half-lives, Δ_λ, and for collapsed cross sections, Δ_σ, which are defined as $\Delta_X = \sqrt{var(X)}/X$. The estimator for the fractional error in the specific rate D is therefore

$$\Delta_{\mathsf{D}} = \frac{1}{\mathsf{D}}\sqrt{(\lambda\Delta_\lambda)^2 + (\sigma\Phi)^2({\Delta_\sigma}^2 + {\Delta_\Phi}^2 + \Delta_\sigma\Delta_\Phi)}. \tag{89}$$

While FISPACT-II is designed to accommodate the uncertainties (including covariances) of incident particle spectra, the current implementation only considers uncertainties in the total flux. Note that a complete covariance treatment of the reaction rate due to cross section energy correlations is implemented, i.e. for a reaction rate R we sum over all energy groups as

$$var(R) = \sum_i \sum_j \phi_i\phi_j cov(\sigma_i, \sigma_j). \tag{90}$$

FISPACT-II outputs the specific depletion rate as well as the percent uncertainty from the equations above. These are also given as a depletion rate using the initial nuclide inventory for each step, as well as a first-order integrated value for the depletion and its uncertainty as a fraction of the final inventory. Note that this is the integrated uncertainty (in atoms) of depletion, which will grow (unbound) monotonically as a percent in pure depletion cases.

In scenarios where a nuclide may be both created and depleted - for example plutonium in a fission reactor, minor actinides, fission products, etc., a combination of both depletion and breeding uncertainties are required. To avoid the complexities and expense of full Monte-Carlo sensitivity-uncertainty analyses, FISPACT-II can be used to calculate depletion and breeding rates with uncertainties. These can be coupled with multiple different approximations. For example, the simplified piece-wise constant equations for a target nuclide of Eq. 87.

If we assume that these terms are constant over the time interval, the solution for this simplified differential equation is simply

$$N_{i+1} = \frac{\mathsf{C}_i}{\mathsf{D}_i} + \left(N_i - \frac{\mathsf{C}_i}{\mathsf{D}_i}\right)\exp\left(-\mathsf{D}_i\Delta t_i\right), \tag{91}$$

and the first order Taylor expansion of the propagated uncertainty yields,

$${\Delta N_{i+1}}^2 = \left(\frac{\partial N_{i+1}}{\partial \mathsf{D}_i}\right)^2 {\Delta \mathsf{D}_i}^2 + \left(\frac{\partial N_{i+1}}{\partial \mathsf{C}_i}\right)^2 {\Delta \mathsf{C}_i}^2,$$

(92)

provides an uncertainty estimate. These methods have been tested with FISPACT-II to generate coupled uncertainties in simulated actinide inventories for fission fuels, as in Fig. 10. These rely upon complete uncertainty data, including the resolved resonance ranges, which are incomplete in the current nuclear data.

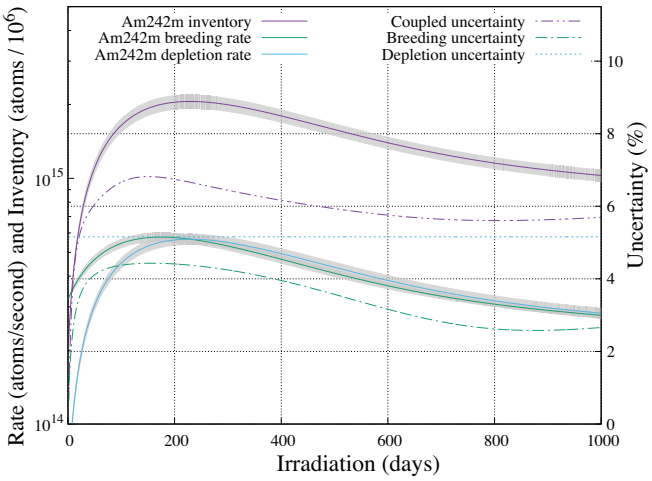

FIG. 10. (Color online) Coupled breeding-depletion uncertainty analysis of Am242m inventory in a PWR MOX spectrum with constant neutron flux of 1.0E+14 n cm^{-2} s^{-1}. The **DEPLETION** uncertainty is constant for this single incident particle spectrum simulation, while breeding paths and their combined uncertainties are time-dependent.

3. Library Data Output

The main FISPACT-II code also provides optional summaries of the collapsed and condensed data libraries in a readable form. The ten options are:

1. decay data, including fission yields if appropriate, for each nuclide
2. the branching ratios of decays for each radionuclide
3. the cross-section data (including uncertainties) for each reaction in the specified projectile spectrum
4. nuclides which will give a bremsstrahlung contribution to the γ dose rate
5. the projectile spectrum used to collapse the cross-section library
6. the photon and particle decay spectral lines energy and intensity for unstable nuclides
7. a list giving the library source of the ENDF cross-section data file for each nuclide (ENDF library input only).
8. a list giving the library source of the ENDF decay data file for each nuclide (ENDF library input only).
9. a compact summary of the decay data, including parent nuclide state, half life, decay modes and decay fractions.
10. a summary of element standard densities and isotope natural abundances used in the code.

M. Recoil Spectra, PKA

The calculation of the energy distributions of residual and emitted particles resulting from nuclear reactions is an important input to the modelling of radiation damage in materials [31]. The recoiling species, or primary knock-on atom (PKA), can induce cascades of atomic displacements, leading to the accumulation of structural damage with component or facility life-limiting consequences. The output of these distributions for an inventory of nuclides exposed to an input neutron spectrum and flux is accomplished via a specially written routine called `spectra-pka`, which updates and improves upon the historical code `specter`, written at Argonne National Laboratory in the 1980s by Greenwood and Smitther [32]. `spectra-pka` collapses the input neutron spectrum with the full set of incident-energy vs. recoil-energy cross-section matrices for every nuclide in the current inventory, which could be at time $t = 0$ or at a later time, perhaps after a period of irradiation and cooling. The resulting recoil distributions, one for every (open) reaction channel of every nuclide in the inventory, are subsequently scaled according to the inventory nuclide fractions and summed appropriately, as a function of both nuclide and element, the latter being particularly relevant to computational atomistic modelling of materials. A fuller description of `spectra-pka` is given in [31, 33].

The recoil or PKA probability matrices themselves are calculated and processed from the raw, point-wise nuclear libraries by the nuclear data processing code NJOY [34] through its `GROUPR` routine, and for an additional library of nuclear data files, complementary to the core ENDF libraries used by FISPACT-II. For each reaction channel, both the recoil matrices of the primary (heavy) residual and and secondary emitted light particle, such as α-particles and protons, are calculated. Figure 11, for example, shows, as cross section versus recoil energy for a range of incident energies, the recoil matrices for the heavy ^{24}Na residual and light ^{4}He α-particle produced from the (n,α) channel on ^{27}Al. The 3D representation used here is particularly useful to compare these two related recoil matrices because there is little or no overlap in the distributions at a given incident neutron energy. The reaction channel itself is threshold-like and the cross section is only significant above 5 MeV, which is thus also true for the matrices in Fig. 11.

Figure 12 shows another example, again for an (n,α) channel, but this time for ^{184}W. In this case note that the energy of the light α-particle can actually be greater than the energy of the incoming neutron (designated by the red line in the figure) because the (n,α) reaction has a positive Q-value on ^{184}W.

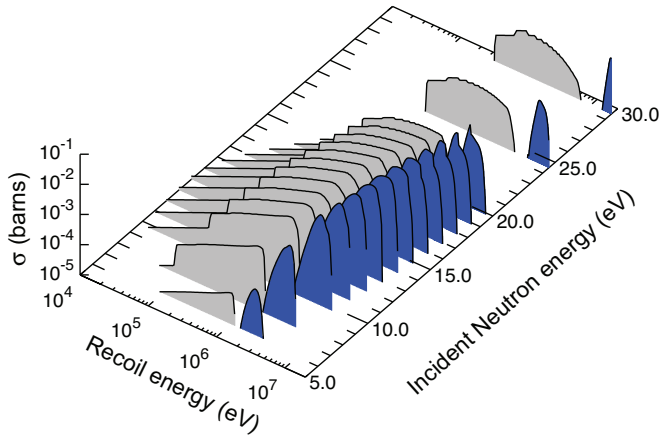

FIG. 11. (Color online) ^{27}Al (n,α) recoil matrices. Both the recoil matrix of the heavy ^{24}Na residual (grey regions) and the light ^{4}He α-particle (blue) are shown. For a given incident neutron energy (plotted at the mid-point of the energy group) the recoil cross section vs. recoil energy curve is plotted. Note that only a subset of the possible incident energies are shown – to aid visualization.

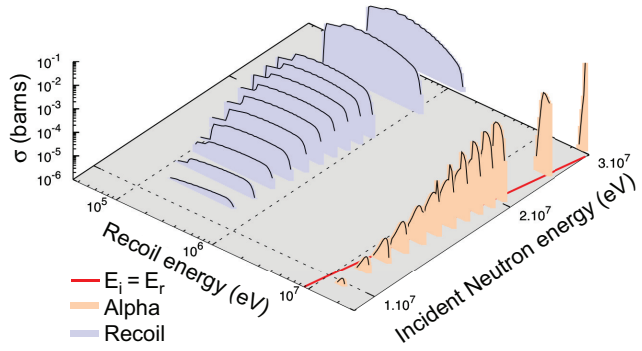

FIG. 12. (Color online) ^{184}W (n,α) recoil matrices. Both the recoil matrix of the heavy ^{181}Hf residual (blue regions) and the light ^{4}He α-particle (red) are shown. For a given incident neutron energy (plotted at the mid-point of the energy group) the recoil cross section vs. recoil energy curve is plotted. Note that only a subset of the possible incident energies are shown – to aid visualization. The red line in the figure represents the line where the energy of the residual is equal to that of the incident neutron.

Figure 13, shows the results obtained when these (n,α) channels and all other possible reaction channels on ^{27}Al are combined, by `spectra-pka`, with a typical neutron irradiation spectrum predicted for the first wall (FW) armour of a demonstration (DEMO) fusion power plant (see [35] for further details). Rather than show the recoil distribution for every product from all possible channels on ^{27}Al, which are nonetheless available as output, in the figure we show the elemental (a) and isotopic (b) sums. From Fig. 13, we see that PKAs of Al (^{27}Al) dominate over the majority of the PKA energy range, reflecting the fact that the simple elastic and inelastic scattering cross section, where the recoil is identical to the target, have very high cross sections compared to the non-elastic reaction channels, particularly at low neutron energies. In Fig. 13(a), only at high energies, in the 100s of keV range and above, do recoil of other heavy particles, in this case magnesium and sodium, become significant compared to the Al recoils of the same energy. Notice that Mg and Na have lower atomic number Z than Al, and it is obviously the case that at time $t = 0$, which the results in Fig. 13 represent, before any transmutation has taken place, there are no reaction channels that would produce residuals with a higher Z than the parent. Only at later times during irradiation exposure, once some higher atomic number elements have been produced by transmutation and decay, would there be a possibility of seeing PKAs of higher Z number compared to the original parent atoms.

The Fig. 13, also gives the PKA distributions for the light secondary emitted gas particles of helium and hydrogen, which are labelled in Fig. 13(a) as protons (p) and α-particles to reflect the fact that these ^{1}H and ^{4}He isotopes will be the overwhelmingly dominant secondary products – as confirmed by Fig. 13(b). ((n,d) and (n,t) involving the heavier H isotopes are rare, and reactions producing other isotopes of He even more so.) As a consequence of their low mass compared to the target and heavy residual, these gas particles take the majority of the kinematic energy of the reaction and so have much higher PKA energies. Thus, for this FW fusion irradiation spectrum, with its dominant 14 MeV neutron peak, the gas particles can be emitted with energies almost up to this 14 MeV level. Such high energy particles may have significant implications for radiation damage in materials, even accounting for their low mass.

`spectra-pka` also automatically outputs total and cumulative distributions, which are the sums over all heavy recoils with gas particles emitted. In principle, these light particles can be added, but this would produce a misleading distribution for materials modelling because the damage created by these high energy light particles will be very different to equivalent-energy heavy recoils. Figure 14 shows cumulative PKA distributions for several important materials under the same fusion irradiation, allowing a direct comparison of the differing recoils, which would, in turn, lead to differing damage rates. The figure shows that Al, being very light, has the highest energy recoils, and heavy W has the lowest energy recoils.

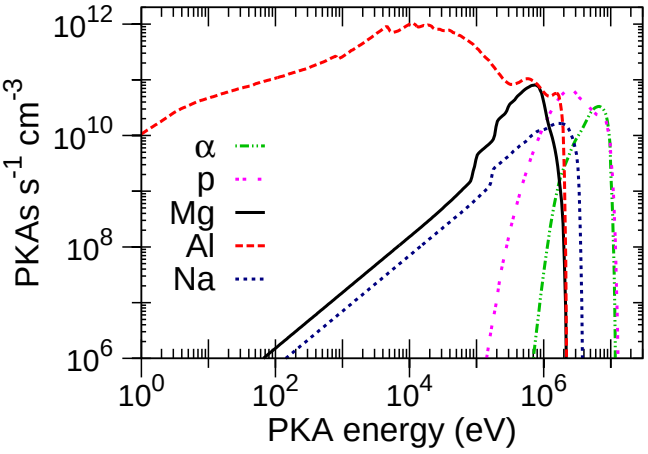

(a)Summed by recoiling Element.

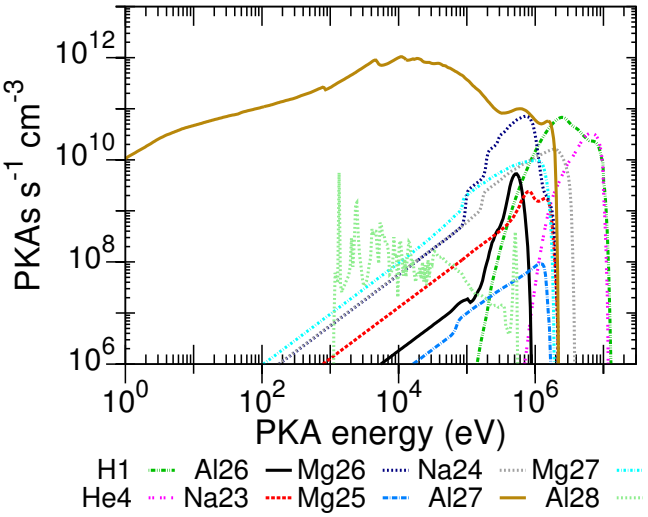

(b)Summed by recoiling Nuclide.

FIG. 13. (Color online) The PKA distributions for Al (in fact ^{27}Al, which makes up 100% of naturally occurring aluminium) under fusion conditions.

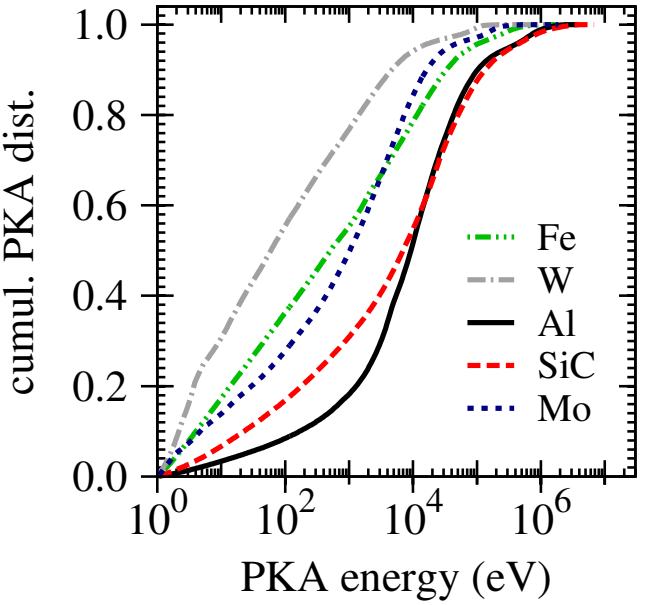

FIG. 14. (Color online) Cumulative PKA distributions for various materials under fusion conditions.

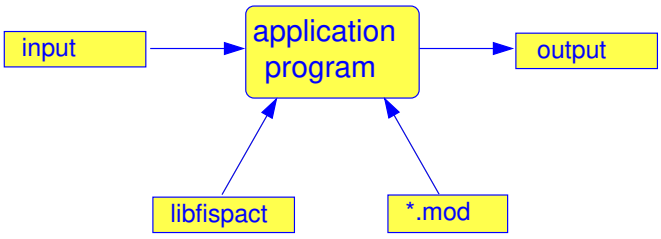

FIG. 15. (Color online) Using the FISPACT-II library with other programs.

N. Auxiliary Programs

The FISPACT-II code comprises a main driver program and a set of encapsulated modules. The main driver delivers the capabilities discussed above, and the modules provide public, shared data structures and subprograms. The public data and subprograms of the modules are fully documented in Ref. [7]. Figure 15 illustrates how the modules may be used by other programs. FISPACT-II provides a library and set of `.mod` files which give other application programs full access to its public data and subprograms. For example, the library may be close-coupled to a Monte-Carlo code to provide much faster two-step transport/activation calculations than is possible with the scripting approach. Examples where a different driver program is used for specific nuclear data or activation computations include:

makenuclideindex: A program that reads the files in directories of ENDF cross-section and decay data and constructs a full master index `ind_nuc` for use by FISPACT-II.

listreactions: This reads the cross-section file for a single nuclide and prints out all the reactions and reaction daughters for that nuclide.

extract_xs_endf: This reads a single cross-section file and a flux file and outputs fluxes, cross sections, reaction rates and uncertainties for each energy group.

compress_xs_endf: This reads the ASCII ENDF cross-section files for all the nuclides in `ind_nuc` and writes a compressed binary version for use by

FISPACT-II. Typically this gives a speedup of a factor of 5 to 10 times for collapse runs (cf. Fig. 1).

fispact_mp: This is a version of FISPACT-II that simultaneously allows more than one projectile irradiation, but at present does not include pathways and uncertainty calculation.

The approach illustrated in Fig. 15 assumes that the application program is written in Fortran95. However, if the coupling is to a C or C++ program, then the derived data types present a problem. To deal with this case, the FISPACT-II library includes an interface module that communicates with the application program only through intrinsic Fortran data types [36]. This interface module allows FISPACT-II to be closely coupled with other codes where inventory calculations for a large number of different fluxes and materials are needed. In particular, it allows coupling to Monte-Carlo codes without the large input/output overhead associated with running the free-standing code many times.

O. Irradiation with Other Projectiles: γ, p, d and α

The previous sections have focused on neutron-induced reactions while FISPACT-II has been engineered to handle simulation with charged-particle reactions in the same manner. Where the ENDF data are available, all of the three subsystems of FISPACT-II; library data reduction, inventory calculation and pathways/uncertainty analysis, can equally be applied to irradiation with other projectiles.

FISPACT-II can accommodate ENDF data for γ, p, d, and α induced reactions. At present, group TENDL cross-section libraries for gamma, proton, deuteron and alpha are provided and recommended as defaults, but without uncertainty data (Section III D). The JENDL-4 α-induced and ENDF/B-VII.1 γ-induced libraries are also distributed with the official code release.

The set of reaction `MT` values recognised by FISPACT-II for these projectiles is the same as those listed in Table I for neutron activation, but with the projectile replaced and values of ΔA and ΔZ being changed as listed in Table XII. Thus, for example, the replacement Table I for deuteron activation would have n replaced by d in column 1, all values of ΔZ increased by 1 and all values of ΔA increased by 1.

TABLE XII. Changes to Table I for different projectiles.

Projectile	$\delta(\Delta Z)$	$\delta(\Delta A)$
n	0	0
γ	0	-1
p	1	0
d	1	1
α	2	3

For all TENDL data above 30 MeV, the use of total residual production cross sections offers complete information for the radionuclide yields from nuclear reactions – the fundamental data for inventory calculations. These include spallation-evaporation reactions and associated yields, as shown in the yields for ^{120}Sn in Fig. 16. These are processed as a (n,O) reaction by FISPACT-II and populate all of the residual production channels in the rate equations.

A single group structure is used for all the charged particle and gamma libraries, employing a coarser grid than the one used for neutrons, primarily due to the lack of resonances in those cross-section sets. The CCFE-162 group structure universally employed is based on the TENDL charged particle incident-energy grid and fully captures the high-energy data that are provided.

III. NUCLEAR DATA LIBRARIES

FISPACT-II requires input from several nuclear data libraries before it can be used to calculate inventories and source terms. While any libraries in the correct ENDF-6 format may be used, the development of FISPACT-II over the last few years has run in parallel with the development of the TALYS-based Evaluated Nuclear Data Library (TENDL) [22] project and those general purpose European libraries are a recommended source of cross-section data for many applications, including activation studies. Together, FISPACT-II and TENDL's nuclear data forms make up an advanced simulation platform for the simulation of inventories, source terms and nuclear observables that is a complete package tailored and predictive for many application needs, including (but not limited to) nuclear fission and fusion, nuclear fuel cycle management, accelerator physics, isotope production, material characterisation, earth exploration, astrophysics, homeland security.

The following data libraries are required to exploit the capabilities of FISPACT-II in full:

1. cross-section data for neutron, proton, deuteron, alpha and gamma-induced reactions;
2. fission-yield data for neutron, proton, deuteron, alpha and gamma-induced reactions;
3. variance and covariance data for neutron-induced reactions;
4. probability table data for neutron-induced reactions in the resonance energy ranges;
5. decay data;
6. radiological data:
   (a) biological hazard data;
   (b) legal transport data;
   (c) clearance data;

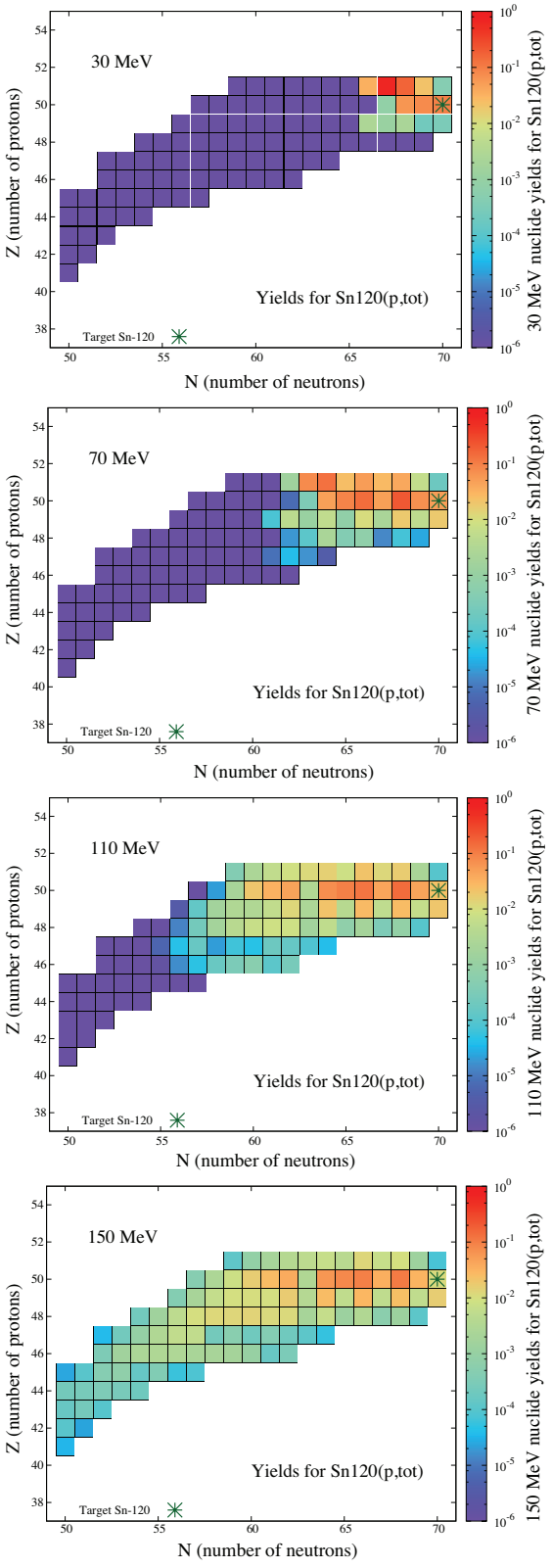

FIG. 16. (Color online) TENDL-2015 total residual nuclide production cross sections from proton-induced reactions on ^{120}Sn. Incident energies for 30, 70, 110 and 150 MeV are shown to demonstrate the range of yields over 30-200 MeV.

7. heavy and light particle recoil matrices.

The preparation of nuclear data from diverse sources for use in FISPACT-II was streamlined and simplified by following as closely as possible the forms of data format described in the ENDF-6 format manual [2].

Three processing codes are used in sequence and in parallel to produce, process, check, and compare the various original nuclear data forms: NJOY12-050 [34], PREPRO-2015 [37] and CALENDF-2010 [14]. No one, or even two, of these processing codes are sufficient to manage all the required steps. In general, a combination of the three is needed to extract the multi-physics data forms that are used to create the most versatile library files for FISPACT-II. A schematic of the processing sequence is shown in Fig. 17.

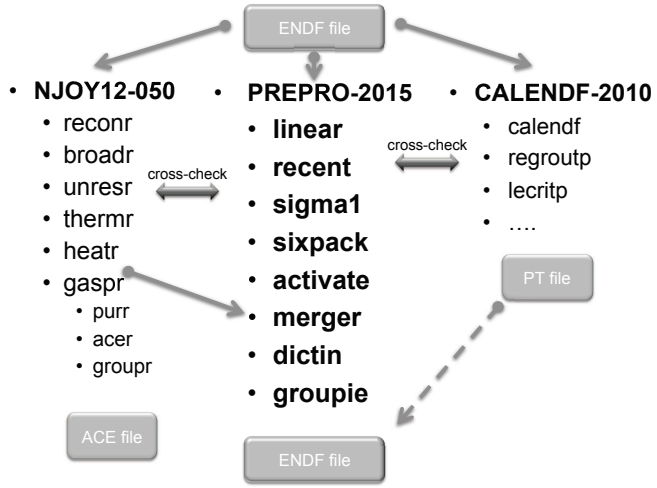

FIG. 17. A schematic of the processing sequence using NJOY, PREPRO and CALENDF.

Further details of the data assimilation processes and their history can be found in [38, 39]. TENDL processed data forms differ in some respects [22, 23]. This is due to often subtle enhancements made in the original but completely ENDF-6 compliant TENDL data format and the way the files themselves are processed. This is particularly noticeable in the partials for kerma, dpa and PKA generated by the latest TALYS and the more complete use made of the variance and covariance information contained in this truly general purpose library.

A. NJOY

The NJOY processing system is widely used to convert evaluated files into forms of interest for numerous practical applications. Many reactor analysis, criticality safety, radiation shielding, inventory simulation codes rely on its powerful processing capabilities to provide their (often specialised) nuclear data forms. Uniquely, in addition

to the processing of cross sections, angular distributions, emitted spectra and other nuclear observables, NJOY can be used to process:

- gas production reactions: `gaspr`;
- heat production cross sections: `heatr`;
- displacement cross sections: `heatr`;
- charged particle and recoil energy group-to-group matrices: `groupr`.

Application forms for FISPACT-II include all the above. The first three, once generated in the specific NJOY pointwise format are extracted and seamlessly embedded into the PREPRO pointwise infrastructure for proper integration and further processing.

The charged particle (A≤4) and residual nucleus (A>4) recoil group-to-group matrices are also produced from the `groupr` module of NJOY in the same fine group structure as for the cross section for each evaluation. Those can then be folded, isotope by isotope, with any neutron spectrum to provide materials science applications with the recoil energies information they need at an elemental level. However, this type of practical information form is satisfactory only if the original evaluation is complete and fully populated. Older evaluations produced specifically for fission reactor physics applications may be inadequate in this respect.

NJOY can also be used to process some parts of the variance and covariance information, however in the case of FISPACT-II requirements it has been necessary to consider a specific development in order to be able to master the full complexity of the data streams necessary to an inventory code. As described in Section II C a projection operator maps the cross-section energy bins to the covariance energy bins.

B. PREPRO

The codes are named the PRE-PROcessing codes, as they have been designed to pre-process ENDF-6 formatted data into forms useful for applications. PREPRO is a modular set currently comprising 18 modules each designed to perform one or more independent operations, that are used in a given sequence. Raw ENDF-6 data files need to have resonance parameters interpreted for cross sections to be constructed, Doppler broadened, thinned and linearised to the desired temperature, with isomeric branching ratio applied when necessary, before being in a form usable for applications.

The recent release of PREPRO consists of an important modernisation of all codes, following the latest requirements linked to the ENDF-6 format, specifically: portability, level of precision and use of the latest Fortran. It also comes with a set of "best input parameters" that allows safe but robust data mining and processing activities.

Application forms of use for FISPACT-II generated from PREPRO (using the `linear`, `recent`, `sigma1`, `sixpack`, `activate`, `merger`, `dictin` and `groupie` modules) include detailed partials, total group cross sections, resonance widths and uniquely high energy (>30 MeV) activation and transmutation cross sections, and radionuclide yields (when provided in the original data set). PREPRO also merges the unique NJOY-produced set of responses, kerma, displacement cross sections and gas production, into its own structures. Finally, one of its modules groups all cross sections into a fine structure using appropriate micro flux weighting spectra.

One tremendous advantage to be gained from this particular suite of modules and processing steps is that at any stage it endeavours to keep the output file structure in ENDF-6 format, file and reaction-type numbers alike. Cross sections constructed from parameters progress from 0 K pointwise data, to 293.6 K pointwise then groupwise data in the same structured file.

C. Cross Section Group Structure

There are three standard group structures in the ENDF-6 format used for the TENDL, ENDF/B.VII.1, JENDL-4.0, CENDL-3.1 and JEFF-3.2 nuclear libraries; data in these structures can be read automatically into FISPACT-II.

They have a fine energy grid, an increased upper energy bound of 1 GeV, and allow the addition of α and γ-induced reactions while permitting more precise modelling of reaction thresholds and the resolved and unresolved resonance ranges. These groups are:

Name	Number of groups
CCFE	162
CCFE	709
UKAEA	1102

The method of presentation in Fig. 18 (energy bin width) and Fig. 19 (lethargy bin width), is designed to make clear in which energy ranges particular structures have the most groups and will therefore give a good, accurate representation of the reaction rates.

The CCFE-162 (up to 200 MeV) structure was introduced for studies of charged-particle projectiles and γ-induced activation and transmutation. This structure includes all legacy ones known to the authors, because past limitations of computing resources are no longer a consideration that can be used in justifying simpler energy structures. The CCFE (709 up to 200 MeV and 660 up to 30 MeV) group structures are extensions of the LLNL (616 up to 20 MeV) structure. They have 50 tally bins per energy decade, equally spaced in the logarithm of the energy between 10^{-5} eV and 10 MeV, 200 keV steps to 30 MeV and thereafter bins with appropriately chosen equally-spaced boundaries in energy up

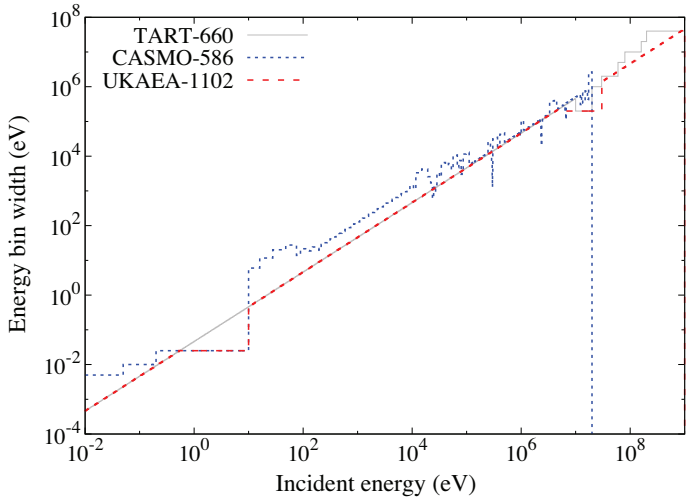

FIG. 18. (Color online) Energy bin widths for the TART-660, CASMO-586 and UKAEA-1102 group structures.

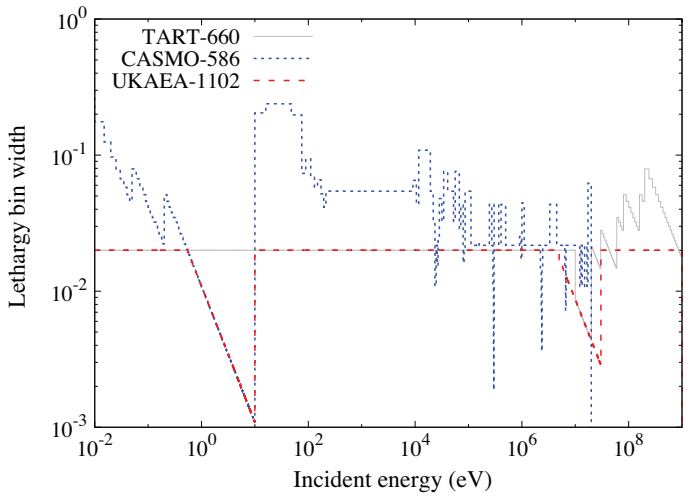

FIG. 19. (Color online) Lethargy bin widths for the TART-660, CASMO-586 and UKAEA-1102 group structures.

to 1 GeV. The UKAEA 1102-group structure is the culmination of extensions of the state of the art thermal fission CASMO (586), the fast LLNL (616) and the fast CCFE (709) structures pushed to 1 GeV. Each specific feature of those three grids have been combined into one single structure: the UKAEA 1102-group structure depicted in Fig. 20.

The generation of reaction rates with multi-group convolution of binned fluxes with cross-sections has always been the subject of intense research in order to satisfy the specific requirements of one application at a time. Recent studies [40, 41] have demonstrated that the fine CCFE-709 and *a fortiori* the UKAEA-1102 group structure have been optimised to comprehensively cover all applications (Fig. 28,29).

D. ENDF Cross Section Libraries

FISPACT-II accommodates a range of nuclear reaction data forms, including induced-reaction cross sections for multiple incident particles, for example, but not limited to TENDL-2015, ENDF/B-VII.1, JEFF-3.2, JENDL-4.0u and CENDL-3.1 nuclear data libraries processed into a fine-group structure. The recommended cross section data libraries for FISPACT-II are the TENDL ENDF-style forms, mainly because they have the ability to provide the most complete datasets and forms including variance and covariance information. Those libraries have been the subject of a wide range of verification and validation processes.

The enhanced cross section and data forms for FISPACT-II are entirely ENDF-6 compliant in nature and are more robust, complete and more exploitable with regard to any application than the raw data they are derived from. The `MF` (files) and `MT` (channels) legacy ENDF-6 infrastructure dictionary is kept and processed (Fig. 22 and 23), but also complemented when needed. Derived, reconstructed `MT`s are added: such as partial gas production, total and partial kerma and dpa (Fig. 26 and 27), complete isomeric channel partial cross sections properly parsed and stored in `MF`=10, as are the light particle (A<4) and heavier radionuclide production cross sections at high energy, above 30 MeV, in a comprehensive `MF`=10, `MT`=5 description that details the production cross sections for up to 200 daughter radionuclides (Fig. 24 and 25).

Cross-section and probability tables are given for three reactor temperatures in the Kelvin range. Two astrophysics temperatures in the keV range are also given for the major libraries.

It should be noted that the full `MF`=2, `MT`=152 data are kept in their original state in the processed file to be used when requested by FISPACT-II's self-shielding keyword. PKA matrices for the heavy recoils and the light particles are also given for all the stable nuclei in the same 709 and 660 -30 MeV group structures (Fig. 11 and 12).

Variance and covariance data are also processed directly with FISPACT-II but then only if they exist in part or in full in the original evaluation and library. Only TENDL systematically and uniformly contains such information. All the libraries are for neutron-induced reactions, but TENDL also provides α, γ, proton and deuteron-induced datasets, ENDF/B-VII.1 provides γ-induced reactions and JENDL-4 also provides a set of high-energy proton, neutron and a few α-induced evaluations.

Each library has its own tree-based directory structure that contains files for single nuclides, named after the isotope they refer to. Such simple storage infrastructure gives robustness, efficiency and flexibility.

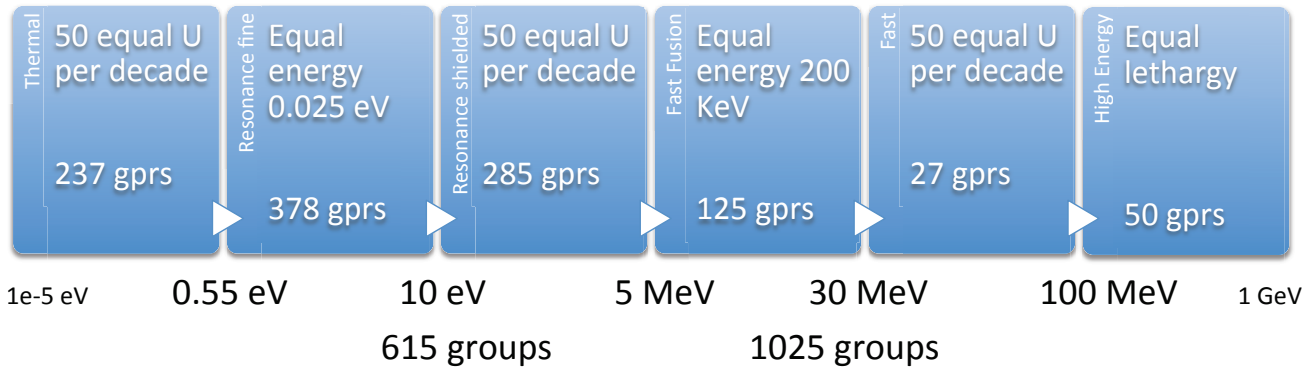

FIG. 20. (Color online) UKAEA-1102 group structure description with alternating regions of equal energy bins and equal lethargy (U) bins.

TABLE XIII. Characteristics of group structures

Group name	Number of target nuclides	Variance and covariance	Number of nuclides with probability tables	Temperatures	PKA matrices
TENDL-2015	2809	Yes	2601	293.6 K 600 K 900 K 5 keV 30 keV	Yes
ENDF/B-VII.1	423	Few	268	293.6 K 600 K	Yes
JENDL-4.0u	406	Few	292	293.6 K 600 K	Yes
JEFF-3.2	472	Few	0	293.6 K 600 K	No
CENDL-3.1	239	Few	0	293.6 K	No

E. ENDF Decay Libraries

In addition to cross sections the other basic quantities required by an inventory code are data on the decay properties (such as half-life, α, β, γ emissions, etc.) of all the nuclides considered as targets or daughters. These data are available in the various evaluated decay data libraries, summarised in Table XIV. FISPACT-II is able to read the data directly in ENDF-6 format; it requires no pre-processing to be done, although file debugging has always been found necessary. Earlier libraries were based primarily on the JEFF-3.1.1 [42] and JEFF-2.2 [43] radioactive decay data libraries, with additional data from the most recent UK evaluations. However, not all of the then 2233 nuclides that were needed at the time are included in such sources. For these nuclides data were taken from sources such as Brown and Firestone [44], and ENDF-6 formatted files have been constructed. Reference [45] documents the earlier library, but in order to handle the extension in incident particle type, energy range and number of targets, many more nuclides are needed. A new 3875-nuclide decay library named UKDD-12 (Table XIV) has been assembled from previous compilations, complemented with all of JEFF-3.1.1, a few nuclides from ENDF/B-VII.1 and other decay files to cover the range of daughters arising from all TENDL reactions and more short-lived fission products.

TABLE XIV. Decay libraries.

Library name	Number of isotopes
UKDD-12	3875
JEFF-3.1.1	3854
ENDF/B-VII.1	3818
JENDL-4.0	1380
JDDF-2015	3237

Care has been taken to ensure that the cross-section and decay data libraries are compatible. All nuclides (including isomeric states) that can be formed from the various reactions as daughters in the cross-section library need to be included in the decay library so long as their half-lives are greater than 0.1 second. Some nuclides with shorter half-lives are also included where it is felt that they are of particular importance (e.g. the metastable states of ^{88}Y). Short-lived (<0.1 s) isomers which would return to the ground state by an isomeric transition usually have little impact on activation calculations and most of these have been ignored so far. However, the effort is now directed towards better physics and completeness, rather than accepting pragmatic solutions.

There are still some issues regarding minor differences

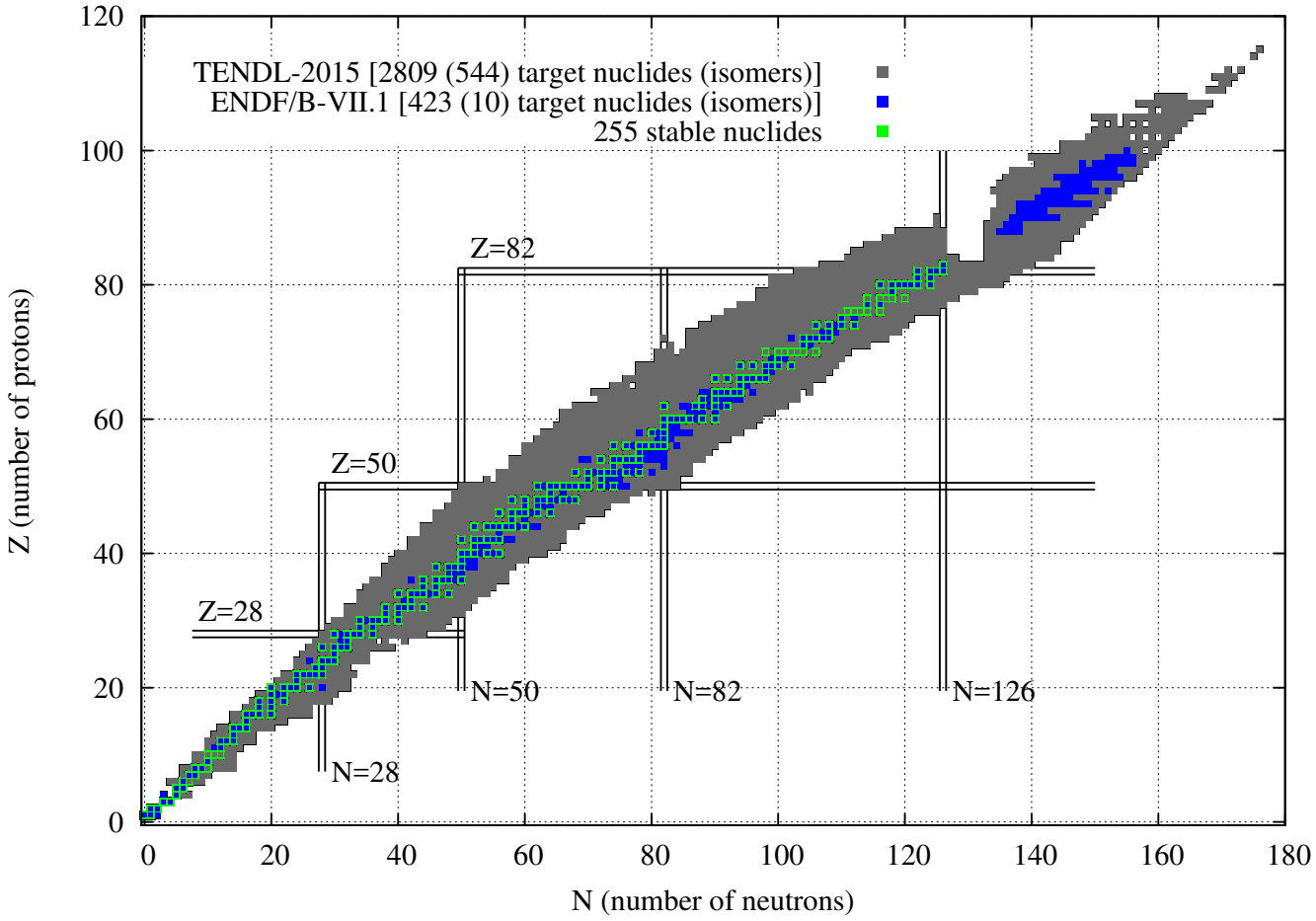

FIG. 21. (Color online) Chart of nuclides showing the range of all TENDL-2015 target files against the same for ENDF/B-VII.1.

between the isomer definitions in the cross-section library (arising from the RIPL-3 database [46] used in the preparation of TENDL) and those in the newly-compiled decay library. FISPACT-II now handles ground states and several isomeric states (g, m, n, o, . . . , t) but there are some inconsistencies in the energy levels of these radionuclide daughter products of reactions and the associated decay data files. These inconsistencies will be addressed fully in a future release of the libraries.

TABLE XV. Fission libraries.

Library name	nFY	sFY	oFY
GEF-5.2	119	109	
UKFY-4.1			21
JEFF-3.1.1	19	3	
ENDF/B-VII.1	31	9	
JENDL-4.0	31	9	

F. ENDF Fission Libraries

The FISPACT-II inventory code allows the use of a variety of neutron-induced (nFY), spontaneous (sFY) and particle-induced (oFY) fission yield libraries. Cumulative or independent yields can be selected. The various libraries contain not only different data for the same nuclides, but also cover different sets of nuclides. This is summarised in Table XV, which shows the number of nuclides with data for neutron-induced fission yield, spontaneous fission yield and alpha, deuteron, proton and gamma fission yield files. The methodologies behind TENDL and GEF [47, 48] allow for more robust files, notably containing any target nuclides, including isomers and a large range of incident neutron energies.

Fission yields are generally stored for three separate incident neutron energies: a thermal value of 25 meV, a fast value of 400 keV and a high-energy value of 14 MeV.

The GEFY-5.2 [49] data sets cover independent and cumulative fission-fragment yields where multi-chance fission is considered, fundamentally modifying the mass and general nuclide yields. The yields cover from thermal en-

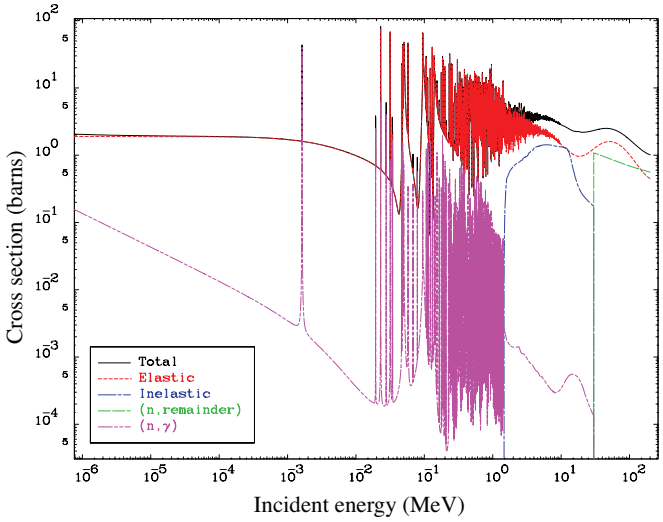

FIG. 22. (Color online) ^{52}Cr at 294 K: major cross sections.

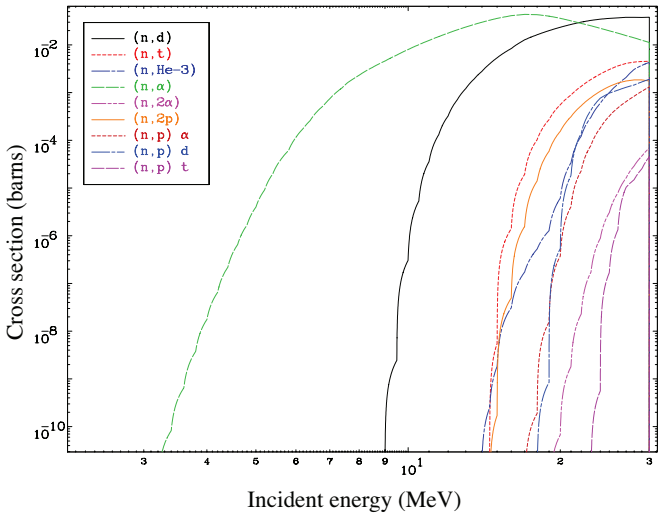

FIG. 23. (Color online) ^{52}Cr: charged particle production cross sections.

ergy (0.0253 eV) to 30 MeV in 59 energy steps for all target isotopes, allowing a more sophisticated interpolation of the yields depending on the incident particle spectrum. Examples of the energy-dependent yields are shown in Fig. 30.

G. Radiological Indices

FISPACT-II can report three types of quantity of radiological interest arising from the irradiation of a sample material:

- biological hazard indices;
- legal transport indices; and
- clearance indices.

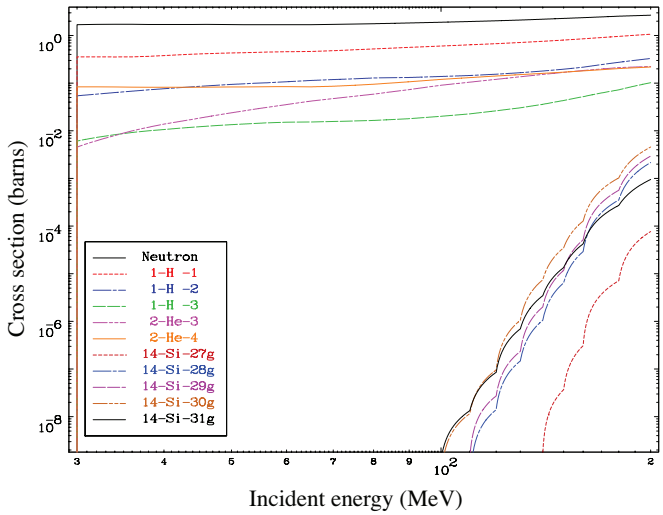

FIG. 24. (Color online) ^{52}Cr: radionuclide production cross sections above 30 MeV, beginning of mf6/mt5.

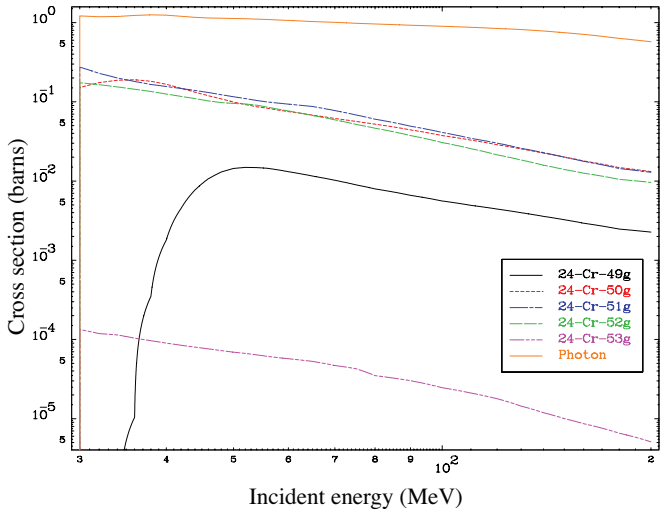

FIG. 25. (Color online) ^{52}Cr: radionuclide production cross sections above 30 MeV, end of mf6/mt5

1. *Biological hazard indices*

Activity is one quantity used to judge the potential hazard of an irradiated material. However, activity takes no account of the biological impact on human beings. To enable FISPACT-II to give some indication of the potential biological hazard of irradiated materials, a library of dose coefficients has been assembled which determine the dose received by a man over his lifetime (50 years) following the ingestion or inhalation of 1 Bq of activity of a particular radionuclide.

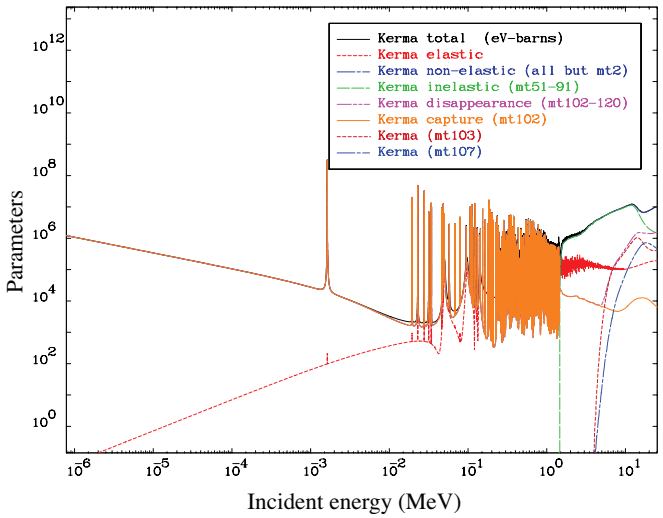

FIG. 26. (Color online) ^{52}Cr at 294 K: Kerma cross sections.

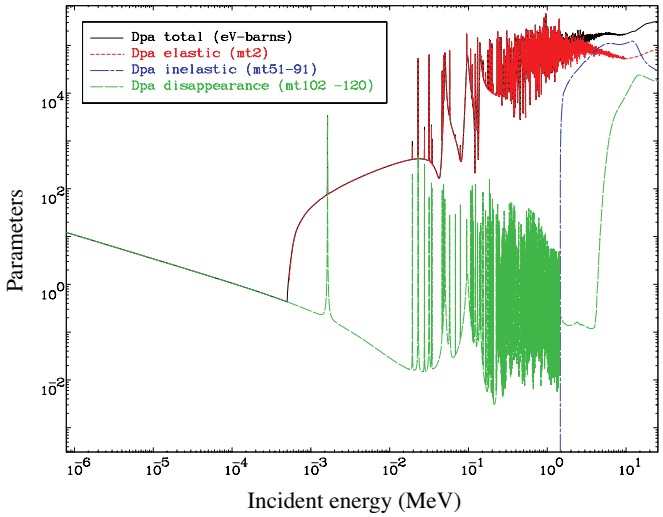

FIG. 27. (Color online) ^{52}Cr at 294 K: displacement cross sections.

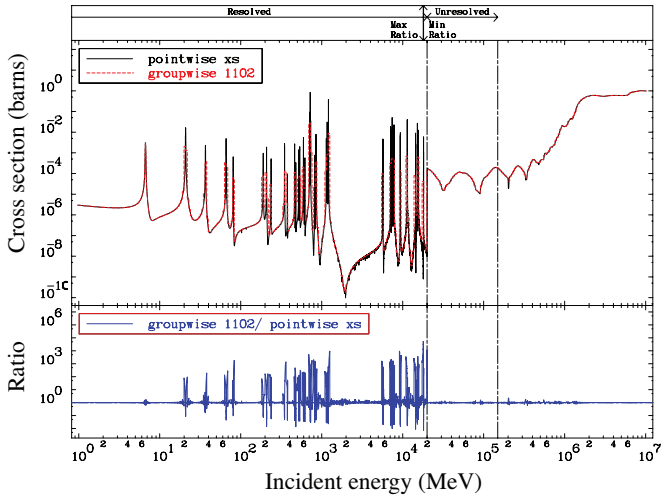

FIG. 28. (Color online) ^{238}U at 294 K: fission pointwise and groupwise cross sections and their ratio.

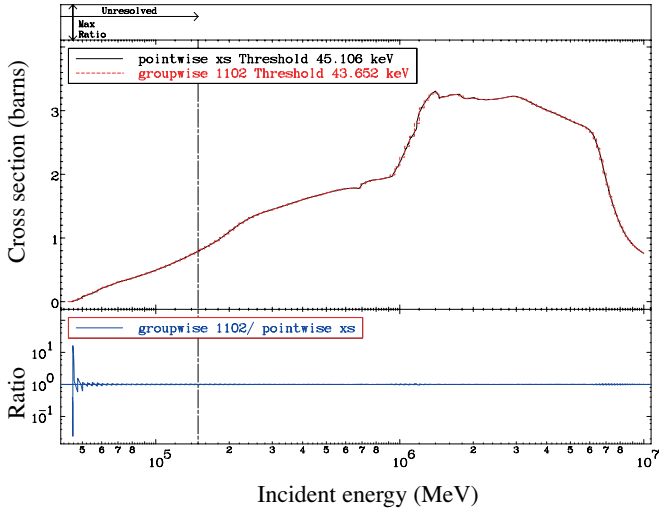

FIG. 29. (Color online) ^{238}U inelastic pointwise and groupwise cross sections and their ratio.

The basic sources for these data are reports published by the ICRP [50, 51] and the NRPB [52, 53]. However, these sources primarily cover radionuclides generated by the fission power producing community and consequently only cover some of the nuclides that can arise in non-fission applications, including: fusion, high-energy physics and medical applications. In order to extend the range of nuclides to all those in the extensive decay library it has been necessary to use an approximate method. Reference [54] describes how available data for an element are used with decay data for a nuclide to derive Committed Effective Doses per unit uptake for ingestion and inhalation for the nuclides with no data. In total more than a thousand nuclides have had data calculated approximately. References [29, 55] document the previous biological hazard library.

2. *Legal transport indices*

Transport of radioactive material from place to place is governed by regulations set up by the IAEA. Reference [56] gives details of A2 transport activity limits for certain radionuclides. Using these values it is possible to calculate how much of a particular mixture of radioactive materials can be packed into a type of container and safely transported. Data from this reference for the nuclides listed are transferred to the A2 indices library, with the default prescription given in reference [55] used for all radionuclides not explicitly listed. References [29, 55]

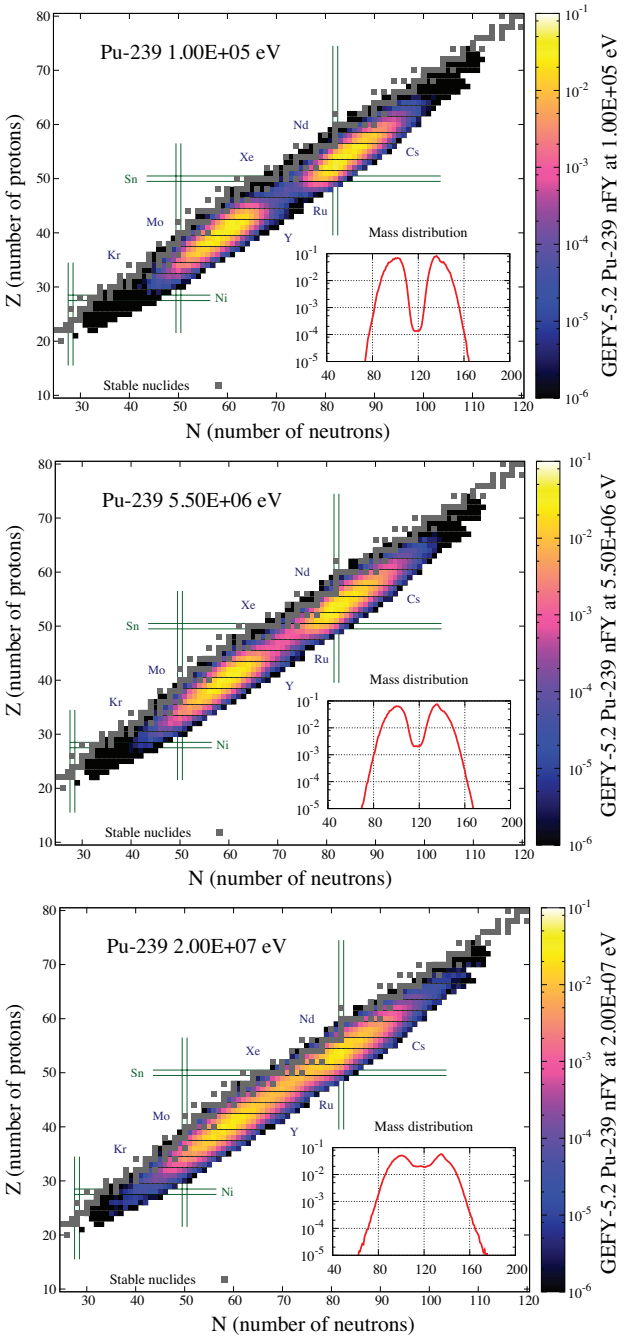

FIG. 30. (Color online) Energy-dependent neutron-induced fission yields from GEFY-5.2, showing the range of distributions. Incident energies shown include 100 keV, 5.5 MeV and 20 MeV.

document the earlier A2 libraries. FISPACT-II can use these data to show the A2 limit for individual nuclides and the effective A2 value for the irradiated material.

3. *Clearance indices*

Disposal of radioactive material in special repositories is expensive. Regulations exist to determine acceptable activity levels for nuclides that then permit materials to be 'cleared' or disposed of as if they were not radioactive. Clearance data are being investigated by the IAEA and recommendations are available. Reference [57] gives details of suggested clearance values for certain radionuclides, while an earlier report [58] gives a formula that allows values for other nuclides to be calculated. Data from these references for the nuclides listed are transferred to the clearance indices library, with the default prescription used for all radionuclides not explicitly listed. References [29, 55] document the earlier clearance-index libraries. FISPACT-II can use these data to show the clearance index for individual nuclides and for the irradiated material.

H. Absorption coefficients

The photon mass attenuation coefficient μ/ρ, and the mass energy-absorption coefficient μ_{en}/ρ for all elements with $Z = 1 - 100$ have been produced using the XGAM program from the National Institute of Standards and Technology [59] The database covers energies of photons (X-ray, γ ray and bremsstrahlung) from 1 keV to 100 GeV and has been processed into a 24-group structure (1 keV - 20 MeV) identical to the FISPACT-II γ group structure. The present compilation follows that used in the previous library, and is an extension of the calculations of Hubble [60]. It replaces the values given in Hubble [61] that were used in earlier FISPACT versions.

The present data differ from the previous set in the following respects:

1. The first 100 elements are included compared to the 40 selected elements previously covered;
2. All edge energies are included and identified and values of μ/ρ and μ_{en}/ρ are given just above and below each discontinuity to facilitate accurate interpolation.
3. Somewhat different values for the atomic photoeffect cross-section have been used for $Z = 2 - 54$;
4. For compounds and mixtures, values for μ/ρ can now be obtained by simple addition, i.e. combining values for the elements according to their proportions by weight. Radiative losses are now included;
5. The total cross-section per atom (σ_{tot}) which is related to μ/ρ can be written as the sum over contributions from the principal photon interactions,

$$\sigma_{tot} = \sigma_{pe} + \sigma_{coh} + \sigma_{incoh} + \sigma_{pair} + \sigma_{trip} + \sigma_{phn} \quad (93)$$

where σ_{pe} is the atomic photoeffect cross-section, σ_{coh} and σ_{incoh} are the coherent (Rayleigh) and incoherent (Compton) scattering cross-sections respectively, σ_{pair} and σ_{trip} are the cross-sections for electron-positron production in the fields of the nucleus and the atomic electrons respectively and σ_{phn} is the photonuclear cross-section. However, the latter contribution has been neglected as well as other less probable photon-atom interactions.

The data file contains the photon mass energy attenuation coefficient (μ/ρ) for all the elements $Z = 1 - 100$ in increasing Z order. The attenuation coefficient (μ) and energy absorption coefficient (μ_{en}/ρ) for air are also listed. All data are stored in the same 24-group energy structure as shown in Table VIII.

I. CALENDF Probability Table Forms

CALENDF is an R-matrix analysis code with unique capabilities that complement the other processing codes. It has been widely used in the multi-physics data processing of the libraries needed by the FISPACT-II code. In the preparation of TENDL, CALENDF has been used both to generate statistical resonances for those target nuclides with no, or only poor, experimental information, and also to extract and assemble the probability tables from all evaluations of resolved and statistical resonance parameters.

Probability table data sets are supplied for each evaluation/library and temperature from the energy of 0.1 eV up to the end of the unresolved energy range of the evaluation in the same fine group structure as the cross sections; 709 or 1102 groups. Several groups are typically not populated as they are outside the resonance energy range of interest. The same probability table forms are used by the Monte Carlo code TRIPOLI [62, 63] in the unresolved energy range and by the fast deterministic code ERANOS [64, 65] in both resolved and unresolved resonance energy range.

The code manipulates these probability tables in various ways, including isotopic smearing, condensation, interpolation and order reduction. Effective cross sections and moments can then be extracted in the resolved and unresolved resonance ranges, while probability table self-shielding factors (ssf) are calculated [11, 66] for any competing channels and isotopic compositions. Note that the effective cross sections and moments derived in this way account not only for contributions to the self-shielding factors from all known channels and energies but also any isotopic mixture. There is an overlap of capabilities with PREPRO, but the different codes are used as appropriate for the different forms of application data.

IV. VERIFICATION AND VALIDATION

Verification and Validation (V&V) activities are essential for the successful development of any well-engineered physics prediction code. An essential activity is verification to ensure that at all stages of the development the code functions in accordance with its user requirements. Successful verification should then be followed by validation involving the comparison of results with external sources of information to ensure that the code produces correct results, or at least results of acceptable accuracy, taking into account the level of physics assumptions and approximations inherent in the design of the code and its input data.

The development of FISPACT-II has proceeded over several stages in recent years, with new features being added at each stage. An extensive set of test cases (currently several hundred) has been produced and extended as the code development has continued. This test set exercises all keywords that users employ in the FISPACT-II `input` file to control a run of the code. The test cases ensure that newly-added keywords have the intended effects.

The test set also provides regression tests so that all the established functionality of the code can be verified each time a new release is prepared.

Verification and validation is a vital part of the processing and production of nuclear data libraries. For an advanced inventory and observables code which covers the complete set of nuclear reactions, this takes several forms:

- validation of input nuclear data against experimental information, both integral and differential;
- verification of the nuclear data, particularly those without experimental information, against systematics, statistical review and consistency checks;
- checking code methodologies for nuclear data interpretation, reading, processing and use in simulations – essential for handling multiple ENDF-6 libraries and technological databases such as TENDL and GEFY;
- validation of code simulations against experiment for all input nuclear data forms.

In the last few years great effort has been expended on producing a set of largely-automated V&V tools. As well as validating the nuclear data libraries themselves, these V&V tools also verify the robustness and accuracy of the FISPACT-II code itself. Each individual report straddles multiple aspects of the general V&V process, for example the integro-differential report tests TENDL effective cross sections against experimental data as well as differential EXFOR and full code simulations against a variety of integral measurements. Each section discusses one aspect of the V&V with a brief summary of salient conclusions from one of the reports. A more general summary of

all experimental and systematic trends of the neutron-induced TENDL-2014 library can be found in [67].

A. Systematic Trends

As a truly general purpose nuclear data library, TENDL provides *complete* data for all target nuclides and reaction channels. This is a double-edged quality, offering new and robust information where none would otherwise exist, but also potentially exposing less predictive regimes of the code system, faults in the input reference data or other general errors in the library production. Previous activation libraries often used (or were simply reflections of) simplified systematics which are typically crude, semi-empirical models with parameters fit to some χ^2 analysis against whatever experimental data are available. For example, the following 14 MeV systematics were employed in the production and validation of EAF libraries [68],

$$\begin{aligned}\sigma_{(n,p)} &= 7.657\left(A^{1/3}+1\right)^2 \times \\ &\quad \times e^{-28.80S-59.24S^2+0.2365A^{1/2}} \\ \sigma_{(n,p)} &= 23.659\left(A^{1/3}+1\right)^2 e^{-23.041\left(S+S^2\right)}.\end{aligned}$$

for $Z < 40$ and $Z \geq 40$, respectively. A is the nuclide mass number and $S = (N-Z)/A$ is the asymmetry number. The constants have been fixed in previous analyses to best match some (static) experimental data. These systematics of course do not represent the complexity of the interaction probabilities, but provide a basis for identifying potential outliers and non-physical trends in a large nuclear reaction database. Examples of the comparisons can be seen in Figs 31 and 32, which show plots of the ratio of calculated (C) to systematic (S) cross sections for 14 MeV (n,p) and the ratio of (n,2p) to (n,p) for TENDL-2014. While the first demonstrates that the systematic prediction does not account for various odd-even or shell effects, it also identifies a potentially curious pattern at the very proton-rich nuclides, which are shown as a blue cluster. These radionuclides will decay through EC or β^+ with a few proton emission decay modes for the far edge, making it noteworthy that the TENDL-2014 (n,p) drops off. This is primarily due to the sharp increase in the competing (n,2p) cross section, which becomes dominant in this region as shown in Fig. 32.

Another simple, yet effective method of identifying trends to find errors is to visualise and inspect various quantities such as cross sections at particular energies, maximum values, yields, etc., over a range of different axes such as mass, neutron or asymmetry number, nuclear shell, skewness, separation energies, etc. An example is shown in Fig. 33, which shows total cross sections at 2 MeV and identifies several nuclides which do not fit the global or local trends. In this example ^{40}Ar has resolved resonances at 2 MeV and the average values are more in agreement, while ^{48}Ca has statistically-resolved resonances which do not follow the expected trends at this energy.

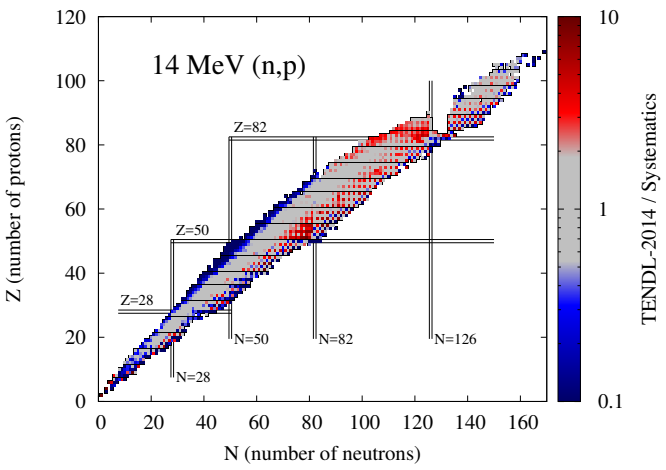

FIG. 31. (Color online) Nuclide chart showing calculation to systematic ratios (C/S) for 14 MeV (n,p) reactions.

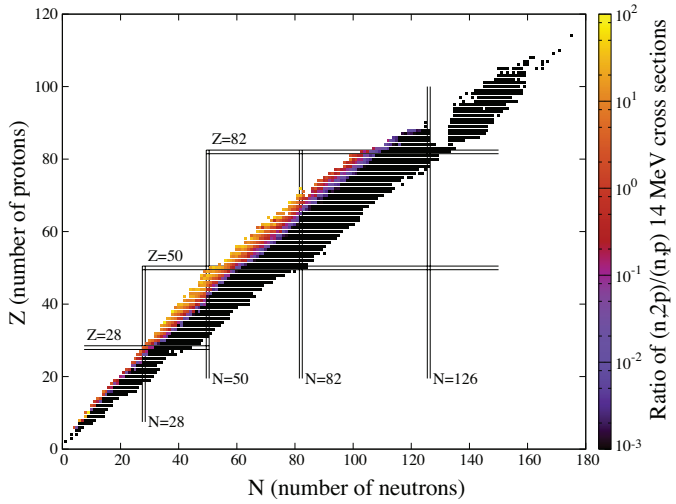

FIG. 32. (Color online) Nuclide chart showing TENDL-2014 ratio of 14 MeV (n,2p) to (n,p) cross sections.

The results of these systematic checks for TENDL-2014 were used to update and correct various input parameter libraries and modify some code methods for the TENDL-2015 and future library releases. The full report [69] includes analyses for each of the major reaction channels.

B. Maxwellian-Averaged

Many reaction channels have little or no experimental data, and for those with some measurements, these do not cover the full range of energies needed to describe the cross sections. In particular, the non-threshold reaction channels require a huge range of measurements to cover the resonance ranges, thermal values and high-

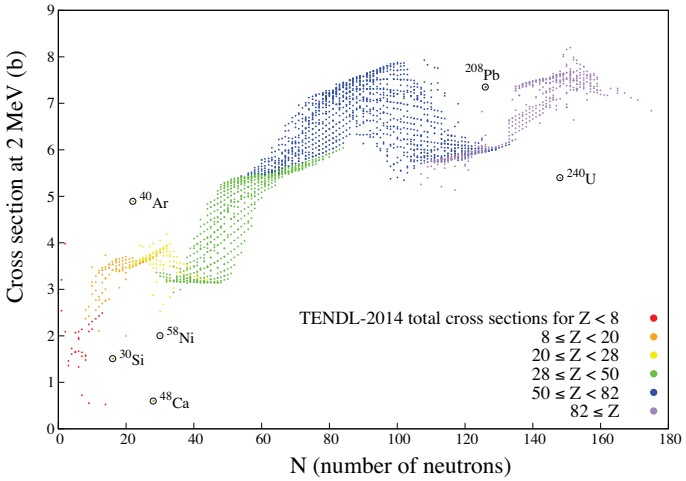

FIG. 33. (Color online) Total cross sections at 2 MeV for all TENDL-2014 nuclides. A few potential outliers are highlighted.

energy components. Resonance parameters are typically generated with generalised least squares methods over a large experimental database [70, 71], but for most nuclides these are unavailable. In many cases not only are there not resolved resonance parameters, but very little or no integral data are available.

The importance of neutron capture and other non-threshold reactions for stellar nucleosynthesis processes has led experimentalists to measure integral cross sections for reactions which would otherwise have little attention. These are used to provide reaction rates in stellar nuclide evolution calculations which model the elemental composition of the observable universe. The importance of these values has led to the production of an evaluated reference database for Maxwellian-averaged cross sections: the Karlsruhe Astrophysical Database of Nucleosynthesis in Stars (KADoNiS) [72]. This contains data for 357 nuclides over a range of 11 temperatures form 5 keV (58 million K) to 100 keV (1.2 billion K). It draws largely upon the well-known compilation of Bao *et al.* [73], which includes an impressive catalogue of experimental and theoretical sources. While several of the nuclides without experimental information within Bao have been updated in the most recent KADoNiS database v0.3, 80 of these nuclides (22%) are based on theoretical, statistical model calculations rather than experimental measurements. Even though not as strong as the C/E validation for the remaining 277 nuclides, these still provide code-to-code comparisons for the TENDL calculated values [74].

The TARES code of the TENDL generation system consistently produces the resonance parameters for the ENDF6 files `MF=2`, `MF=32` and `MF=33`, the last of which can be used with in the FISPACT-II uncertainty covariance collapse to generate specific rate uncertainties for each such non-threshold reaction channel. TARES also employs CALENDF resonance sampling methods [23] to statistically generate extended resolved resonance regions with enhanced capabilities for temperature-dependent broadening and self-shielding. These 'high-fidelity resonances' (HFR) play a central role in the Maxwellian averaged values, particularly where no resonance data are available and step-function discontinuities between the low-energy region set by a thermal cross section and the higher-energy region can produce problematic temperature-dependent shapes. A prime example of this is shown in Fig. 34, where the TENDL HFR produces a more realistic cross section which produces a superior agreement with the KADoNiS values.

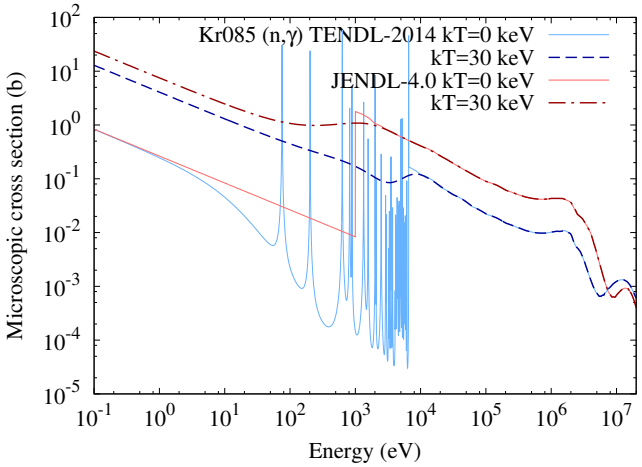

FIG. 34. (Color online) TENDL-2014 and JENDL-4.0u microscopic cross sections for ^{85}Kr, showing the unbroadened 0K and broadened 30 keV data. The TENDL-2014 C/E with KADoNiS is 0.92 at 30 keV.

A study of the MACS for all KADoNiS nuclides was performed using several methods, including the well known utility code `inter` [75], the Japanese `maxwav` [76] and FISPACT-II collapses which offered the complete covariance uncertainty for each reaction. Of course, this is limited to files which possess a full `MF=33` file and only where they are meaningful, so that resonance range treatment is still not fully implemented for any library. However, for some examples the TENDL nominal and uncertainty values are due to TALYS calculations where the full uncertainty is already available in the 2014 release, for example in Cd106 as shown in Fig. 35. The ability to not only offer predictive capture cross sections, but also predict realistic uncertainty bounds which match beautifully with the experimental data is a unique feature of TENDL.

C. Thermal Cross Section, Resonance Integral

Thermal cross sections for non-threshold channels and resonance integrals are standard values which are com-

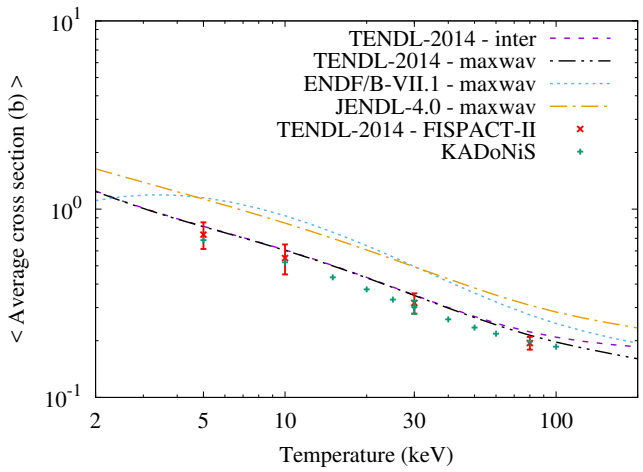

FIG. 35. (Color online) TENDL-2014, JENDL-4.0u and ENDF/B-VII.1 Maxwellian averaged cross sections for ^{106}Cd, showing the range of temperatures which cover the KADoNiS data points.

piled into well-known databases [77]. Thermal cross sections are essential data for thermal reaction rates – of particular importance for heavily moderated spectra such as those found in thermal fission reactors. The integral values summarised by a $1/E$ spectrum collapsed with the resolved resonances between the cadmium cutoff and 100 keV are typically referenced in systems with such spectra but also are widely quoted values which should be reproduced by nuclear data libraries. Verifying the values for TENDL-2014 with multiple electronically-stored databases for these values has proven fruitful for correcting errors in both reference databases and the TENDL-2014 library (and therefore its own reference input data). These were few and isolated cases which have been completely resolved for subsequent releases.

The general result from this validation exercise was to find that the vast majority of values corresponded exactly to those found the in reference databases for thermal with some slightly greater variation in the resonance integrals. The resonance integrals are slightly more complex, involving numerous resonance parameters and choices of resonance formalism. Again the distribution of C/E values was very tightly centred around 1, with some anomalies due primarily to isomeric production pathways.

D. Fusion, Fast Events

Few experimental data exist for structural material samples irradiated under all nuclear plant types relevant neutron spectra, and even when data do exist the measured quantities are either specific activity and/or γ spectroscopy. In particular, no or very few experimental data on decay power have previously existed for fission plant structural materials and for materials under high neutron energy irradiation conditions (i.e. fusion, fast fission). It was to fill this gap that a series of experiments were performed using the Fusion Neutron Source (FNS) facility at the Japan Atomic Energy Agency JAEA [78–80]. Material samples were irradiated in a simulated D-T neutron field and the resulting decay power was measured for cooling times of up to thirteen months. Using the highly sensitive Whole Energy Absorption Spectrometer (WEAS) method, both β and γ emission decay energies were measured at selected cooling times and, quite impressively, as soon as a few tens of seconds after the end of irradiation.

Validation of decay power predictions by means of direct comparison with integral data measurements of sample structural materials under neutron spectra allow confidence to be given to the decay power values calculated. It also permits an assessment of the adequacy of the methods and nuclear data, and indicates any inaccuracy or omission that may have led to erroneous code predictions. It is clear that certain safety margins can be derived from such a validation exercise, if relevant to plant operation, materials and design, and applied as bounding conditions in operational Safety and Environmental (S&E) analyses.

1. *FNS Assembly*

14 MeV neutrons are generated by a 2 mA deuteron beam impinging on a stationary tritium-bearing titanium target. The total neutron flux at the sample location, for this experiment, is in the range of 1.0×10^{10} [n cm^{-2} s^{-1}], the same order of magnitude as in the first wall of the Joint European Torus (JET) fusion experiment when operating with D-T plasma. However, the irradiation time at the FNS were of 5 minutes and 7 hours in comparison with the few seconds flat burn achieved during the DTE1 JET fusion 1996 campaign. As a point of reference the total flux in a power plant is typically expected to be in the region of 10^{13} or 10^{15} [n cm^{-2} s^{-1}], three to five orders of magnitude higher than in JET or FNS, and also for much longer irradiation times.

Thin samples, 25x25 mm^2 in area, and typically 10 μm thick, have been used, either as metallic foil or powder sandwiched between tape. Use of a thin sample minimises the self-absorption of β rays emitted in the sample itself and allows their measurement. A total of 74 different materials have been used across the different phases of the experiment.

The decay energy in each irradiated sample was measured in the Whole Energy Absorption Spectrometer (WEAS) comprised of two large bismuth-germanate BGO scintillators in a geometric arrangement, which provides almost 100 % detection efficiency for both β and γ-rays. Correction factors need to be applied for γ-ray efficiency and for β and electron energy loss in the sample itself (less than 15% generally), and for other effects such as the decay heat due to the plastic tape used for the pow-

der samples. The overall experimental uncertainty totals between 6 to 10% in most cases, although it rises to higher levels at particular cooling time for certain samples. The WEAS provides high sensitivity, down to powers less than 1 pW, which is valuable for measurement of some nuclides with long half-lives. It also has a wide dynamic range: measurements of up to a few mW have been achieved in the experiments.

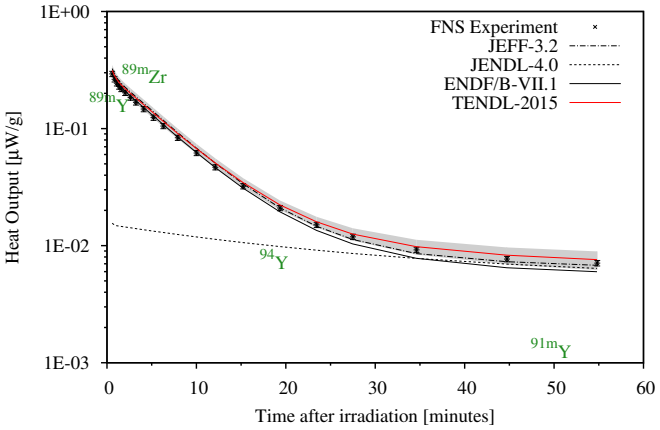

FIG. 36. (Color online) Decay heat production and cooling in zirconium irradiated for five minutes in the JAEA FNS experiment, compared with FISPACT-II predictions.

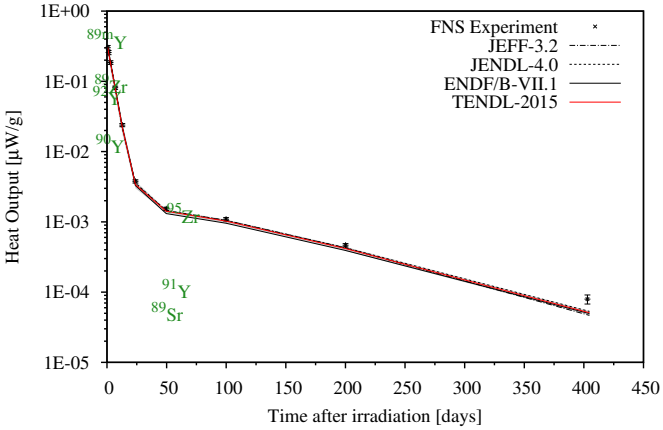

FIG. 37. (Color online) Decay heat production and cooling in zirconium irradiated for seven hours in the JAEA FNS experiment, compared with FISPACT-II predictions.

2. *Comparison of the Results*

For each material sample and irradiation condition, FISPACT-II, combined with the TENDL-2015, ENDF/B-VII.1, JEFF-3.2 and JENDL-4.0, calculations have been performed [81–83]. Graphical comparisons of the results are presented. On the graphs FNS experimental measurements are also plotted and include the uncertainties as vertical lines, while the grey shadow area corresponds to the calculation uncertainty derived from TENDL-2015. The 5 minutes or 7 hours irradiation results can be presented. Care needs to be taken when interpreting the graphs, particularly in view of the log-linear scales. Such plots allow a direct visual interpretation of nuclide half-life at times when one isotope is clearly dominant. A departure from equivalence in the decay profile between experiment and calculation would indicate a mismatch in terms of half-life in one or more of the important nuclide.

The full report details the analyses for each of the 74

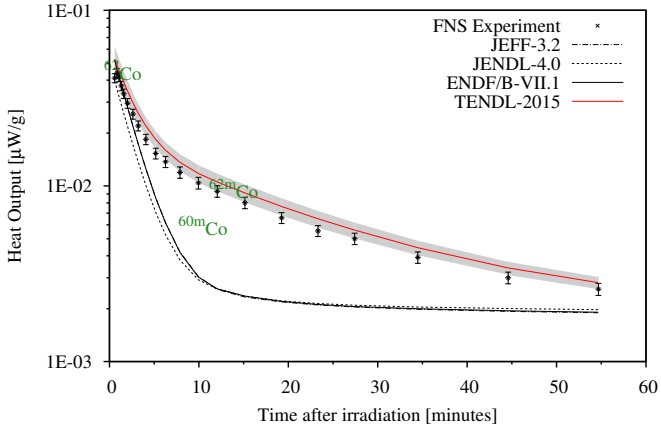

FIG. 38. (Color online) Decay heat production and cooling in nickel irradiated for five minutes in the JAEA FNS experiment, compared with FISPACT-II predictions.

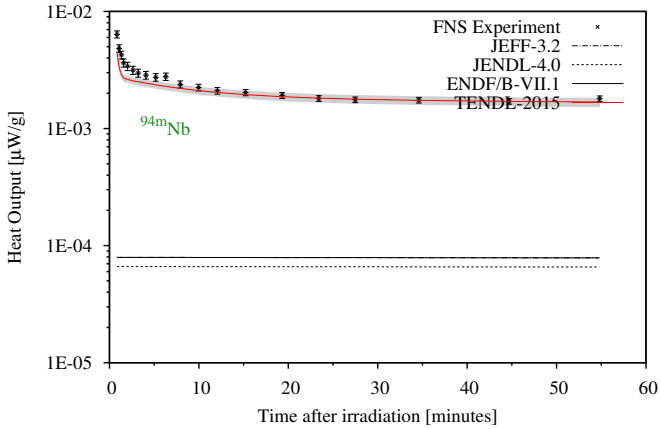

FIG. 39. (Color online) Decay heat production and cooling in niobium irradiated for five minutes in the JAEA FNS experiment, compared with FISPACT-II predictions.

materials samples that have been irradiated in the two campaigns. To complement the analysis of total heat, an appendix has been included showing the TENDL-2014 differential cross sections against EXFOR [84] for all reactions leading to the production of dominant nuclides. Further details of these plots can be found in [85].

There is some interest in focusing on irradiated samples of importance for one application. Zirconium is largely employed as cladding material in many LWR plant worldwide, and as such deserves some attention. From Fig. 36 one immediately notices a good agreement amongst the different nuclear databases except for JENDL-4.0 which is unable to produce ^{89m}Zr, predominant in the first half hour of cooling. Time dependent calculation over experiment (C/E) values (2-18%) also compare nicely with the TENDL-2015 derived uncertainty (8-20%). For the longer irradiation, Fig. 37 shows a good agreement for all nuclear data libraries. Note that the decay heat dropped by over 2 orders of magnitude within a month of cooling.

Nickel and niobium, Fig. 38 and 39 are also elements of importance in the next generation of power plants, either fusion or fast fission, however in those particular cases one has to note the lack of isomeric production channels from the legacy libraries. Only the truly general purpose TENDL library seems to be capable of reproducing the more exact time dependent decay heat profile arising after irradiation of those elements. What is also of concern is the systematic under-prediction, due to the absence of isomeric state branching ratios, from the other libraries.

3. FNS Analyses

The experimental time-dependent decay-power measurement program at JAEA FNS, combined with the FISPACT-II simulations, performed provide a unique check of the calculational method and nuclear databases associated with the prediction of decay power for the set of material samples analysed. The results of the comparison give confidence in most of the decay heat values calculated, although the predominantly 14 MeV neutron spectrum in FNS means that the low neutron energy reactions of importance in other devices have not yet been fully considered [86]. This fact limits the scope of validation and possible conclusions reached in this study of the decay power predicted through the identified pathways. However, it covers the decay data of all the isotopes involved irrespective of their production routes.

The experimental uncertainty, calculational uncertainty and E/C values have been systematically produced. Their direct comparison demonstrates that the method chosen to calculate and propagate these calculational uncertainties in the FISPACT-II code system is verified and validated (V&V), and that the TENDL uncertainties file could be further improved along the same lines.

From the overall results, a set of inadequacies, not only in the cross sections but also in the decay libraries, has been identified that will require some corrective actions to be taken. These corrections and/or amendments will benefit the next generation of the TENDL library cross sections, associated variance and covariances, and decay data files. As expected, they impact both the production paths and/or decay data of some specific radionuclides without impairing the overall picture. A large proportion of the decay powers calculated in this validation exercise with TENDL-2015 are in good agreement (within a few %) with the experimental values for cooling times spanning from tens of seconds, and this is a unique insight in the isomers space, ranging up to more than a year.

E. Integro-differential

For a great many target nuclides and reactions, there are few experimental measurements to rely upon in the nuclear data evaluation process. Many energies are too difficult to probe, for example resonance regions or energies between a few MeV and 14 MeV for neutrons. These limitations in the data force us to be more proactive in validation, drawing upon different, complementary sources to draw conclusions where individual sets of differential measurements are lacking.

A series of irradiations of various materials in several complementary neutron fields have been carried out over several decades. Analyses of the results have produced integrated effective cross sections attributed to various nuclear interactions. Neutron spectra calculated for each experiment can be convolved over energy with library cross sections for comparison with experimental results. The measurement techniques vary between experiments, from calorimetric to spectroscopic, fairly mono-energetic to 'white' spectra. Each presents its own challenges, but the extraction of useful data on individual reaction channels can be done even in calorimetric measurements such as those performed with total decay heat from FNS.

To best gauge the quality and extent of the conclusions that can be drawn from the available set of integral measurements, differential data from EXFOR are compared against the evaluated cross sections with all isomeric production, if present. The combination of these has great value in highlighting areas for re-evaluation or providing the most robust activation validation possible.

The combination of multiple, complementary integral measurements with differential cross-section data from EXFOR has been used to validate the TENDL-2014 neutron-induced nuclear data library. The integral measurements use incident particle spectra from a variety of sources including:

- Fusion D-T with various amounts of scattering, 14 MeV peaked
- Deuterium beam on beryllium target 'fast white' spectrum above 20 MeV
- Deuterium beam on lithium target 'IFMIF-like' spectrum up to 60+ MeV

- Proton beam on deuterium targets 'fast white' spectrum above 20 MeV
- Spontaneous ^{252}Cf fission neutrons

The measurement techniques typically include HPGe gamma spectroscopy to identify individual nuclides, spectroscopic or total heat measurements. Normalisations and spectra are determined through various means, from activation foils to ToF and alpha-monitors. Not all experiments are of the same quality and this fact is extremely important when making judgements on the quality of an evaluated file using few measurements.

Identification of individual reaction channels within integral measurements poses a few challenges, including the separation of production of decaying, precursor nuclides (cumulative effects) and isolation of multiple reaction channels, which occur through multiple target elements, multiple target isotopes and multiple reaction channels per nuclide. Care must be taken not to mistakenly identify only one reaction channel when multiple ones are involved, which could either throw into question an accurate evaluation or 'validate' a spurious cross section. The approach taken by the UKAEA is to establish a set of criteria for inclusion and remove those which fail the tests. In those (few) removed cases which were used in previous EAF validations, it is unlikely that the experiments measured the specific reaction channel(s) in question.

For all integral measurements new pathway analysis using the FISPACT-II pathways search features have been done. These identify the % contribution from each reaction channel and verify that the channel of interest is dominant for the measurement. Even with high-purity samples this can be quite complex due to multiple isotopes or reactions, for example consider the FNG nickel irradiation shown in Fig. 40. As in several cases, the total heat measurements reflect multiple nuclides contributing at every time-step. However, at specific points one nuclide is strongly dominant, for example the ^{62}Co and ^{62m}Co at the first and last measurements shown in this figure. Decay data can provide an additional concern due to potential misallocation of beta/gamma heat (and other simpler issues such as half-life uncertainty). The apparent discrepancies between beta and gamma heat in the first measurement are reconciled in the total, which has a less uncertain energy per decay. ^{60m}Co dominates the gamma heat at 500 s and ^{62m}Co dominates the beta and total in the final data point. The production pathways for nickel are quite simple, with ^{60}Ni(n,p) and ^{62}Ni(n,p) generating the cobalt isotopes and isomers. This allows specific identification of each as an integral measurement of a reaction channel.

This level of analysis has been performed in the recent report for the FNS and FNG heat measurements. Results from other laboratories were tested with pathways analyses and verification of the reaction channels available.

Care must be taken when claiming that a reaction has been 'validated', since the detailed structure of a cross

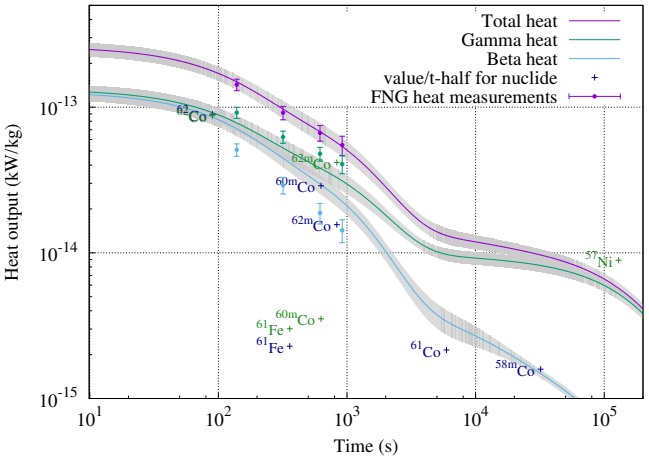

FIG. 40. (Color online) Total and spectroscopic decay heat measurements from an FNG irradiation of nickel with FISPACT-II predictions. Dominant nuclides are placed at coordinates which reflect their half-life and end-of-irradiation heat.

section is not fully probed (even with multiple experiments using complementary spectra) and a new experiment using a different spectrum could find discrepant results. Aside from the differences in experimental design, there is tremendous deviation in the quality of the spectral characterisations, simulation tools used to calculate data (ultimately including the effective cross section) and reporting of measurement methodologies.

The distributions show a generally superior agreement for TENDL-2014, with 12% more values between 0.94 and 1.06. The log-mean C/E value,

$$\log\left(\overline{C/E}\right) = \frac{1}{n}\sum_{i=1}^{n}\log\left(C_i/E_i\right) , \tag{94}$$

for TENDL-2014 is 0.993, while the EAF-2010 data yields a surprising 0.850. This can be intuitively seen in the skewed EAF distribution of C/E values, indicating a systematic under-prediction for the integral values of this report. The fact that TENDL provides a more symmetric distribution should not be surprising; the data are derived from physical parameters which globally govern the production of reaction information and both under- and over-prediction should be equally likely. In comparison, the asymmetry of EAF belies its methodology, where pathways are included depending on an evaluator's judgement. As a result, pathways are missing or under-represented and this results in an overall under-prediction for nuclide production.

It should be noted that the EAF library was constructed and modified with knowledge of these integral measurements, which were used as justification for renormalisations leading to better agreement with the experiments. That TENDL blindly predicts these effective cross sections, using physical parameters, with greater accu-

racy than a library tuned by renormalisations is quite remarkable. When the standard international libraries are used to calculate the effective cross sections considered, the distribution shows a tremendous lack of data, as depicted in Fig. 41. The most notable difference here is that approximately one third of the C/E values are less than 0.1, with the vast majority of these being precisely zero due to missing reactions. This is not unexpected, since these libraries do not contain the data required for activation-transmutation simulations and should not be relied upon or trusted for such analysis. However, it is troublesome since it is often claimed that those libraries are validated for various applications that require these (and many other) reactions.

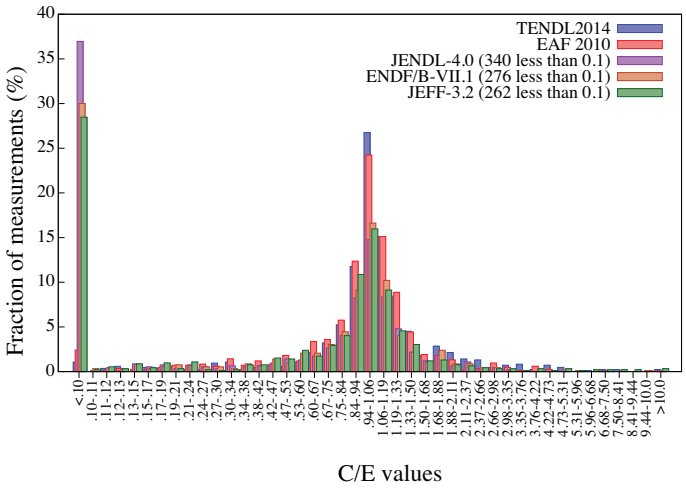

FIG. 41. (Color online) Distribution of integral measurement C/E values for TENDL-2014, EAF-2010, ENDF/B-VII.1, JENDL-4.0u and JEFF-3.2 neutron libraries. Note that values less than 0.1 also include zero, which is the case for around 1/3 in the legacy libraries.

F. Fission Events

Decay heat and inventory calculations for irradiated fission fuels comprise two of the fundamental tasks for time-dependent Bateman solvers in the nuclear industry. Detailed and accurate knowledge of these time-dependent characteristics, as well as trustworthy uncertainty values, are of primary importance for reactor safety cases and the handling of irradiated fuel issues which cover a great many activities representing billions of dollars in current and future effort.

Development of the FISPACT-II code has resulted in new and unique simulation methods for a variety of nuclear observables, including fission decay heat and inventory calculations. To perform these simulations, massive libraries which contain the complete probability distributions for fission product formation, as well as the complete decay data for all of these products (reaching from the long-lived to those with sub-second half-lives), must be maintained and validated with sophisticated and sturdy simulation software. All of the physics of nuclear interactions, fissions and decays is contained within the nuclear data files, which hide one half of the simulation within the evaluation method behind those files.

While most time-dependent inventory and observables codes rely upon one bespoke nuclear data library, the ability to harness any dataset affords a unique opportunity to cross-check data and provide feedback which ultimately improves the code/data system. By performing a verification and validation on FISPACT-II with all of the major international nuclear data libraries, this exercise goes beyond demonstrating the capabilities of the code/data system in simulating decay heat and inventories, giving precise information on which nuclides should have their fission yield or decay data re-evaluated and in which library.

1. *Fission Experiments*

To ensure that this validation [87] is as robust as possible, a thorough effort has been made to revisit as many high-quality decay heat experiments with complementary neutron spectra, irradiation schedules, measurement techniques and nations of origin. Simulations from theoretical fission bursts to full-day irradiations have been performed, using a variety of nuclear data combinations, and compared with the available experiments, which are summarised in Table XVI. Good agreement between calculation and experiment (C/E) is found for total heat from the major fresh fuel components in actual LWRs, however spectroscopic partial heat and decay heat in thorium fuel cycle nuclides remains discrepant both in C/E and code to code ratios C/C where different nuclear data libraries are used. For minor actinides where no experimental data were available, C/C comparisons also show substantial differences between data libraries.

Detailed (spectroscopic and total) decay heat breakdown by nuclide is also performed for select cooling times and fissile nuclides, using different decay or fission yield libraries to demonstrate the precise cause of the C/C discrepancies. These are found to primarily be due to incomplete adoption of Total Absorption Gamma Spectroscopy (TAGS) results for Pandemonium nuclides [88], but many other decay data and fission yield differences have been identified. Given the tendency for relative agreement on total values, it is clear that many compensating effects are still present.

a. Thermal pulse experiments A large set of thermal decay heat experiments have been performed for ^{235}U and ^{239}Pu, so that some statistical meta-analysis is necessary to handle the range of experimental values and uncertainties. While a chi-squared analysis may be proposed, the systematic issues with multiple experimental techniques, quality of campaigns and other factors must be taken into account. For these reasons, evaluated datasets

TABLE XVI. Decay heat data sources with a primary author, experimental information and indicative year.

Author	Nuclide(s)	Method	Irrad. (s)	Year
Fisher	$^{232}\mathrm{Th_f}$, $^{233}\mathrm{U_f}$, $^{235}\mathrm{U_f}$, $^{238}\mathrm{U_f}$, $^{239}\mathrm{Pu_f}$	γ	< 1	1964
McNair	$^{235}\mathrm{U_{th}}$, $^{239}\mathrm{Pu_{th}}$	β	10–10^5	1969
MacMahon	$^{235}\mathrm{U_{th}}$	β	10–10^4	1970
Scobie	$^{235}\mathrm{U_{th}}$	β	10^4–10^5	1971
Lott	$^{235}\mathrm{U_{th}}$	Total	100–5000	1973
Yarnell	$^{233}\mathrm{U_{th}}$, $^{235}\mathrm{U_{th}}$, $^{239}\mathrm{Pu_{th}}$	Total	2×10^4	1978
Jurney	$^{233}\mathrm{U_{th}}$, $^{235}\mathrm{U_{th}}$, $^{239}\mathrm{Pu_{th}}$	γ	2×10^4	1979
Murphy	$^{235}\mathrm{U_f}$, $^{239}\mathrm{Pu_f}$	β	10^5	1979
Dickens	$^{235}\mathrm{U_{th}}$, $^{239}\mathrm{Pu_{th}}$, $^{241}\mathrm{Pu_{th}}$	γ & β	1–100	1980
Baumung	$^{235}\mathrm{U_{th}}$	Total	200	1981
Akiyama	$^{233}\mathrm{U_f}$, $^{235}\mathrm{U_f}$, $^{238}\mathrm{U_f}$, $^{239}\mathrm{Pu_f}$	γ & β	10–300	1982
Akiyama	$^{232}\mathrm{Th_f}$, $^{\mathrm{nat}}\mathrm{U_f}$	γ	10–300	1983
Johansson	$^{235}\mathrm{U_{th}}$	γ & β	4–120	1987
Tobias	$^{235}\mathrm{U_{th}}$, $^{239}\mathrm{Pu_{th}}$	Stat.	—	1989
Schier	$^{235}\mathrm{U_{th}}$, $^{238}\mathrm{Pu_f}$, $^{239}\mathrm{Pu_{th}}$	γ & β	<1	1997
Ohkawachi	$^{235}\mathrm{U_f}$, $^{237}\mathrm{Np_f}$	γ & β	10–300	2002

have been produced, for example the Tobias evaluations or ANS/ANSI-5.1. Comparisons with predictions from FISPACT-II and other high-quality experiments (Fig. 42) show excellent agreement in total heat for all libraries, with some unresolved gamma/beta partial heat discrepancies due to TAGS data adoption.

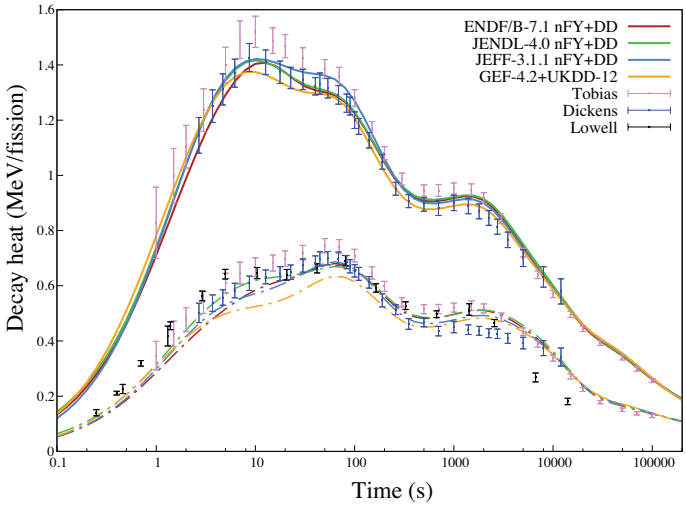

FIG. 42. (Color online) Total and gamma decay heat following thermal neutron pulse fission on ^{235}U, comparing well-known experimental data with FISPACT-II and all major libraries.

The remaining spectroscopic issues are largely related to the misallocation of gamma/beta energy in decay processes due to a lack of knowledge about beta decay feeding to high-energy excited daughter states. These low probability events are difficult to measure, and consequently the average gamma energies are skewed toward lower values, resulting in an incorrect apportionment of decay heat to the beta decay. Totals remain largely insensitive to the choice of decay library, but ENDF/B-VII.1 and JENDL-4.0u generally have more complete adoption of the most recent data which corrects these problems. As FISPACT-II has been engineered to accomodate any and all nuclear data, the user is able to choose the most appropriate physics based on the results of UKAEA validation.

b. Fast pulse experiments The range of fast fission pulse experiments includes the Akiyama et al. measurements using the YAYOI reactor for a variety of nuclides including ^{233}U, ^{235}U, ^{238}U, ^{239}Pu (Fig. 43) and ^{232}Th. These are complemented by UM Lowell data for ^{238}U and measurements of gamma heat from experiments using a Godiva device from Fisher & Engle. Non-pulse fast measurements are also compared, for example from the UKAEA Zebra reactor.

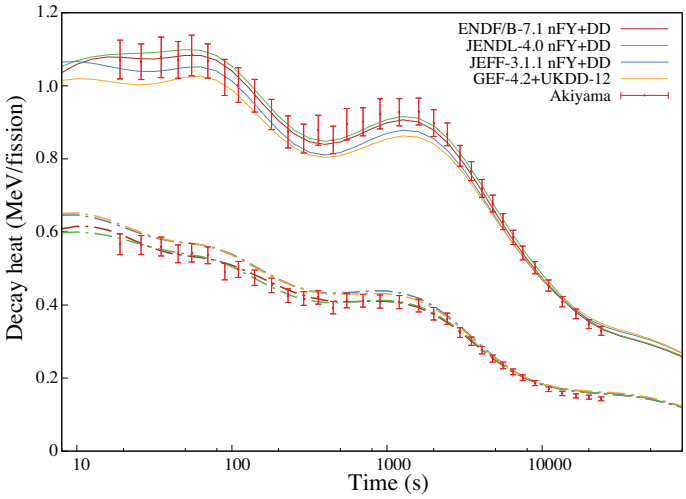

FIG. 43. (Color online) Total and beta decay heat following fast neutron pulse fission on ^{239}Pu, comparing well-known experimental data with FISPACT-II and all major libraries.

Except for some irregularities with the capture correction in the ^{232}Th gamma measurement, these are largely in agreement for all of the systems considered. Some differences were noted using previous GEFY-4.2 data which led to significantly different total heat predictions in short cooling times, typically less than 10 seconds. In some cases these are not within the scope of the available experiments to adequately probe, and it should be noted that the GEF code has enjoyed significant and continued development in recent years and months. At present it is not the recommended library for typical thermal or fast reactor decay heat simulations, but its impressive capabilities make it the only option for many advanced applications, and updated versions are continually in de-

velopment and testing.

c. Finite duration experiments Several non-pulse experiments were considered which employed a variety of neutron spectra, types/techniques, irradiation durations and cooling times. These vary from seconds to years post-irradiation (in some cases both in one experimental campaign), boil-off calorimetry to shielded gamma measurements and fast reactors to thermal columns. Quite importantly, they also include experiments from several countries and continents, including the UKAEA, LANL, Studsvik, CEA, ORNL, CENBG, Uppsala, KfK, SRRC and JAEA. Agreement with FISPACT-II predictions are generally very good, particularly better than the pulse cases where nuclides which suffer from the Pandemonium effect are less significant and numerous.

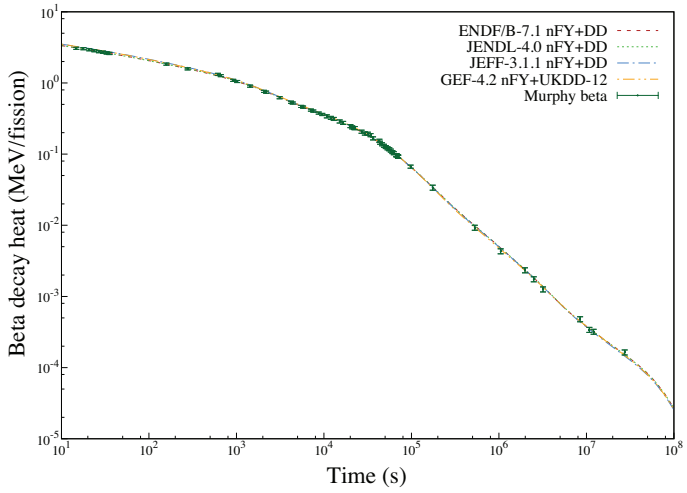

FIG. 44. (Color online) β decay heat following fast neutron irradiation for 10^5 seconds on ^{239}Pu at the UKAEA Zebra reactor, comparing experimental data with FISPACT-II and all major libraries.

The example in Fig. 44 shows a 100,000 second irradiation in the UKAEA Zebra reactor followed by beta heat measurements at a huge range of cooling times from just over ten seconds to nearly one year. The impressive agreement for all nuclear data libraries is in part attributable to the lower total number of nuclides with a significant role in a long (cumulative/equilibrium) irradiation.

2. *Nuclear Data Probing*

The use of different nuclear data libraries can have a profound effect on the simulation of decay heat for all fissile nuclides, including the main constituents of LWR fuel, for example. To better understand the root cause of these differences, FISPACT-II can be employed by swapping individual decay or fission files and comparing heat and inventories at a selection of cooling times. By doing this, the effects of library differences can be easily discovered and nuclides which both contribute non-negligibly to decay heat and have discrepant yields or decays can be identified.

The robust and open nature of the nuclear data functionalities of FISPACT-II allow it to follow all nuclides and precisely identify those nuclides which are responsible for discrepancies. For the nuclides which suffer from the Pandemonium effect, the beta heat is over-expressed due to mis-allocation of the heat due to high-energy gammas. This is not the only error possible with decay data files—misreading of data from ENSDF, dubious splitting of totals and simple typographical mistakes could also be at fault—but it is the most prevalent problem. To find the root cause, the decay data files must be interrogated by hand (ultimately by decay data evaluators). The example in Fig 45 is the set of ^{233}U gamma heat contributors with nominal values on the left y-axis and ratios to the ENDF/B-VII.1 simulations on the right y-axis. In this comparison JEFF-3.1.1 fission yields are used exclusively to ensure that any effects are solely due to the decay files. Note also the absence of ^{98}Zr gamma heat in all libraries except ENDF/B-VII.1, which is due to files where only the ground state is populated in the beta decay.

Two supplements to the V&V report were prepared as compilations of nuclear data comparisons for general use; one with constant fission yields which compared the effects of varied decay data on decay heat [89] and another with constant decay data which tested fission yields [90].

G. Materials Database Handbooks

As well as the validation against experiment exercises discussed above, a further set of verifications has been developed to, in particular, demonstrate the robustness and test extended features of FISPACT-II. A fixed group of irradiation scenarios, simulations and visual presentations, chosen for a specific engineering need such as for a fusion or fission power plant, is automatically applied to a large set of materials to produce a scoping study of the nuclear irradiation response space.

The various outputs are automatically compiled into extensive reports, building on the work in earlier, non-automated reports [91, 92]. This automation makes it relatively straightforward to produce reports for different irradiation conditions and different materials. So far, two fusion power-plant [35, 93] and three fission-plant [94–96] handbooks have been produced to present TENDL results for all naturally occurring elements up to Bismuth, with each report containing between 650 and 800 pages! Most recently, a handbook has been produced for the first-wall conditions expected in the under-construction ITER fusion experiment [97], which, as well as the elemental responses, also includes data for the material alloys that are to be used in its construction. The calculations for each handbook have also been repeated for different nuclear data libraries, with some of the compar-

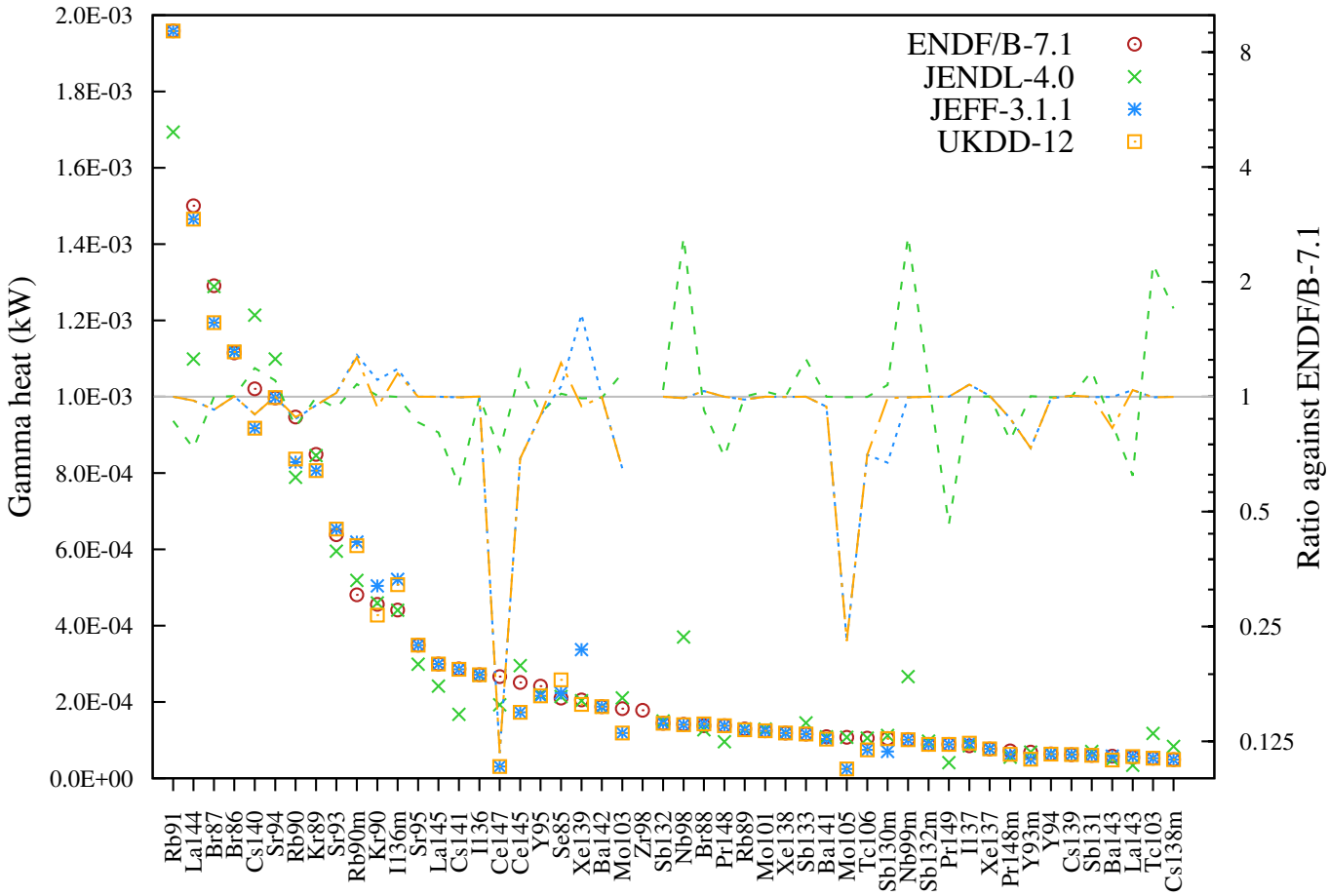

FIG. 45. (Color online) Comparison of the gamma heat at 100 s cooling following a fast neutron pulse on ^{233}U. Ratios are given on the right y-axis. Nuclides are listed by magnitude of heat in the ENDF/B-VII.1 simulation.

ison between TENDL-2014, ENDF/B-VII.1, JEFF-3.2, and JENDL-4.0 presented in [98].

A description of the different data components for each material in these 'handbooks' – focussing on the latest database of response results under fusion power plant conditions [35] is presented below, with examples.

1. *Activation Tables*

The first section for each element in the fusion DEMO handbook [35] is a set of six activation tables, which display the important radionuclides produced by the irradiation of the element for 2 fpy (full power years) in a typical fusion DEMO power plant first wall (FW) armour neutron spectrum. Data are presented at different decay times following irradiation, as shown in the total or specific activity (measured in Bq kg^{-1}) table for pure Cu in Table XVII—with the other tables showing results for decay power, γ dose rate, ingestion and inhalation dose, and IAEA Clearance index. As well as the total activity at each decay time the table displays all of the nuclides, with their percentage contributions, that contribute more than 1% of the activity at any cooling time. The Table XVII example, for instance, shows that immediately after shutdown, and for a short time afterward, ^{64}Cu is the dominant radionuclide in terms of total activity. At 3.7 days ^{60}Co becomes dominant, followed by ^{63}Ni at 100 years and then ^{59}Ni at the longest cooling time. The time evolution of the picture is primarily controlled by the relative half-lives of the different contributing nuclides – ^{64}Cu, for example, has a 12.7 hour half-life, compared to the 5.27 years of ^{60}Co, which explains why the former is over-taken by the latter at the 3.7-day cooling time.

2. *Activation Graphs*

In this part three pairs of plots are given, one for each of specific activity, decay power or heat output (in kW kg^{-1}), and γ dose rate (Sv h^{-1}). For each radiological quantity, one plot presents, as curves and points

TABLE XVII. The total activity in Bq kg^{-1} for various cooling times after irradiation of copper and the percentage contributions to those totals from significant nuclides.

	Cooling time					
	0s	5.3m	3.7d	1y	100y	10^4y
Total activity	6.20×10^{14}	5.28×10^{14}	9.19×10^{13}	5.45×10^{12}	3.08×10^{11}	3.79×10^{4}
^{64}Cu	55.6	65.0	31.4			
^{62}Cu	34.1	27.6				
^{66}Cu	5.9	3.4				
^{60m}Co	2.1	1.8				11.4
^{60}Co	0.9	1.0	58.6	86.9		11.4
^{63}Ni	0.1	0.1	6.7	11.2	100.0	
^{65}Zn			2.1	1.3		
^{59}Ni						65.8
^{60}Fe						11.4

with uncertainties the total decay response of the material after 2 fpy exposures to three different fusion DEMO irradiation spectra: the same FW armour spectrum used for the activation table (total flux 5.04×10^{14} n cm^{-2} s^{-1}); a characteristic spectrum from the deeper rear-casing (backplate) of the tritium breeding blanket modules (1.12×10^{13}); and a third spectrum from the vacuum vessel VV (2.45×10^{11}) of the reactor. The second graph in the pair shows the FW response again, but additionally shows the important radionuclides that contribute to the activity. Nuclides appear in such plots at the position on the time (x) axis corresponding to their half-life and on the activity (y) axis corresponding to their contribution to activity at shutdown after the 2 fpy irradiation. This type of plot is a feature built directly into FISPACT-II and provides a visual indication of which nuclides produce a particular level of activity in the element.

Figure 46 shows the pair of plots produce for total heat output from pure chromium. Note that in all such plots in [93] the equivalent results for pure iron are given in grey in the first plot as a visual comparison to this most important of structural materials. From Fig. 46(a), we see that Cr performed better than Fe at almost all cooling times under DEMO FW and blanket-case conditions, demonstrating that it would not increase decay heat (relative to Fe) were it used in certain steel alloys for in-vessel components of fusion reactor. However, in the much-deeper VV, where the neutron spectrum is highly moderated, it is, in fact, Fe that performs better at short cooling times. Meanwhile, in Fig. 46(b), notice how the the heat is dominated by vanadium nuclides at short cooling times, and that at longer cooling times the production of tritium ^{3}H directly from Cr (as opposed to its large production and use in fusion reactors in general) is responsible for much of the decay heat from the material.

3. *Activation graphs: radionuclide breakdown*

Another new visualization feature prototyped for the latest DEMO handbook [35], which was not available in the first series of automated handbooks [93–96], is the ability to plot the full time-evolution of the contributions of individual radionuclides to a particular radiological response. Two examples of these plots are given in Figure 47, for (a) the decay heat response of Mn, and (b) the total Becquerel activity of Sn – in each case following 2 fpy irradiations under DEMO FW conditions. These plots are created automatically using processed data from the raw FISPACT-II output, with the time-evolution curve for a particular radionuclide shown if it contributes significantly to a radiological quantity at anytime during the simulated decay.

Such plots give much more information than the standard activation plots with nuclide-name labels at half-life against shutdown-activity coordinates (see section IV G 2, above), and, in general, can be understood even in very complex situations, which is not always the case for the other plots where overlapping labels can make reading difficult. For example, from Fig. 47(a), one can immediately identify that, in increasing decay-time order, first ^{56}Mn ($T_{1/2}$ = 2.6 hours), then ^{54}Mn ($T_{1/2}$ = 312 days), then ^{3}H ($T_{1/2}$ = 12.3 years), and finally ^{53}Mn ($T_{1/2} = 3.7\times10^6$ years) dominate (at near-100% levels) the decay heat output from Mn at various times during the cooling, before decaying away according to their half-lives (except for ^{53}Mn on this timescale).

Meanwhile, in the very complex situation depicted in Fig. 47(b), for the total activity cooling of pure Sn, it is still possible to pick-out the dominance of ^{121}Sn ($T_{1/2}$ = 1.1 days) and ^{121m}Sn ($T_{1/2}$ = 43.9 years) on decay timescales of 10-1000 years, with the long-lived latter continuously feeding the short-lived former.

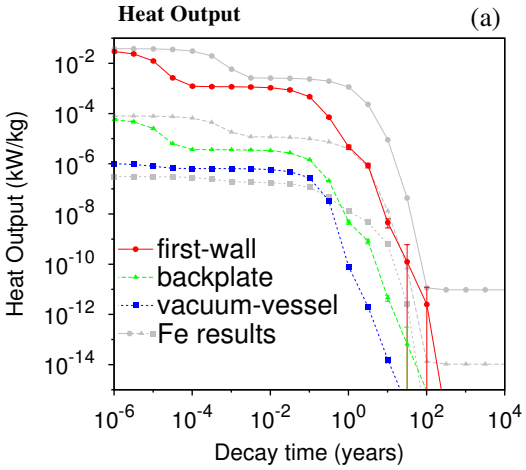

(a)Cr at the first wall, blanket and manifold, with equivalent results for Fe shown lightly.

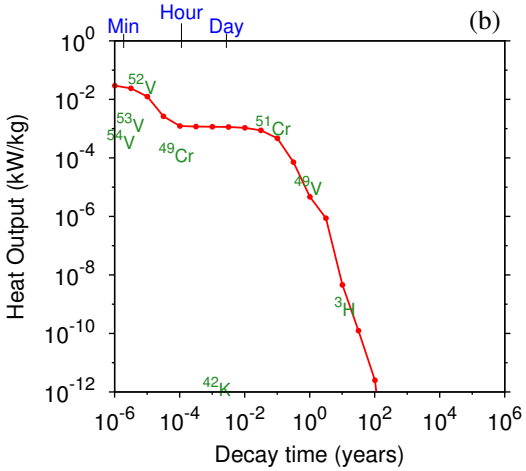

(b)Cr, following the DEMO FW irradiation, and also showing important nuclides, plotted at their half-live and shutdown activity.

FIG. 46. (Color online) The time-evolution in heat output from chromium and iron following two full-power-years of irradiation in three DEMO fusion reactor locations.

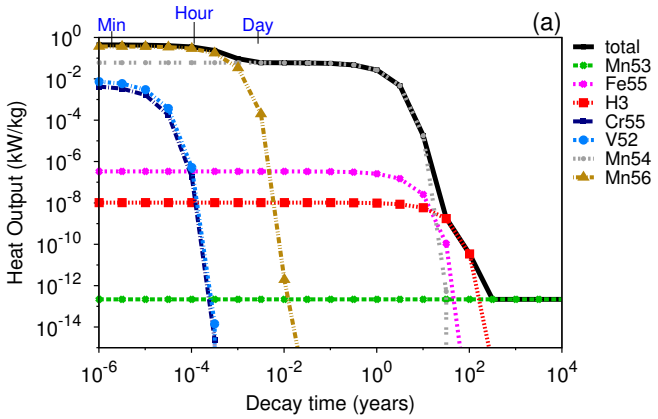

(a)Mn decay heat

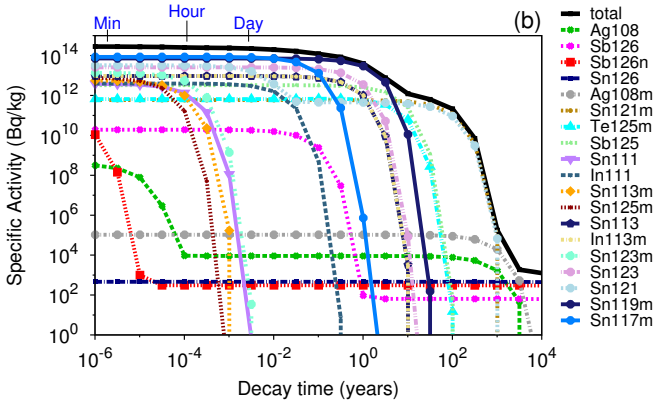

(b)Sn total activity

FIG. 47. (Color online) The time-evolution in radionuclide contributions to radiological responses following 2-year irradiations in DEMO FW conditions

4. *Importance Diagrams*

Importance diagrams [99, 100] are another unique feature available within the FISPACT-II system. Full details of these diagrams are given in [99] and the routines to generate them have been recently prototyped and discussed by Gilbert *et. al.* [100]. In essence they show the regions of the incident-neutron-energy versus decay-time landscape where a single radionuclide dominates a particular activation quantity, and provide a general visual representation of the post-irradiation response of a material that is independent of the neutron spectrum.

In [35], the diagrams for each material are produced by performing a sequence of 2 fpy, single neutron energy-group irradiations at a total flux of 10^{15} n cm^{-2} s^{-1}. The resulting set of inventory outputs are then processed to define and plot regions of the neutron-energy decay-time landscape where particular nuclides contribute more than 50% of (i.e., are important for) a radiological quantity – in the handbook the diagrams are presented for the same three quantities considered in the activation graphs (Section IV G 2).

For each radiological quantity, two diagrams are presented in the handbook: one with a logarithmic energy scale ranging from 10 meV to 30 MeV, exemplified by the γ dose rate importance diagram for tungsten shown in Fig. 48(a); and a second with a linear energy scale ranging from 1 to 30 MeV—see Fig. 48(b) for W dose rate—which provides additional visual detail in the important MeV ranges of fusion and fast fission neutrons. Figure 48(a) shows that, for pure W, three radionuclides dominate the majority of the dose rate importance map below 1 MeV, ^{187}W, ^{182}Ta, and ^{186m}Re at short, medium, and long decay times, respectively. Figure 48(b), shows that the importance of ^{182}Ta extends to longer cooling times at higher neutron energies, while ^{184}Re is important in a region containing the 14 MeV fusion DT neutrons at cooling times up to 1 year.

In Fig. 48(a) notice also the thin horizontal bands of importance regions. These are primarily caused by the giant resolved resonances in the neutron capture (n,γ) cross-section channels on the naturally occurring isotopes of W. They are only visible in this diagram (and in others in [35]) because of the new, efficient computational approach, which enables the high resolution 709-group energy structure of the TENDL libraries to be considered in the sequence of single energy-group simulations.

5. *Transmutation Results*

The transmutation or burn-up response, where a material's composition changes with time due to irradiation, is calculated for each material for the same DEMO FW 2-fpy irradiation scenario as elsewhere. The resulting FISPACT-II simulation output is then processed to define the evolution in concentration of the different elements in the inventory as a function of time. Figure 49(a) demonstrates the typical graphical presentation of the results, in this case for the transmutation of pure nickel. The figure shows that the primary transmutant metals produced in Ni are Co (mainly from the relatively high cross section threshold (n,p) and (n,np) reaction channels) and Fe (from (n,α) channels), with associated significant production of the gas elements hydrogen and helium.

In this section of each material in the handbook the end-of-life composition from the 2-fpy irradiation is also presented in a 'chart of the nuclides' tableau [100], which is a newly developed visualization approach, again prototyped with new routines within the FISPACT-II system. Nuclides are displayed individually in boxes with atomic number Z increasing vertically and the neutron number N increasing horizontally, with the shading of the box indicating the concentration in atomic parts per million (appm) of that nuclide at the indicated inventory time. This representation allows the full complexity of an inventory simulation to be graphically represented, and is particularly powerful when animated as a function of time. However, in the static images of the handbook only a single snapshot is given, at 2 fpy, see for example the result for Ni in Fig. 49(b). Interestingly, this figure shows that the Fe produced in Ni is not made up of ^{56}Fe, which is iron's dominant natural isotope (~92 atm.%), but rather two of its minor constituents ^{57}Fe and ^{58}Fe.

For the most recent addition to the series of handbooks, which presents results under conditions predicted for the ITER experimental reactor [97], complex alloys are also evaluated. In such situations, a single block of the nuclide map is insufficient to fully represent the nuclides present in the material at the end of the irradiation, which in the case of ITER is a 14-year experimental campaign. Therefore, for alloys in [97], a full nuclide map – split into four – is presented instead. Figure50 shows a typical result, in this case for the transmuted composition of Inconel-718 (52.5 wt.% Ni, 19% Cr, 17.7% Fe, 5.1% Nb, 3% Mo, and other minor impurities). Note that the nuclides shown in the tableau are not all of those present in the TENDL libraries, but rather a subset, with those far from the line-of-stability removed to improve readability. The figure shows that Inconel-718 is represented by five distinct groupings in the plot (the one centered on Fe/Cr/Ni overlaps two of the blocks).

6. *PKA Distributions*

As discussed elsewhere (see Section II M and [31]), the calculation of radiation damage source terms – the energy spectra of primary knock-on atoms (PKAs) – has recently been incorporated into the FISPACT-II system. In the handbook [35], PKA distributions for DEMO FW conditions at time $t = 0$ (i.e. before any transmutation has taken place) summed as a function of element (see the Al example in Fig. 13) and isotope are presented in separate plots for each material.

Many aspects of nuclear research and development have long relied on an accurate knowledge of only the principal cross-sections of a selected few nuclides important for the fission industry. When considering fields and technologies which are less established, such as fusion [101], the need to probe and predict further afield has shifted the emphasis to other types of nuclear data. Deep penetration issues, emitted particles and their energy spectra are examples of these new data needs which are at the forefront of fusion (and other advanced system) requirements.

7. *Pathway Analysis*

For each element a pathway analysis (see Section V) is presented for every radionuclide considered important for that element because it appears in either the importance diagrams (Section IV G 4) or activation tables (IV G 1) of the same element. A standard pathway analysis is performed for the element using the **UNCERTAINTY** keyword (see Section II J and the FISPACT-II manual for details [1]) in a 2-fpy, 10^{15} n cm^{-2} s^{-1} irradiation followed by several cooling steps, where the **LOOKAHEAD** keyword—see the manual [1]—identifies important nuclides from these cooling steps to add to those from the irradiation steps, where the default pathway analysis is performed. For each material, this simulation is repeated for four different neutron energy regions: thermal neutrons from 20 to 50 meV; intermediate neutrons from 20 to 40 keV; fast neutrons at typical fission energies of 1 to 3 MeV; and the fusion relevant range from 13 to 15 MeV. In each simulation the 10^{15} n cm^{-2} s^{-1} flux is distributed uniformly across the energy groups covering the energy range of interest. The outputs are then processed to extract the pathways for the important nuclides and these are presented in a table with the non-zero percentage contributions of each pathway to the production of the nuclide given for each neutron energy range. Path-

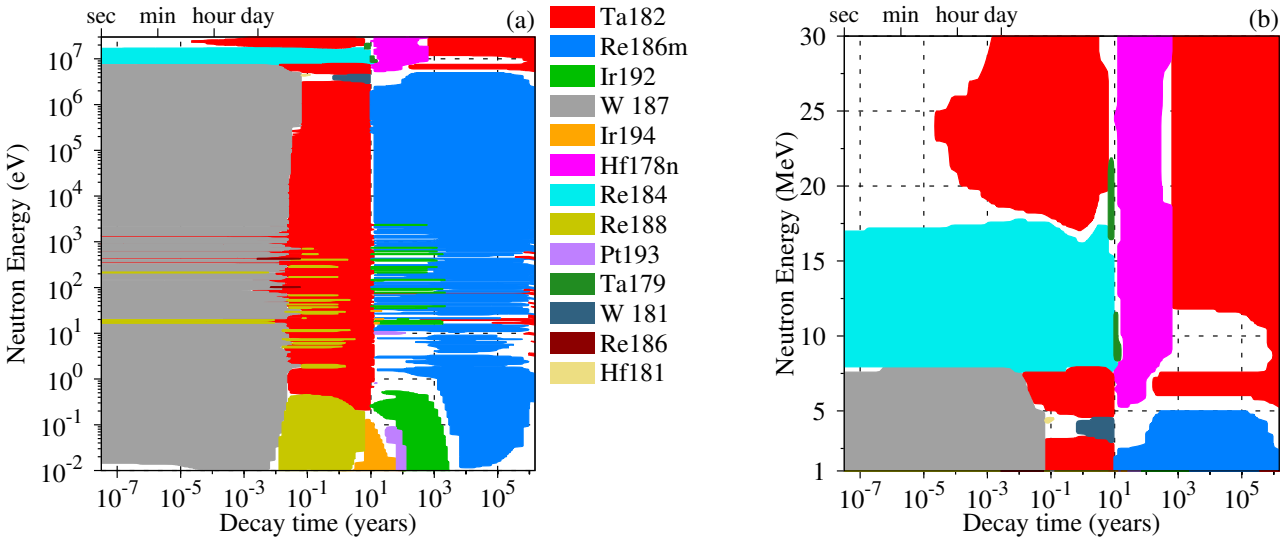

(a)Logarithmic energy scale. (b)Linear energy scale.

FIG. 48. (Color online) The γ-dose rate importance diagram of pure tungsten. The logarithmic energy scale shows regions of dominance at all energies from 10 meV to 30 MeV. The linear energy scale emphasises the important fusion range from 1 to 30 MeV.

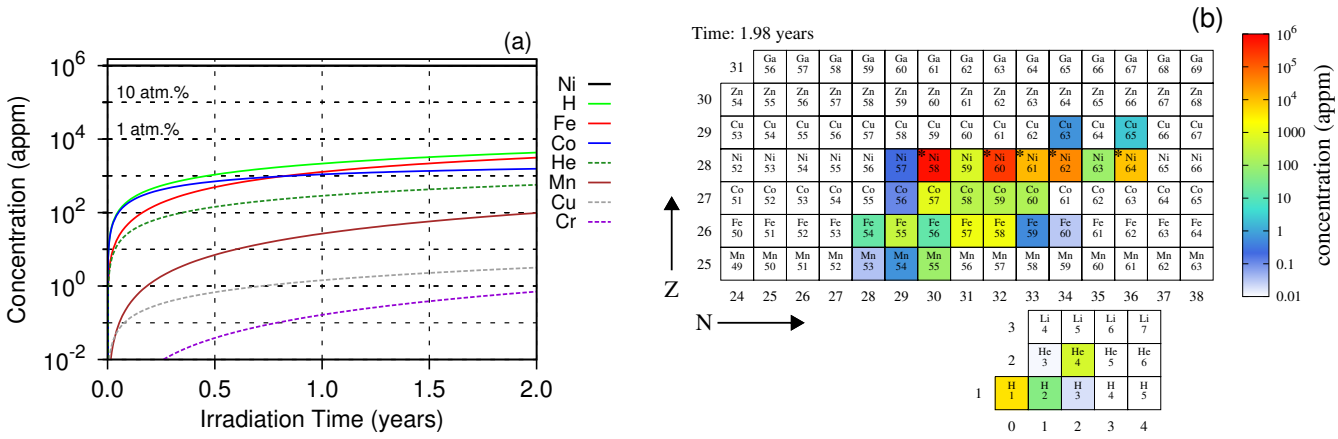

(a)Elemental transmutation response. (b)Nuclide map.

FIG. 49. (Color online) The elemental transmutation response of pure nickel during a two full-power-year irradiation in DEMO first-wall conditions and a nuclide map showing the transmuted composition of the sample at the end of the irradiation.

ways are only listed if they contribute more than 1% of a nuclide in any of the four energy ranges. Note that the standard uncertainty analysis used in the automated production of the handbook does not always produce results for every important nuclide across all four energy ranges.

Table XVIII, shows the handbook pathway analysis result for pure iron. The important target nuclides are listed in half-life order (also given in the table), with the pathways for each listed in decreasing order of contribution at a given energy range and then in increasing order of neutron energy range. As can be seen even from this result for simple iron, the pathway tables can be quite detailed, extending for several pages in the most complex cases.

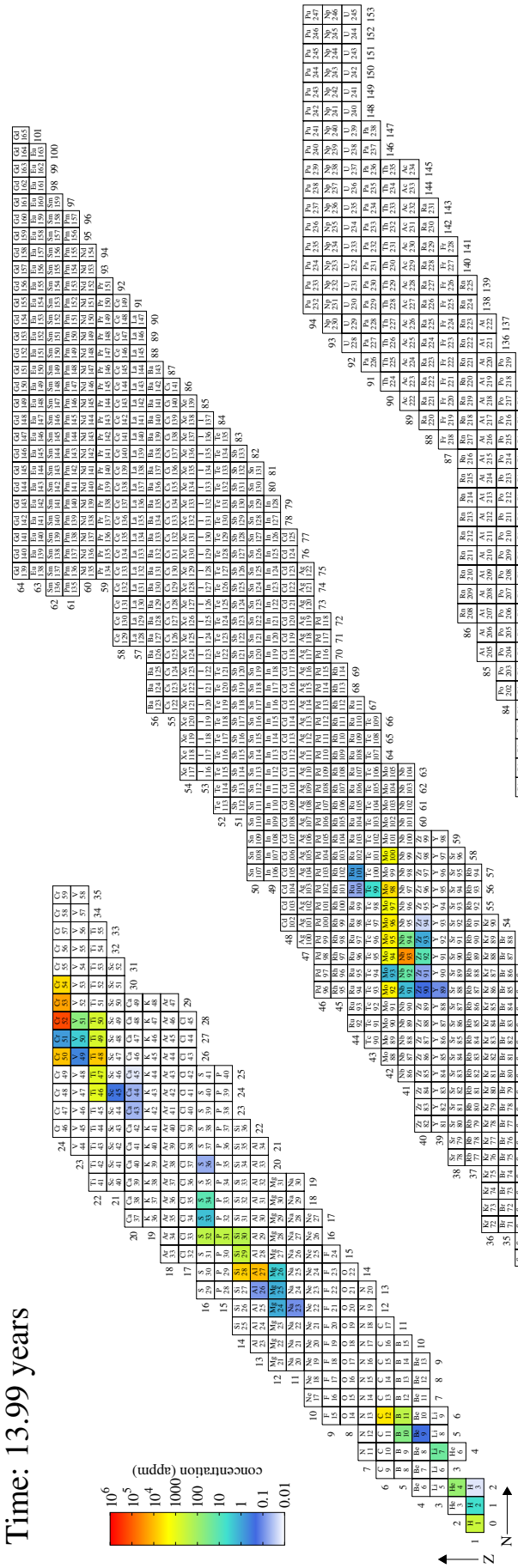

FIG. 50. (Color online) A nuclide map showing the predicted transmuted composition of Inconel-718 at the end of the 14-year experimental campaign in ITER.

TABLE XVIII: Iron pathway analysis: important target nuclides, their half-lives and the pathways leading to them. The percentage contribution of each pathway is shown for neutron fluxes in four energy ranges.

Nuclide	Half-life	Pathway	20–50 meV	20–40 keV	1–3 MeV	13–15 MeV
^{56}Mn	2.58h	^{54}Fe(n,γ)^{55}Fe(β^+)^{55}Mn(n,γ)^{56}Mn	99.6	100.0	99.1	
		^{56}Fe(n,p)^{56}Mn				99.0
^{44}Sc	3.97h	^{54}Fe(n,α)^{51}Cr(n,α)^{48}Ti(n,α)^{45}Ca(β^-)^{45}Sc(n,2n)^{44}Sc				31.1
		^{54}Fe(n,α)^{51}Cr(β^+)^{51}V(n,α)^{48}Sc(β^-)^{48}Ti(n,α)^{45}Ca(β^-)^{45}Sc(n,2n)^{44}Sc				24.9
		^{54}Fe(n,α)^{51}Cr(n,α)^{48}Ti(n,α)^{45}Ca(β^-)^{45}Sc(n,2n)^{44m}Sc(IT)^{44}Sc				22.5
		^{54}Fe(n,α)^{51}Cr(β^+)^{51}V(n,α)^{48}Sc(β^-)^{48}Ti(n,α)^{45}Ca(β^-)^{45}Sc(n,2n) ^{44m}Sc(IT)^{44}Sc				18.0
^{51}Cr	27.70d	^{54}Fe(n,α)^{51}Cr	100.0		100.0	98.8
^{59}Fe	44.50d	^{56}Fe(n,γ)^{57}Fe(n,γ)^{58}Fe(n,γ)^{59}Fe	59.0			
		^{58}Fe(n,γ)^{59}Fe	20.9	97.0	99.9	99.6
		^{57}Fe(n,γ)^{58}Fe(n,γ)^{59}Fe	20.0	3.0		
^{54}Mn	312.16d	^{54}Fe(n,p)^{54}Mn			100.0	81.4
		^{56}Fe(n,2n)^{55}Fe(n,np)^{54}Mn				7.7
		^{56}Fe(n,2n)^{55}Fe(β^+)^{55}Mn(n,2n)^{54}Mn				6.2
		^{56}Fe(n,np)^{55}Mn(n,2n)^{54}Mn				3.6
^{55}Fe	2.73y	^{54}Fe(n,γ)^{55}Fe	100.0	100.0	100.0	
		^{56}Fe(n,2n)^{55}Fe				99.5
^{60}Co	5.27y	^{58}Fe(n,γ)^{59}Fe(β^-)^{59}Co(n,γ)^{60m}Co(IT)^{60}Co	31.0	58.2	48.2	49.8
		^{56}Fe(n,γ)^{57}Fe(n,γ)^{58}Fe(n,γ)^{59}Fe(β^-)^{59}Co(n,γ)^{60m}Co(IT)^{60}Co	19.5			
		^{58}Fe(n,γ)^{59}Fe(β^-)^{59}Co(n,γ)^{60}Co	18.7	40.7	50.9	49.8
		^{56}Fe(n,γ)^{57}Fe(n,γ)^{58}Fe(n,γ)^{59}Fe(β^-)^{59}Co(n,γ)^{60}Co	11.9			
		^{57}Fe(n,γ)^{58}Fe(n,γ)^{59}Fe(β^-)^{59}Co(n,γ)^{60m}Co(IT)^{60}Co	11.8			
		^{57}Fe(n,γ)^{58}Fe(n,γ)^{59}Fe(β^-)^{59}Co(n,γ)^{60}Co	7.2			
^{3}H	12.33y	^{54}Fe(n,γ)^{55}Fe(n,p)^{1}H(n,γ)^{2}H(n,γ)^{3}H	100.0			
		^{54}Fe(n,p)^{1}H(n,γ)^{2}H(n,γ)^{3}H			99.9	
		^{57}Fe(n,t)^{3}H				65.5
		^{56}Fe(n,2n)^{55}Fe(n,t)^{3}H				16.3
		^{56}Fe(n,2n)^{55}Fe(β^+)^{55}Mn(n,t)^{3}H				5.0
		^{56}Fe(n,t)^{3}H				3.7
		^{56}Fe(n,np)^{55}Mn(n,t)^{3}H				3.3
		^{54}Fe(n,p)^{54}Mn(n,t)^{3}H				2.2
		^{56}Fe(n,α)^{53}Cr(n,t)^{3}H				2.1
^{63}Ni	100.62y	^{58}Fe(n,γ)^{59}Fe(β^-)^{59}Co(n,γ)^{60m}Co(IT)^{60}Co(n,γ)^{61}Co(β^-)^{61}Ni(n,γ) ^{62}Ni(n,γ)^{63}Ni	40.7	57.8		
		^{58}Fe(n,γ)^{59}Fe(β^-)^{59}Co(n,γ)^{60}Co(n,γ)^{61}Co(β^-)^{61}Ni(n,γ)^{62}Ni(n,γ)^{63}Ni	24.5	40.4		
		^{57}Fe(n,γ)^{58}Fe(n,γ)^{59}Fe(β^-)^{59}Co(n,γ)^{60m}Co(IT)^{60}Co(n,γ)^{61}Co(β^-)^{61}Ni(n,γ) ^{62}Ni(n,γ)^{63}Ni	7.5			
		^{56}Fe(n,γ)^{57}Fe(n,γ)^{58}Fe(n,γ)^{59}Fe(β^-)^{59}Co(n,γ)^{60m}Co(IT)^{60}Co(n,γ)^{61}Co(β^-) ^{61}Ni(n,γ)^{62}Ni(n,γ)^{63}Ni	7.0			
		^{58}Fe(n,γ)^{59}Fe(n,γ)^{60}Fe(n,γ)^{61}Fe(β^-)^{61}Co(β^-)^{61}Ni(n,γ)^{62}Ni(n,γ)^{63}Ni	4.7			
		^{57}Fe(n,γ)^{58}Fe(n,γ)^{59}Fe(β^-)^{59}Co(n,γ)^{60}Co(n,γ)^{61}Co(β^-)^{61}Ni(n,γ) ^{62}Ni(n,γ)^{63}Ni	4.5			

continued on next page

continued from previous page

Nuclide	Half-life	Pathway	20–50 meV	20–40 keV	1–3 MeV	13–15 MeV
		^{56}Fe(n,γ)^{57}Fe(n,γ)^{58}Fe(n,γ)^{59}Fe(β^-)^{59}Co(n,γ)^{60}Co(n,γ)^{61}Co(β^-)^{61}Ni(n,γ)^{62}Ni(n,γ)^{63}Ni	4.2			
		^{58}Fe(n,γ)^{59}Fe(β^-)^{59}Co(n,γ)^{60m}Co(IT)^{60}Co(β^-)^{60}Ni(n,γ)^{61}Ni(n,γ)^{62}Ni(n,γ)^{63}Ni	2.2			
		^{58}Fe(n,γ)^{59}Fe(β^-)^{59}Co(n,γ)^{60}Co(β^-)^{60}Ni(n,γ)^{61}Ni(n,γ)^{62}Ni(n,γ)^{63}Ni	1.3			
		^{56}Fe(n,γ)^{57}Fe(n,γ)^{58}Fe(n,γ)^{59}Fe(n,γ)^{60}Fe(n,γ)^{61}Fe(β^-)^{61}Co(β^-)^{61}Ni(n,γ)^{62}Ni(n,γ)^{63}Ni	1.1			
		^{57}Fe(n,γ)^{58}Fe(n,γ)^{59}Fe(n,γ)^{60}Fe(n,γ)^{61}Fe(β^-)^{61}Co(β^-)^{61}Ni(n,γ)^{62}Ni(n,γ)^{63}Ni	1.0			
^{60}Fe	1.5×10^6y	^{58}Fe(n,γ)^{59}Fe(n,γ)^{60}Fe	41.0	98.5	100.0	99.5
		^{56}Fe(n,γ)^{57}Fe(n,γ)^{58}Fe(n,γ)^{59}Fe(n,γ)^{60}Fe	39.2			
		^{57}Fe(n,γ)^{58}Fe(n,γ)^{59}Fe(n,γ)^{60}Fe	19.8	1.5		
^{53}Mn	3.7×10^6y	^{54}Fe(n,np)^{53}Mn				96.7
		^{54}Fe(n,d)^{53}Mn				1.7

V. PATHWAY ANALYSIS

This chapter contains a detailed description of the method of pathway analysis implemented in FISPACT-II (Section V A). Output from pathway analysis by FISPACT-II is described in Section V A 3, which supplements that already presented for the activation handbooks in Section IV G 7 above. Section V B and Section V C demonstrate the new method's versatility compared to its predecessor in FISPACT 2007, including the two orders of magnitude speed gains in execution times over a range of test cases.

A. Details of Analysis and Output

1. *Digraph Iteration*

The inventory of a given nuclide computed using the rate equations may equivalently be found by a superposition of contributions of flows along a network of pathways to that nuclide, where a pathway is the combination of a linear chain of reactions between different nuclides (a path), plus a number of loops from a nuclide to itself. Pathways analysis finds the significant pathways by automatically combining paths and loops, and these pathways are used in performing uncertainty and sensitivity calculations.

Source nuclides for the pathways calculation are the initial inventory, and target nuclides are dominant nuclides at the current timestep. A dominant nuclide is one that gives a major contribution to a radiological quantity, such as activity, gamma dose, heating, inhalation dosage, etc.

Brute-force searching for pathways rapidly fails owing to the combinatorial growth of possibilities. The chain of nuclear reactions and decays may be interpreted in graph theory as an instance of a directed graph (known as a 'digraph' [102]), and this has allowed us to use graph theory to develop a new algorithm. In graph theory, each vertex on the digraph corresponds to a particular nuclide, and the 'edges' connecting the vertices describe the flow through decays and reactions from nuclide to nuclide. The digraph is conventionally represented by a tree data structure, and this is stored as a linked-list queue in FISPACT-II. All paths from a source nuclide may be represented by the tree, with vertices connected by edges. The known flows along the edges provide an upper bound on the contribution of a given path. When this bound falls below the cutoff threshold, then the branch of the tree is terminated, a process known as 'pruning'. A second method of reducing the tree size is to follow descendents of a given nuclide only once, building a single-visit tree. All branches from second and subsequent occurrences of the nuclide are pruned, and information from the first instance is used to construct paths.

The new graph-theoretic algorithm for finding pathways developed for FISPACT-II leads to much faster and lower-storage computations than were possible with the brute-force method employed in FISPACT 2007. Simple algebraic tests, derived from rigorous upper bounds on the path weights, are used to prune the number of paths to a relatively small number of candidates for which the stiff-ode solver is used to calculate accurate weights. These weights are used in the final determination of pathway significance. Pathway analysis for the large number of nuclides in the TENDL data libraries, for long paths (tree depths), paths with fission and loops, and for multiple irradiation steps can be readily handled.

The algorithm, which is illustrated below by a simple example, may be summarised as

1. create a single-visit digraph with edge-weight pruning;

2. iterate on the digraph to extract all edges on significant paths and loops;
3. use these edges to build a tree with weight, loop and depth pruning;
4. combine resulting paths and loops to make pathways;
5. compute inventories along pathways and discard those below a user-specified threshold.

In contrast to FISPACT 2007, the implementation of this algorithm in FISPACT-II has no arbitrary constraints on its complexity; computer memory size and running time are the only limitations. Pathways are discarded only if their significance falls below thresholds set by the user. Another advantage of the graph-theoretic algorithm is that any loops from a nuclide to itself (for example, via an isomeric state) are found automatically and are included if the flow around a loop significantly modifies the weight of the pathway on which that loop resides.

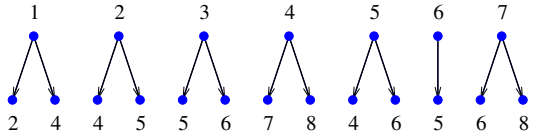

FIG. 51. (Color online) Adjacency list for the 8-nuclide example.

To illustrate the method we consider the eight nuclide example whose adjacency list is shown in Fig. 51. Parent 1 has daughters 2 and 4, etc. To find paths originating at nuclide 1, a single-visit tree is built breadth-first (Fig. 52). At the second level, children of 2 (4 and 5) and 4 (7 and 8) are added. At the third level, children of 4 are not added because nuclide 4 has already been visited as a parent at level 1 and only the first occurrence of nuclide 6 has its children added. The tree is completed at level 4. All the leaves of the tree are nuclides that have appeared earlier.

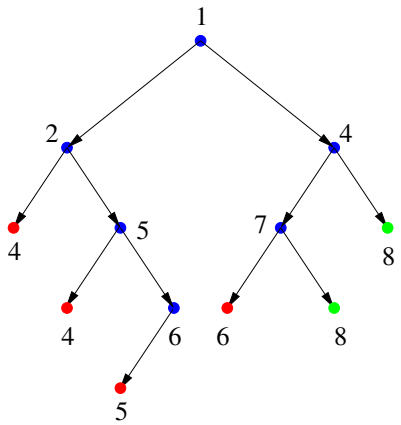

FIG. 52. (Color online) A parent single-visit tree for nuclide 1.

Graph edges are extracted from the digraph of Fig. 52 by iteration. Consider for example paths from nuclide 1 to 4. At the first iteration, edges with nuclide 1 or 4 as children are extracted, giving edges (14), (24) and (54), and adding target nuclides 2 and 5. At the next iteration, edges with children 2 and 5 are extracted, giving edges (12), (25) and (65), and target 6. The third iteration gives (56) and (76) and target 7. The final iteration finds edge (47) and introduces no further target nuclides so the iteration terminates.

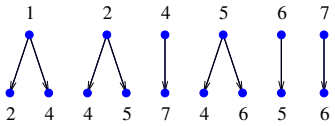

FIG. 53. (Color online) Reduced adjacency list for pathways between nuclides 1 and 4.

Figure 53 shows the reduced set of edges that are involved in pathways from nuclide 1 to 4. In this trivial example, only nuclide 8 is pruned, but in real cases many are excluded from the reduced adjacency lists. If we excluded pathways with loops on the final nuclide (4), then branches of the full tree could be terminated at occurrences of nuclide 4. Instead, we collect paths and loops separately, and use the following criteria to terminate branches:

1. a loop is found (i.e., a nuclide is encountered that has already occurred on the path from the root to the leaf);
2. the leaf has a weight below the path floor value;
3. the depth exceeds the maximum depth.

In Fig. 54, the solid horizontal (red) line shows a branch terminated by criterion 1, and the broken lines show branches terminated by criterion 2. Traversing the tree reveals paths 1-4, 1-2-4 and 1-2-5-4 at levels 1, 2 and 3, and loop [56] at level 4.

The pruning weight criteria (Section V A 2 below) are sufficient conditions for a pathway to be discarded. The final list is found by integrating the rate equations along the pruned list and discarding those below the chosen thresholds. Figure 55 shows the resulting pathways from nuclide 1 to 4.

Loops are discarded if they increase the inventory of a path by less than the loop floor fraction. The weights for discarding paths are discussed in the section below.

Note in this example if we had a smaller path floor, then the loop [5476] would have been found and would have been combined with the paths shown in Fig. 55 if its contribution exceed the loop floor criterion.

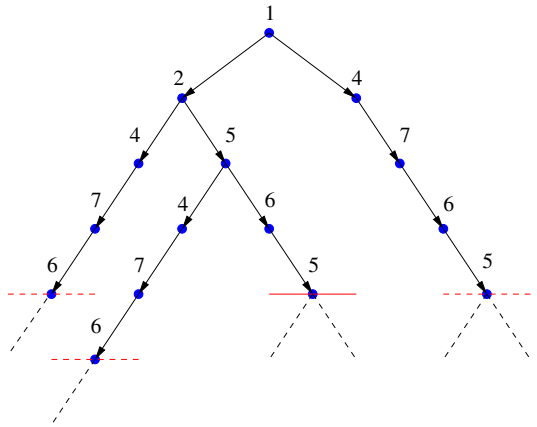

FIG. 54. (Color online) The breadth-first tree for the adjacency list of Fig. 53.

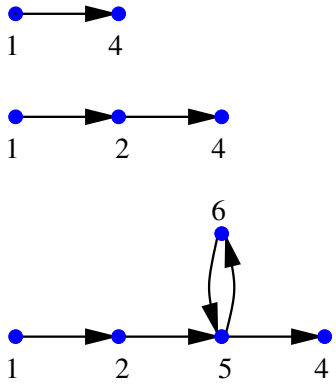

FIG. 55. (Color online) The pathways obtained from the tree in Fig. 54.

2. *Threshold Pruning*

Pathways are assigned importance based on the fractions of the inventory at the target nuclide that come via them from the source nuclide. Each intermediate step i from nuclide i to $i+1$ along a dominant pathway between the source and the target introduces a reduction in the flow that can be bounded by a reduction factor less than unity.

If N_s and N_t are respectively the initial number of source atoms and the final number of target atoms given by the full inventory calculation, and ϵ is the threshold fraction of N_t below which the pathway is not considered significant, then any partial pathway with inventory N_D at depth D for which

$$\rho_D = N_D/N_s < \epsilon N_t/N_s \tag{95}$$

can be pruned. Estimated bounds on ρ_D can be found from the rate equation coefficients and the time interval being considered, but the final pruning and pathway assessment will require integration of the inventory along the pathway.

An upper bound for ρ_i at level i can be found by considering the flow along the linear chain that forms a path. The evolution of the inventory is given by

$$\frac{dN_1}{dt} = -\alpha_1 N_1 \tag{96}$$

and for subsequent nuclides ($i > 1$)

$$\frac{dN_i}{dt} = -\alpha_i N_i + \beta_{i-1} N_{i-1}\,, \tag{97}$$

where α_i gives the total rate of decay and induced destruction of a nuclide, and β_i is the rate of decay and transmutation of nuclide i specifically to nuclide $i+1$ along the path. The coefficients α_i and β_i are extracted directly from the rate equation matrix.

For constant flux, α_i and β_i are constant, so Eq. (97) may be integrated to give

$$N_i(t) = e^{-\alpha_i t}\left(A_i + \int_0^t e^{\alpha_i t'}\beta_{i-1}N_{i-1}(t')dt'\right)\,, \tag{98}$$

where for $i > 1$, the initial conditions give $A_i = 0$.

The total number of nuclides created at vertex $i+1$ in time interval $[0, T]$ is

$$F_{i+1} = \int_0^T \beta_i N_i dt\,. \tag{99}$$

Substituting Eq. (98) into Eq. (99), interchanging the order of integration and integrating over t gives

$$\begin{aligned} F_{i+1} &= \frac{\beta_i}{\alpha_i}\left(F_i - e^{-\alpha_i T}\int_0^T dt'\; N_{i-1}(t')\beta_{i-1}e^{\alpha_i t'}\right) \\ &\leq \frac{\beta_i}{\alpha_i}F_i(1 - e^{-\alpha_i T})\,, \end{aligned} \tag{100}$$

where the final inequality was obtained by replacing the exponential in the integral by its lower bound ($= 1$) in Eq. (100).

Setting $F_1 = 1$ and computing F_{i+1} using the inequality in Eq. (100) gives an upper bound on ρ_i, and so provides a sufficient pruning condition for terminating branches in trees such as that illustrated in Fig. 54.

The tree-pruning criterion for a single pulse of irradiation may be extended to multi-pulse irradiation of J pulses by replacing F by a vector of length J. A sufficient condition for the pathway to be discarded at depth D (> 0) is

$$F_{D+1}(T_J) < \epsilon\frac{N_t(T)}{N_s(0)}\,, \tag{101}$$

where this inequality is applied only to the final components of the vectors F at time T_J. The total fluxes satisfy initial conditions

$$F_i(T_0) = 0; \quad i > 1 \tag{102}$$

and at the end of time interval j (> 0)

$$F_{i+1}(T_j) \leq F_{i+1}(T_{j-1}) + \frac{\beta_i^j}{\alpha_i^j} F_i(T_j)[1 - \exp(-\alpha_i^j \Delta T_j)], \quad (103)$$

where $\alpha_i^j > 0$, $F_1(T_j) = N_{1,j-1}$ and $\Delta T_j = T_j - T_{j-1}$.

Pruning weights using Eqs (100)–(103) are implemented in the FISPACT-II pathways calculations.

3. *Pathway Output*

Pathways are output in order of decreasing dominance of the target nuclide as ordered in the dominant nuclide tables. Individual pathways are retained if they contribute more than the (adjustable) minimum percentage of the number of target atoms given by the full rate equation solution for the time interval. Loops are retained in a pathway if they contribute more than the (adjustable) loop minimum percentage of the number of target atoms created along the pathway. There is also a maximum number of parent-daughter pairs (edges) that are considered in a path. The target nuclides are those on the merged dominant nuclides list at the end of the irradiation or optionally those that appear on the merged dominant list at any step after the end of the irradiation period. Another option is to repeat the pathways calculation after any cooling step. These options are useful if one wishes to capture pathways to nuclides that only become dominant in late cooling times.

The pathways calculation prints lists of all significant paths and loops ordered by target nuclide. An extract of a pathways output is shown in Fig. 56. The first line for each target nuclide gives the nuclide name and the percentage of the total number of atoms given by the number of significant paths shown. The first line for each pathway identifies a path or loop, gives its number and its respective percentage contribution to the target nuclide inventory. The remainder of the line gives the nuclides on the path (or loop) from source to target, and the type of graph edge joining them. Edge types (r,R), (d,D) and (b,B) respectively denote reaction, decay and combined reaction and decay edges from short (lower case) and long lived (upper case) parents. L and S denote short and long lived target nuclides. Short-lived nuclides have half lives less than the time interval and long-lived have half lives greater. Shown below each edge is a list giving the percentage contributions that each reaction and decay make towards the total rate for the edge for primary products. If the daughter of an edge is a secondary then the isomeric state of the primary product of the reaction or decay is also displayed. Significant loops are displayed directly after their path, with the percentages of their part of the total path percentage.

B. Model Reduction

FISPACT-II usually runs with the full TENDL-2015 master index of 3875 nuclides. Nuclides that are present in the master nuclide index used by the code are included in a calculation. For single inventory calculations, the cpu time used is small (typically less than a minute on a 3GHz desktop PC), with the dominant time often being that taken to read and collapse the 9 Gigabytes of ASCII data in the TENDL-2015 library. Nuclides may be excluded from the calculation by removing them from the master index file, `ind_nuc`.

FISPACT-II has the capability to produce a reduced index in a pathways inventory run, where only those nuclides that appear on pathways from the initial inventory to the dominant nuclides are included. Using a reduced index leads to much faster library reading. Memory allocation in the code is all dynamic, and so calculations with a reduced number of nuclides in the index also use less memory. Sensitivity calculations can also benefit from the model reduction capability. Repeating calculations using this reduced master index usually accurately reproduces the results from the full calculation as was demonstrated in [103], as follows.

To capture as much as possible of the vast range of activation problems treatable by FISPACT-II, the seven nuclide mixtures listed in Table XIX were composed. Most of the mixtures consist of 1 kg of material subject to a neutron flux of $10^{15}\,\mathrm{cm^{-2}s^{-1}}$, for a year, without any cooling period. However, to produce a fission problem, an existing test case with a smaller sample, flux and irradiation time was used. Further, to compare with experimental data for Y_2O_3, a much smaller sample, flux and irradiation time was used.

The mixtures were used in eight test cases, with the Alloy case extended to include a cooling phase. Each test case was run using the full TENDL 2012 database with pathway analysis to identify the dominant nuclides and important reactions, total numbers of which are listed in Table XX. The sole exception was the YO_2 case where a single nuclide, ^{86}Rb was selected for study. Monte-Carlo solution of the full problem was then performed in the sequence of increasing sample size per reaction, M_s = 10, 40, 160, ... up to the maximum value specified in the table. It was confirmed, for each mixture separately, that provided the same machine was used, the cost of a FISPACT-II calculation scaled linearly with M_s, the total number of samples, to a very good approximation.

The distributions of activity per sample obtained from the pathways-reduced calculations were examined, and compared with those produced by full FISPACT-II calculations. Numerical parameters for Gaussian and log-normal distributions fitted to the computed activities agreed to at least 2 significant figures, often 3, as shown in Tables 3 and 4 of [103]. The histograms in [103] showed detailed agreement, any discrepancies probably no larger than those due to sampling effects. Standard deviations of distributions of separate nuclides were shown to agree

```
Target nuclide Sc 44     99.557% of inventory given by  8 paths
--------------------

path  1  20.048% Ti 46 ---(R)--- Sc 45 ---(R)--- Sc 44 ---(S)---
                       98.16%(n,np)   100.00%(n,2n)
                        1.84%(n,d)

path  2  12.567% Ti 46 ---(R)--- Sc 45 ---(R)--- Sc 44m---(b)--- Sc 44 ---(S)---
                       98.16%(n,np)   100.00%(n,2n)   100.00%(IT)
                        1.84%(n,d)                      0.00%(n,n)

path  3  11.143% Ti 46 ---(R)--- Sc 45m---(d)--- Sc 45 ---(R)--- Sc 44 ---(S)---
                       96.62%(n,np)   100.00%(IT)     100.00%(n,2n)
                        3.38%(n,d)
```

FIG. 56. An example of pathways output.

TABLE XIX. Test cases from [103]. Apart from the Fiss mixture, each consists of numbers of atoms of the listed elements with their natural abundances of nuclides, given as percentages of the whole.

Test Label	Constituents of Mixture	Sample Mass	Irradiation Period	Cooling Period	Neutron flux $\mathrm{cm^{-2}s^{-1}}$
Alloy	Fe 40.0 : Ni 20.0 : Cr 20.0 : Mn 20.0	1 kg	1 yr	0	10^{15}
Alloy+c	Fe 40.0 : Ni 20.0 : Cr 20.0 : Mn 20.0	1 kg	1 yr	1 yr	10^{15}
Fe	Fe	1 kg	2.5 yr	0	10^{15}
Fiss	U235 3.7 : U238 96.3	8.7 g	3 mo	0	2.59032×10^{14}
LiMix	Li 40.0 : Be 30.0 : O 30.0	1 kg	1 yr	0	10^{15}
WMix	W 20.0 : Re 20.0 : Ir 20.0 : Bi 20.0 : Pb 20.0	1 kg	1 yr	0	10^{15}
Y2O3/YO2	Y 78.74 : O 21.26	1 g	300 s	0	1.116×10^{10}

to similar accuracy between reduced and full calculations, except for one or two extremely minor reactions.

In conjunction with this excellent agreement, it is noteworthy that Monte-Carlo sensitivity calculations using the reduced master index required much smaller cpu time and memory resources, specifically typical speed-up factors of order 10^3 appear in Table XX. In the context, this is a significant gain from using the pathways-reduced approach. The next Section V C shows how it can also be used to provide a cheap way of ranking the important reactions.

C. Ranking the Importance of Nuclear Reaction and Decay

Since as shown in Section II J, it is challenging to determine uncertainties in reaction cross sections, it is important to examine techniques that can identify which reactions most require further examination. Three different ranking techniques were described in [104]. The most innovative uses pathways-based reduction, see Section V C 1 below, although a new technique was also employed in the calculation of the direct sensitivity, viz. matrix Fréchet derivative, see Section V C 2, rather than the more usual decoupled direct method DDM [105]. The third is closely related to the Pearson product-moment correlation. Techniques for ranking the interactions A_{ij} were analysed in the context of a single constant irradiation in the time interval $(0, T)$, producing an inventory $N(T)$. Only the total activity

$$Q = \sum_{t \in S_t} q_t, \quad \text{where} \quad q_t = \alpha_t N_t(T) \tag{104}$$

was considered where α_k is the decay rate of the nuclide k with the convention that α_k is zero for stable nuclides.

1. *Pathways Based Metric*

The Pathways Based Metric (PBM) is calculated straightforwardly from the output of the pathways-reduced approach in Section V A 3, using auxiliary software not currently integrated into standard FISPACT-II. For a given interaction A_{ij}, all the number M_p of pathways upon which it lies are identified and the PBM calculated as

$$S^{ij}_{PBM} = \sum_{k=1}^{M_p} p_l \alpha_t N_t I_{kl} \,, \tag{105}$$

where p_l is the fractional contribution of pathway l to the number of atoms N_t (evaluated at time T) in the inven-

TABLE XX. Test cases statistics, from [103]. The entries in the columns labelled 'Full' and 'Pathways Reduced' are the numbers of dominant nuclides.

Test Label	I, Reactions Examined	Full	Pathways Reduced	Matrix A Size	Max. M_x, Samples per Reaction	M_s, Total Sample	Reduced cpu (s)	Full cpu (s)
Alloy	76	23	23	53	640	48 640	82.053	44 136
Alloy+c	50	13	13		640	32 000	56.494	38 623
Fe	26	20	13	23	640	16 640	9.6355	13 995
Fiss	1	47	47		2 560	2 560	33.143	10 143
LiMix	17	9	9	23	640	10 880	4.0664	8 011
WMix	71	29	29	69	640	45 440	96.947	47 019
Y2O3	12	11	11	16	2 560	30 720	4.7893	13 526
YO2	2	1	1		10 240	20 480	2.1057	8 944

tory with decay rate α_t and the indicator matrix $I_{kl} =$ 1 or 0 depending whether or not a reaction contributing to the interaction lies on the pathway. To date, the loops identified by the graph-based approach used by FISPACT-II have been ignored.

Figure 57 illustrates the definition in a simplified case where irradiation of an initial sample consisting of N_1 atoms of nuclide 1 and N_2 atoms of nuclide 2 produces an inventory containing numbers N_5 and N_6 of radioactive nuclides 5 and 6 respectively, with three important pathways. The first pathway contributes $p_1 N_5$ atoms and the third $p_3 N_5$ atoms of nuclide 5. The sensitivity of the inventory to the reaction with coefficient A_{32} (the large arrowheads in Fig. 57), is then

$$S^{32}_{PBM} = p_1\alpha_5 N_5 + p_2\alpha_6 N_6\,, \tag{106}$$

where α_5 is the decay rate of nuclide 5 etc.

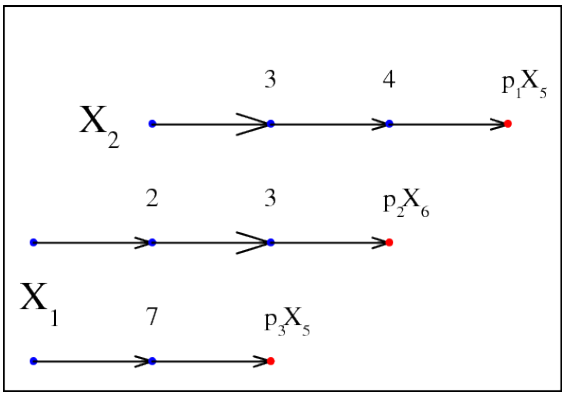

FIG. 57. (Color online) An example illustrating how the Pathways Based Metric S_{PBM} is calculated when the three pathways shown are highlighted by the pathways-reduced analysis. The pathways are numbered in order 1, 2 and 3 from the top. Pathway 1 starts with nuclide 2 and generates via a sequence of reactions involving nuclides 3 and 4, $p_1 N_5$ atoms of nuclide 5, whereas the other pathways begin with nuclide 1 and generate nuclides 6 and 5 respectively. The larger arrowheads indicate reactions with the coefficient of interest A_{32}.

2. *Direct Method*

The Direct Method (DM) works directly with the triply-subscripted array describing the rate of variation of the number of atoms of nuclide k, N_k, with respect to nuclear reaction coefficients. For initial investigative purposes it is sufficient to consider the partial derivative with respect to A_{ij}. Differentiating Eq. (56) with (i, j) regarded as fixed, gives

$$\frac{d}{dt}\left(\frac{\partial \mathbf{N}}{\partial A_{ij}}\right) = \mathsf{A}\frac{\partial \mathbf{N}}{\partial A_{ij}} + \frac{\partial \mathsf{A}}{\partial A_{ij}}\mathbf{N}\,. \tag{107}$$

The sensitivity of the total activity is, using Eq. (104)

$$S^{ij}_{DM} = \sum_k \alpha_k \frac{\partial N_k(T)}{\partial A_{ij}}\,. \tag{108}$$

Unlike in the decoupled direct method, S_{DM} is calculated using the matrix Fréchet derivative as explained in the Appendix to [104], viz.

$$S^{ij}_{FDM}(T) = T\sum_k \alpha_k L_{\exp}(T\mathsf{A}, \mathsf{E}_{ij})N(0)\,, \tag{109}$$

where $L_{\exp}$ is the matrix Fréchet derivative with E_{ij} each direction in which it has to be taken. Equation (109) defines the Fréchet direct method, although for the purposes of comparison with S_{PBM} in [104], S_{FDS}, equal to S_{FDM} weighted by $\epsilon_{ij}\bar{A}_{ij}$, the relative error in the distribution of the coefficient A_{ij} times the mean coefficient. Both these quantities are returned by FISPACT-II, which did however require modification to output the matrix A in a format suitable for input to the external MATLAB [106] code that actually calculates $L_{\exp}N(0)$.

3. *Comparison of Methods*

From the definitions, the main distinction between the PBM and the other two measures is that the pathways-based method is 'global', capturing the whole variation of the inventory as parameters are varied, although having

the disadvantage that it cannot measure sensitivity to diagonal entries of A. The other two techniques are more local, indeed the DM returns directly only a coefficient at the mean of the distribution of Q. The Pearson coefficient is somewhere in-between, using global variations, but making a local linear assumption about the mean.

To compare them more directly, the three techniques were each applied to a wide range of test cases similar to that introduced in the previous Section V B, except that the tiny YO2 case and the fission case were omitted, and data from TENDL-2013 were used instead of TENDL-2012. It is not critical that the three techniques agree completely, since the objective is only to identify reactions to which the total inventory is sensitive. Nonetheless, the measures frequently returned top ten rankings sharing 7 or more reactions, which is as good as might be expected allowing for missing data and other effects mentioned in the list immediately below. Thus the simple pathways-based metric (PBM) gives a sensitivity ranking of interactions comparable to ranking based on the more conventional measures obtained either by the direct method or in terms of Pearson correlation coefficients. Moreover, the PBM was found to be superior in that it

1. is quick to calculate once the principal pathways have been identified

2. does not suffer from numerical difficulties such as underflow (Fréchet direct) or round-off (Pearson) in its evaluation

3. may be generalised to the case of multiple irradiation periods in the same way as the pathways-reduced approach itself.

4. unlike Pearson, does not require error estimates for every interaction coefficient.

Underflow results because the range of number needed to compute the Frechet derivative increases with the ratio of absolute largest to smallest eigenvalue of the rate matrix, so may not be adequately represented in 8-bytes of precision when very long and short-lived nuclides are present.

VI. CONCLUSIONS

The FISPACT-II system brings many new capabilities to the long established family of inventory codes. At the core of the main code is a modern rate equation solver that exploits the most advanced physics provided in modern nuclear data forms. This has primarily been driven by the development of the technological TENDL nuclear data libraries that, when coupled with FISPACT-II, allow truly general-purpose simulations for neutron-induced inventory calculations, as well as charged-particle simulations for proton, deuteron, alpha and gamma-ray irradiation.

The use of modern nuclear data forms opens up many novel features. New data forms for probability tables offer adaptable self-shielding calculations for any isotopic composition of materials and any irradiation scenarios, as well as geometry-specific self-shielding for several configurations. Complete recoil spectra information provides material science with the data needed to simulate the evolution of material properties under irradiation. The inclusion of all (partial and total) reaction channels offers robust simulation of all inventory response functions, including source terms, gamma-dose, decay heat, activation-transmutation, depletion, gas production and dpa. These also provide new functionalities, such as the renormalisation of incident particle flux, through total or any partial kerma, to volumetric power rating. The availability of complete covariance data for all reaction channels, at least in TENDL, combined with the sophisticated pathways-based and Monte-Carlo sensitivity methods of FISPACT-II offers novel uncertainty quantification and propagation methods for all physical systems. The high-energy residual nuclide production data of TENDL, as read by FISPACT-II, allows fully tabulated nuclear data to be used in simulations of incident particles up to several hundred MeV.

Accessing all ENDF-6 nuclear data files, including both the well-known international libraries and the modern, technological files such as TENDL and GEFY has allowed FISPACT-II to be used to perform rigorous testing of the data against experimental values. These have verified the code capabilities, validated simulation results and offered a new method for probing nuclear data files to find weaknesses when used for various applications.

With the new code functionalities, access to all general-purpose nuclear data and suite of modern V&V, FISPACT-II serves as a truly 21st software system capable of leading the way safely, securely and predictively into the simulation needs of the present and future.

ACKNOWLEDGMENTS

We would like to gratefully acknowledge the invaluable collaborations with A.J. Koning, D.A. Rochman, D.E. Cullen, R.E. MacFarlane and P. Ribon, J. Kopecky and R.A. Forrest, as well as their support, patience and advice over the years. They have paved the way and we have followed with our own technologies and experience.

We also recognise the challenge and motivations given by walking along the path of other renowned simulation tools including, but by no means limited to, CASMO, SCALE/ORIGEN, MCNP/CINDER, SERPENT and MC21.

This work was funded by the RCUK Energy Programme under grant EP/1501045. The simulation system is distributed under license through the OECD/NEA Databank and ORNL/RSICC. To obtain further informa-

tion on the data and models underlying this paper please contact PublicationsManager@ccfe.ac.uk

[1] J.-Ch. Sublet, J.W. Eastwood, J.G. Morgan, M. Fleming, and M.R Gilbert, "FISPACT-II User Manual," Technical Report UKAEA-R(11)11 Issue 7, UK Atomic Energy Authority (2015). http://fispact.ukaea.uk.

[2] M. Herman and A. Trkov, editors, "ENDF-6 Formats Manual, Data Formats and Procedures for the Evaluated Nuclear Data File ENDF/B-VI and ENDF/B-VII" (Brookhaven National Laboratory, 2011).

[3] R.A. Forrest and J.-Ch. Sublet, "FISPACT-3: User Manual," Technical Report AEA-FUS 227, AEA Technology, Culham Laboratory (1993). AEA-Intec 1293.

[4] R.A. Forrest and J.-Ch. Sublet, "EASY-97: a multipurpose activation and transmutation code system," FUS. ENG., 17TH IEEE/NPSS SYMPOSIUM **1**, 119 – 124 (1997).

[5] R.A. Forrest, "FISPACT-2007: User Manual," Technical Report UKAEA FUS 534, EURATOM/UKAEA Fusion Association (2007).

[6] R.F. Burstall, "FISPIN - A computer code for nuclide inventory calculations," Technical Report ND-R-328(R), UKAEA (1979).

[7] J.W. Eastwood and J.G. Morgan, "The FISPACT-II Software Specification Document," Technical Report CEM/130516/SD/2 Issue 9, Culham Electromagnetics Ltd (2015). part of the FISPACT-II development documentation series available at http://culhamem.co.uk/fispact/.

[8] K. Radhakrishnan and A.C. Hindmarsh, "Description and use of LSODE, the Livermore solver for ordinary differential equations," Technical Report LLNL Report UCRL-ID-113855, LLNL (1993). https://computation.llnl.gov/casc/odepack/odepack_home.html.

[9] J.-Ch. Sublet, L.W. Packer, J. Kopecky, R.A. Forrest, A.J. Koning, and D.A. Rochman, "The European Activation File: EAF-2010 neutron-induced cross section library," Technical Report CCFE-R(10)05, CCFE (2010).

[10] J.-Ch. Sublet and P. Ribon, "A Probability Table Based Cross Section Processing System: CALENDF - 2001," J. NUCL. SCI. TECH. **Supplement 2**, 856–859 (2002).

[11] J.-Ch. Sublet, R. Blomquist, S. Goluoglu, and R. Mac Farlane, "Unresolved resonance range cross section probability and self shielding factors," Technical Report CEA-R-6227, ISSN 0429-3460, CEA (2009).

[12] A.C. Hindmarsh (2001) http://www.netlib.org/odepack/opkd-sum.

[13] A.C. Hindmarsh, L.R. Petzold, and A.H. Sherman (2005) http://www.oecd-nea.org/tools/abstract/detail/USCD1229.

[14] J.-Ch. Sublet, P. Ribon, and M. Coste-Delclaux, "CALENDF-2010: User Manual," Technical Report CEA-R-6277, ISSN 0429-3460, CEA (2011).

[15] I.I. Bondarenko, editor, "Group Constants for Nuclear Reactor Calculations" (Consultant Bureau, New York, 1964).

[16] G.I. Bell and S. Glasstone, "Nuclear Reactor Theory" (Van Nostrand Reinhold, New York, 1970).

[17] V. Gopalakrishnan and S. Ganesan, "Self-Shielding and Energy Dependence of Dilution Cross-Section in the Resolved Resonance Region," ANN. NUCL. ENERGY **25**, 839–857 (1998).

[18] E. Martinho, I.F. Gonçalves, and J. Salgado, "Universal curve of epithermal neutron resonance self-shielding factors in foils, wires and spheres," APPL. RADIATION ISOTOPES **58**, 371–375 (2003).

[19] E. Martinho, J. Salgado, and I.F. Gonçalves, "Universal curve of the thermal neutron self-shielding factor in foils, wires, spheres and cylinders," J. RADIOANAL. NUCL. CHEM. **261**, 637–643 (2004).

[20] J. Salgado, E. Martinho, and I.F. Gonçalves, "The calculation of neutron self-shielding factors of a group of isolated resonances," J. RADIOANAL. NUCL. CHEM. **260**, 317–320 (2004).

[21] N.P. Baumann, "Resonance integrals and self-shielding factors for detector foils," Technical Report DP-817, du Pont de Nemours, Savannah River Laboratory (1963).

[22] A.J. Koning and D. Rochman, "Modern Nuclear Data Evaluation with the TALYS Code System," NUCL. DATA SHEETS **113**, 2841–2934 (2012).

[23] D. Rochman, A. J. Koning, J. Kopecky, J.-Ch. Sublet, P. Ribon, and M. Moxon, "From average parameters to statistical resolved resonances," ANN. NUCL. ENERGY **51**, 60–68 (2013).

[24] F.H. Fröhner, "Evaluation and analysis of nuclear resonance data," Technical report, Nuclear Energy Agency (2000). JEFF Report 18.

[25] R.G. Jaeger, editor, "Engineering Compendium on Radiation Shielding" (Springer-Verlag, 1968).

[26] O.N. Jarvis, "Low-activity materials: reuse and disposal," Technical Report AERE-R-10860, Atomic Energy Research Establishment (1983).

[27] H. Bateman, "The Solution of a system of Differential Equations Occurring in the Theory of Radio-active Transformations," PROC. CAMB. PHIL. SOC. **16**, 423 (1910).

[28] J.W. Eastwood, J.G. Morgan, and J.-Ch. Sublet, "Inventory uncertainty quantification using TENDL covariance data in FISPACT-II," NUCL. DATA SHEETS **123**, 84 – 91 (2015).

[29] L.W. Packer and J.-Ch. Sublet, "The European Activation File: EAF-2010 biological, clearance and transport libraries," Technical Report CCFE-R(10)04, CCFE (2010).

[30] R.E. MacFarlane and A.C. Kahler, "Methods for Processing ENDF/B-VII with NJOY," NUCL. DATA SHEETS **111**, 2739–2890 (2010).

[31] M.R. Gilbert, J. Marian, and J.-Ch. Sublet, "Energy spectra of primary knock-on atoms under neutron irradiation," J. NUCL. MATER. **467**, 121–134 (2015). http://dx.doi.org/10.1016/j.jnucmat.2015.09.023.

[32] L. R. Greenwood and R. K. Smither, "SPECTER: Neutron damage calculations for materials irradiations" (January 1985) Document Number: ANL/FPP/TM-197. SPECTER and SPECOMP are available from the NEA databank http://www.oecd-nea.org/tools/abstract/detail/psr-0263.

[33] M. R. Gilbert and J.-Ch. Sublet, "PKA distributions: Contributions from transmutation products and from radioactive decay," NUCL. MATER. ENERGY , (2016). In press. http://dx.doi.org/10.1016/j.nme.2016.02.006.
[34] R. E. MacFarlane, D. W. Muir, R. M Boicourt, and A. C. Kahler, "The NJOY Nuclear data processing system – LA-UR-12-27079" (Version 2012-032) http://t2.lanl.gov/nis/publications/NJOY2012.pdf.
[35] M. R. Gilbert and J.-Ch. Sublet, "Handbook of activation, transmutation, and radiation damage properties of the elements simulated using FISPACT-II & TENDL-2015; Magnetic Fusion Plants," Technical Report CCFE-R(16) 36, CCFE (2016). http://fispact.ukaea.uk.
[36] J.W. Eastwood, "FISPACT-II Applications Program Interface: Software Specification Document," Technical Report cem/130516/sd/10, Culham Electromagnetics Ltd (2015).
[37] D.E. Cullen, "PREPRO-2015, 2015 ENDF-6 Preprocessing codes," Technical Report IAEA-NDS-39 (Rev. 16), IAEA (2015). http://www-nds.iaea.org/ndspub/endf/prepro/.
[38] J.-Ch. Sublet, A.J. Koning, R. A. Forrest, and J. Kopecky, "The JEFF-3.0/A Neutron Activation File - EAF-2003 into ENDF-6 format," Technical Report JEFFDOC-982, NT DER/SPRC/LEPH 03/220, OECD, CEA (2003).
[39] J.-Ch. Sublet, A.J. Koning, and D.A. Rochman, "Toward a unified ENDF-6 formatted file frame," Technical Report CCFE-R(11)16, CCFE (2012).
[40] A.P.J Hodgson, R.W. Grimes, M.J.D. Rushton, and O.J. Masden, "The impact of neutron cross section group structures on the accuracy of radiological source models," NUCL. SCI. ENG. **181**, 1–8 (2015). http://dx.doi.org/10.13182/NSE14-156.
[41] M. Fleming, L.W.G. Morgan, and E. Shwageraus, "Optimisation algorithms for multi-group energy structures," NUCL. SCI. ENG. **183**, 179–184 (2016). http://dx.doi.org/10.13182/NSE15-55.
[42] OECD NEA, "The JEFF-3.1/-3.1.1 Radioactive Decay Data and Fission Yields Sub-libraries", OECD NEA (2009) JEFF Report 20.
[43] OECD NEA, "The JEFF-2.2 Radioactive Decay Data", OECD NEA (1994) JEFF Report 13.
[44] E. Brown and R.B. Firestone, "Table of Radioactive Isotopes" (John Wiley and Sons, 1996).
[45] L.W. Packer and J.-Ch. Sublet, "The European Activation File: EAF-2010 decay data library," Technical Report CCFE-R(10)02, CCFE (2010).
[46] R. Capote, M. Herman, P. Oblozinski, P.G. Young, S. Goriely, T. Belgya, A.V. Ignatyuk, A.J. Koning, S. Hilaire, V.A. Plujko, M. Avrigeanu, O. Bersillon, M.B. Chadwick, T. Fukahori, Zhigang Ge, Yinlu Han, S. Kailas, J. Kopecky, V.M. Maslov, G. Reffo, M. Sin, E.Sh. Soukhovitskii, and P. Talou, "RIPL Reference Input Parameter Library for Calculation of Nuclear Reactions and Nuclear Data Evaluations," NUCL. DATA SHEETS **110**, 3107 – 3214 (2009).
[47] K.-H. Schmidt, B. Jurado, C. Amouroux, and C. Schmitt, "Special issue on nuclear reaction data general description of fission observables: Gef model code," NUCL. DATA SHEETS **131**, 107 – 221 (2016).
[48] K.-H. Schmidt, B. Jurado, and C. Amouroux, "General view on nuclear fission," , 1–208 (2014).
[49] K.-H. Schmidt, "GEFY: GEF-based fission-fragment Yield library in ENDF format" (2016) www.khs-erzhausen.de/GEFY.html.
[50] International Commission on Radiological Protection, editor, "Dose Coefficients for Intakes of Radionuclides by Workers" (Pergamon Press, Oxford, 1995).
[51] International Commission on Radiological Protection, editor, "Age-dependent Doses to Members of the Public from Intake of Radionuclides: Part 5 Compilation of ingestion and inhalation dose coefficients" (Pergamon Press, Oxford, 1996).
[52] A.W. Phipps, G.M. Kendall, J.W. Stather, and T.P. Fell, "Committed Equivalent Organ Doses and Committed Effective Doses from Intakes of Radionuclides," Technical Report NRPB-R245, NRPB (1991).
[53] A.W. Phipps and T.J. Silk, "Dosimetric Data for Fusion Applications," Technical Report NRPB-M589, NRPB (1991).
[54] R.A. Forrest, "Dosimetric data for FISPACT2," Technical Report AEA FUS 182, UKAEA (1992).
[55] R.A. Forrest, "The European Activation System: EAF-2007 biological, clearance and transport libraries," Technical Report UKAEA FUS 538, UKAEA (2007).
[56] IAEA, "Regulations for the safe transport of radioactive material 1985 edition (and supplement 1988)," Technical Report Safety Series No. 6, IAEA, Vienna (1988).
[57] IAEA, "Application of the Concepts of Exclusion, Exemption and Clearance," Technical Report Safety Standards Series No. RS-G-1.7, IAEA, Vienna (2004).
[58] IAEA, "Clearance levels for radionuclides in solid materials: application of exemption principles, 1994 Draft Safety Guide," Technical Report IAEA Safety Series No. 111.G-1-5, IAEA, Vienna (1994).
[59] NIST, "NIST X-ray and gamma-ray attenuation coefficients and cross section database," Technical report, U.S. Department of Commerce National Institute of Standards and Technology, Standard Reference Data Program, Gaithersburg, Maryland 20899 (1995).
[60] J.H. Hubble and S.M. Seltzer, "Tables of X-ray mass attenuation coefficients and mass energy-absorption coefficients, 1 keV to 20 MeV for elements Z = 1 to 92 and 48 additional substances of dosimetric interest," Technical Report NISTIR 5632, NIST, U.S. Department of Commerce (1995).
[61] J.H. Hubble, "Photon Mass Attenuation and Energy-absorption Coefficients from 1 keV to 20 MeV," INT. J. APPLI. RADIAT. ISOT **33**, 1269 (1982).
[62] C. Jouanne and J.-Ch. Sublet, "TRIPOLI-4.4 JEFF-3.1 Based Libraries," Technical Report CEA-R-6125, ISSN 0429-3460, CEA (2006).
[63] J.-Ch. Sublet, "JEFF-3.1, ENDF/B-VII and JENDL-3.3 Critical Assemblies Benchmarking With the Monte Carlo Code TRIPOLI," IEEE TRANS. NUCL. SCI. **55**, 604–613 (2008).
[64] J M Ruggieri and et Al., "ERANOS 2.1:International Code System for GEN IV Fast Reactor Analysis," INTERNATIONAL CONGRESS ON ADVANCES IN NUCLEAR POWER PLANTS (ICAPP 2006) , (2006). http://www.ans.org/store/item-700324-CD/.
[65] J.-Ch. Sublet, C. Dean, and D. Plisson-Rieunier, "ECCOLIB-JEFF-3.1 Based Libraries," Technical Report CEA-R-6100, ISSN 0429-3460, CEA (2006).
[66] A.C. Kahler, R.E. MacFarlane, R.D. Mosteller, B.C.

Kiedrowski, S.C. Frankle, M.B. Chadwick, R.D. McKnight, R.M. Lell, G. Palmiotti, H. Hiruta, M. Herman, R. Arcilla, S.F. Mughabghab, J.-Ch. Sublet, A. Trkov, T.H. Trumbull, and M. Dunn, "ENDF/B-VII.1 neutron cross section data testing with critical assembly benchmarks and reactor experiments," NUCL. DATA SHEETS **112**, 2997 – 3036 (2011).

[67] J.-Ch. Sublet, M. Fleming, J. Kopecky, M. Gilbert, D. Rochman, and A. Koning, "Summary of TENDL-2014 Verification & Validation outcomes and recommendations for future libraries," Technical Report UKAEA-R(15)35, UKAEA (2015).

[68] R.A. Forrest, J. Kopecky, and J.-Ch. Sublet, "The European Activation File: EAF-2007 neutron-induced cross section library," Technical Report UKAEA FUS 535, UKAEA (2007).

[69] M. Fleming, J.-Ch. Sublet, J. Kopecky, D. Rochman, and A. Koning, "Probing experimental and systematic trends of the neutron-induced TENDL-2014 nuclear data library," Technical Report UKAEA-R(15)30, UKAEA (2015).

[70] M. C. Moxon, T. C. Ware, and C. J. Dean, "REFIT-2009 A Least-Square Fitting Program for Resonance Analysis of Neutron Transmission, Capture, Fission and Scattering Data," Technical Report UKNSF(2010)P243, UKAEA (2010).

[71] M. C. Moxon, "The measurement of average neutron capture cross-sections in the mass region above 100" (1968) PhD Thesis, London University.

[72] I. Dillmann, M. Heil, F. Käppeler, and T. Rauscher. "KADoNiS v0.3 - The third update of the Karlsruhe Astrophysical Database of Nucleosynthesis in Stars,". In Proceeding of the workshop EFNUDAT Fast Neutrons - scientific workshop on neutron measurements, theory and applications, Geel, Belgium (2009).

[73] Z.Y. Bao, H. Beer, F. Käppeler, F. Voss, K. Wisshak, and T. Rauscher, "Neutron Cross Sections for Nucleosynthesis Studies," ATOMIC DATA AND NUCLEAR DATA TABLES **76**, 70 – 154 (2000).

[74] J.-Ch. Sublet and M. Fleming, "Maxwellian-Averaged Neutron-Induced Cross Sections for kT=1 keV to 100 keV, KADoNiS, TENDL-2014, ENDF/B-VII.1 and JENDL-4.0u nuclear data libraries," Technical Report CCFE-R(15)29, CCFE (2015).

[75] C.L. Dunford and A. Trkov, "ENDF Utility Codes version 7.02-8.2" http://www.nndc.bnl.gov/nndcscr/endf/endf-util/index.html.

[76] Keiichi Shibata, Private communication (2014).

[77] Said F. Mughabghab, "Atlas of neutron resonances: Resonance parameters and thermal cross sections. z=1-100" (Elsevier, 2006), 5 edition.

[78] F. Maekawa et al., "Compilation of benchmark results for fusion related nuclear data," Technical Report JAERI-Data/Code 98-024, JAEA (1998). http://www.jaea.go.jp/jaeri/.

[79] F. Maekawa et al., "Data collection of fusion neutronics benchmarking experiment conducted at FNS/JAERI," Technical Report JAERI-Data/Code 98-021, JAEA (1998). http://www.jaea.go.jp/jaeri/.

[80] F. Maekawa, M. Wada, and Y. Ikeda, "Decay Heat Experiment and Validation of calculation code systems for fusion reactor," Technical Report JAERI 99-055, JAEA (1999). http://www.jaea.go.jp/jaeri/.

[81] J.-Ch. Sublet and M.R. Gilbert, "Decay heat validation, FISPACT-II&TENDL-2015, JEFF-3.3, ENDF/B-VII.1 and JENDL-4.0 nuclear data libraries," Technical Report UKAEA-R(16)36, UKAEA (2016). http://fispact.ukaea.uk.

[82] J.-Ch. Sublet and M.R. Gilbert, "Decay heat validation, FISPACT-II&TENDL-2014, JEFF-3.2, ENDF/B-VII.1 and JENDL-4.0 nuclear data libraries," Technical Report CCFE-R(15)25, CCFE (2015). http://fispact.ukaea.uk.

[83] J.-Ch. Sublet and M. Gilbert, "Decay heat validation, FISPACT-II&TENDL-2012,-2011, and EAF-2010 nuclear data libraries," Technical Report CCFE-R(13) 20, CCFE (2013).

[84] N. Otuka, E. Dupont, V. Semkova, B. Pritychenko, A.I. Blokhin, M. Aikawa, S. Babykina, M. Bossant, G. Chen, S. Dunaeva, et al., "Towards a more complete and accurate experimental nuclear reaction data library (EXFOR): international collaboration between nuclear reaction data centres (NRDC)," NUCL. DATA SHEETS **120**, 272–276 (2014).

[85] M. Fleming, J.-Ch. Sublet, and J. Kopecky, "Integro-differential Verification and Validation, FISPACT-II & TENDL-2014 nuclear data libraries," Technical Report CCFE-R(15)27, CCFE (2015).

[86] J.-Ch. Sublet and G. J. Butterworth, "Fusion Activation of Ferrous Alloys," FUS. ENG. DES. **22**, 279–321 (1993).

[87] M. Fleming and J.-Ch. Sublet, "Validation of FISPACT-II decay heat and inventory predictions for fission events," Technical Report CCFE-R(15)28, CCFE (2015).

[88] J.C. Hardy, L.C. Carraz, B. Jonson, and P.G. Hansen, "The essential decay of pandemonium: A demonstration of errors in complex beta-decay schemes," PHYS. LETT. B **71**, 307 – 310 (1977).

[89] M. Fleming and J.-Ch. Sublet, "Decay data comparisons for decay heat and inventory simulations of fission events," Technical Report CCFE-R(15)28/S1, CCFE (2015).

[90] M. Fleming and J.-Ch. Sublet, "Fission yield comparisons for decay heat and inventory simulations of fission events," Technical Report CCFE-R(15)28/S2, CCFE (2015).

[91] M. R. Gilbert and R. A. Forrest, "Comprehensive handbook of activation data calculated using EASY-2003," FUS. ENG. DES. **81**, 1511–1516 (2006). http://dx.doi.org/10.1016/j.fusengdes.2005.08.067. Original report no. UKAEA FUS 509.

[92] R. A. Forrest, A. Tabasso, C. Danani, S. Jakhar, and A. K. Shaw, "Handbook of Activation Data Calculated Using EASY-2007," Technical Report UKAEA FUS 552, UK Atomic Energy Authority (2009).

[93] M. R. Gilbert, J.-Ch. Sublet, and R. A. Forrest, "Handbook of activation, transmutation, and radiation damage properties of the elements simulated using FISPACT-II & TENDL-2014; Magnetic Fusion Plants," Technical Report CCFE-R(15) 26, CCFE (2015).

[94] M. R. Gilbert and J.-Ch. Sublet, "Handbook of activation, transmutation, and radiation damage properties of the elements simulated using FISPACT-II & TENDL-2014; Nuclear Fission plants (PWR focus)," Technical Report UKAEA-R(15) 31, UKAEA (2015).

[95] M. R. Gilbert and J.-Ch. Sublet, "Handbook of activation, transmutation, and radiation damage properties of the elements simulated using FISPACT-II & TENDL-

2014; Nuclear Fission plants (HFR focus)," Technical Report UKAEA-R(15) 32, UKAEA (2015).

[96] M. R. Gilbert and J.-Ch. Sublet, "Handbook of activation, transmutation, and radiation damage properties of the elements simulated using FISPACT-II & TENDL-2014; Nuclear Fission plants (FBR focus)," Technical Report UKAEA-R(15) 33, UKAEA (2015).

[97] M. R. Gilbert, J.-Ch. Sublet, and A. Turner, "Handbook of activation, transmutation, and radiation damage properties of the elements and of ITER materials simulated using FISPACT-II & TENDL-2015; ITER FW armour focus," Technical Report CCFE-R(16) 37, CCFE (2016).

[98] M. R. Gilbert and J.-Ch. Sublet, "Scoping of material response under demo neutron irradiation: comparison with fission and influence of nuclear library selection," FUS. ENG. DES. , (2016). Submitted for publication. https://arxiv.org/abs/1604.08496.

[99] R.A. Forrest, "Importance diagrams - a novel presentation of the response of a material to neutron irradiation," FUS. ENG. DES. **43**, 209–235 (1998). http://dx.doi.org/10.1016/S0920-3796(98)00418-9.

[100] M.R. Gilbert, L.W. Packer, J.-Ch. Sublet, and R.A. Forrest, "Inventory simulations under neutron irradiation: visualization techniques as an aid to materials design," NUCL. SCI. ENG. **177**, 291–306 (2014). http://dx.doi.org/10.13182/NSE13-76.

[101] T. Hutton, J.-Ch. Sublet, L. Morgan, and T.W. Leadbetter, "Optimising differential data formats for monte-carlo radiation transport in the fusion regime," ANN. NUCL. ENERGY **98**, 36–42 (2016).

[102] J. Bang-Jensen and G. Z. Gutin, "Digraphs: theory, algorithms and applications" (Springer Science & Business Media, 2008).

[103] W. Arter and J.G. Morgan. "Sensitivity analysis for activation problems,". In Joint International Conference on Supercomputing in Nuclear Applications and Monte Carlo 2013, page 02404 (2014). http://dx.doi.org/10.1051/snamc/201402404.

[104] W. Arter, J.G. Morgan, S.D. Relton, and N.J. Higham, "Ranking the importance of nuclear reactions for activation and transmutation events," NUCL. SCI. AND ENG. , (2016). To appear, see http://arxiv.org/abs/1502.07137.

[105] A.M. Dunker, "Efficient calculation of sensitivity coefficients for complex atmospheric models," ATMOSPHERIC ENVIRONMENT **15**, 1155–1161 (1981).

[106] The MathWorks, "MATLAB" (The MathWorks, Inc., Natick, Massachusetts, United States, Release 2012a).